

**NUMERICAL MODELING OF STORM SURGES
IN THE BEAUFORT AND CHUKCHI SEAS**

by

Zygmunt Kowalik

**Geophysical Institute
University of Alaska
Fairbanks, Alaska 99701**

**Final Report
Outer Continental Shelf Environmental Assessment Program
Research Unit 627**

May 1984

ACKNOWLEDGMENTS

I would like to express my gratitude to A. Thorndike (Polar Science Center, University of Washington) for his help in preparing the atmospheric pressure data for the wind calculation and discussion of the air-ice interaction problems.

I am grateful to the following for offering me unpublished data on sea level variation in the **Chukchi** and Beaufort seas: D. **Bain** (State of Alaska, Department of Natural Resources), B. Matthews (University of Alaska, Fairbanks), F. E. Stephenson (Institute of **Ocean** Sciences, Sidney, Victoria, B.C.), and J. Nasr (Fisheries and Oceans, Ottawa).

Discussions with T. Fathauer (National Weather Service, Fairbanks) and Al Comiskey (University of Alaska, Anchorage) helped me understand the climatology of the storm surges and discussions with R. F. Henry and T. **Murty** (Institute of Ocean Sciences, Sidney, Victoria, B.C.) elucidated the problems related to the surge modeling in the polar seas.

I am greatly indebted to M. **Pelto (NOAA, OCSEAP, Juneau)** and G. Weller (University of Alaska, Fairbanks) for help and discussions throughout the work.

This is the final report of OCSEAP Research Unit 627, Contract Number **NA-81-RAC-00048**.

ABSTRACT

Specific problems of storm-surge modeling in ice-covered seas are analyzed and **discussed. First, the system of equations of motion and continuity in the ice-covered sea is introduced.** The idea is to apply the vertically integrated equations of motion and continuity to the prediction of the storm surge wave both in **ice-free and ice-covered seas.** The interaction of atmosphere, ice, and water is expressed by the **normal and tangential stresses.** **To include ice in the storm surge model we have to formulate the equations of motion and continuity for the ice cover. It is reasonable to assume** that the storm surge is a phenomenon of relatively short duration; the thermodynamic behavior of ice can, therefore, be neglected **and only** the mechanical properties of ice are included **in the equations. This brings into the scope of this work** the various methods to describe interactions between the ice floes. A few possible ways to express the internal ice stresses are listed. Because the system of equations **will be solved by numerical methods, the new numerical problems are scrutinized** and criteria of numerical stability are examined. Before starting the computation of a storm surge **in the Beaufort and Chukchi seas, a simulated surge is investigated in a square basin.** The computations are performed with the same wind distribution for both ice-free and ice-covered areas.

In the next step a numerical grid is set over the **Chukchi** and Beaufort seas and three storm surges are simulated and described. The charts of the sea level, current and ice **distribution are related to the large scale of the wind pattern** used to simulate the driving force for the surge. The charts **also** allow estimates of the potential for the storm surge at various locations along the **Chukchi** and Beaufort coasts. First, a positive surge of October, 1963, generated by a low pressure "center traveling from Siberia to Banks Island, is studied. On its way the storm was a source of the strong northwest and west winds which caused the **sea level to rise** to a record height of about 3 m along the **Alaskan coast of the Chukchi Sea. Next we** simulated a negative surge which occurred **in the fall of 1979. This surge was**

generated by the stationary high pressure system centered between Barrow and the North Pole. This is a typical wind pattern which feeds the Beaufort Gyre motion. Comparison of the measured and computed sea level and observed and computed ice edge **position** proves that the model is suitable to reproduce both water and ice motion. Finally, the storm surge in the late summer of 1981 is studied and the results are compared against eight tide gauges deployed along the Beaufort coast. Temporal variations of the recorded and computed sea level support the application of the model **for short time predictions of the sea level during storms.**

Results from the storm surge computations show relation of the sea level and current distribution. Due to the depth and shoreline geometry the pattern of motion in the **Beaufort** Sea is quite different from that **in the Chukchi Sea.** **In both basins** the storm surge tends to develop a dome structure **in the sea level distribution.** **The negative sea level at the center** of the dome in one sea basin is coupled with a positive **level at the dome in** the second basin. Velocity tends to be parallel to **the sea level contours according to the geostrophic adjustment; therefore, two gyres are observed in which motion takes place around the domes.** In the Chukchi Sea both current and sea level display strong variations not only at the shore but at large distances from the coast as well. In the Beaufort Sea, on the other hand, the changes are usually confined to the nearshore region. Also during major surges a **coastal jet current develops along the shelf from Mackenzie Bay to Point Barrow.**

All simulations are done for the ice-free and ice-covered sea surface, but the influence of the ice is practically negligible because major surges took place in summer and fall when the **Chukchi** and Beaufort seas were only partly covered by ice.

TABLE OF CONTENTS

	<i>Page</i>
Acknowledgments.	251
Abstract	253
1. Formulation of basic equations	257
2. Short discussion of certain terms in the equation of motion	260
3. Constitutive law to express internal ice stresses	264
4. Numerical problems related to the storm surge modeling in the polar seas	267
5. Storm surges in ice-covered sea basins	269
6. Storm surges in the Beaufort and Chukchi seas - introduction	270
7. Numerical modeling - area, grid and boundary conditions	275
8. Storm surge of October 1963	279
8.1 Short analysis of the storm	279
8.2 Results of numerical simulations	279
9. Negative surges - open-water season, 1979	283
10. Storm surge of August 30 - September 1, 1981	285
References	286
Figures.	289

1. Formulation of basic equations

Storm surge modeling is a subject area where numerical-hydrodynamical methods are quite successful. The storm surge propagation is usually studied through the vertically integrated equations of motion; therefore, complicated problems of exchange of momentum along the vertical direction are diverted to simpler problems of defining the tangential stresses at the sea surface and at the bottom.

The air-sea interaction in the polar seas is impeded by the presence of ice. The prediction of the pack ice influence on the storm surge propagation would not be so complicated if fairly general laws of the ice floe mechanics had been specified and tested experimentally (Rothrock, 1975).

The basis of calculations presented here will be the vertically integrated equations of water motion and continuity, written in the Cartesian coordinate system $\{x_i\}$, with x_1 directed to the east and x_2 directed to the north:

$$\frac{\partial u_i}{\partial t} + \varepsilon_{ij} u_j + \frac{\partial}{\partial x_j} (u_i u_j) = -g \frac{\partial \zeta}{\partial x_i} + \frac{(1-c)\tau_i^a}{H\rho_w} + \frac{c\tau_i^w}{H\rho_w} - \frac{\tau_i^b}{\rho_w H} + A \frac{\partial u_i^2}{\partial x_j^2} \quad (1)$$

$$\frac{\partial \zeta}{\partial t} + \frac{\partial (H u_i)}{\partial x_i} = 0 \quad (2)$$

The ice motion induced by wind will be studied through the following equations of motion:

$$m \frac{\partial v_i}{\partial t} + m \frac{\partial}{\partial x_j} (v_i v_j) + m \varepsilon_{ij} v_j - mg \frac{\partial \zeta}{\partial x_i} - c (\tilde{\tau}_i^a - \tau_i^w) + F_i \quad (3)$$

Rate of change of the ice mass (m) over **specific area is equal to the net influx of mass to that area plus all sources and sinks (ϕ)-Rothrock** (1970). The equation of continuity for the ice mass consistent with the above considerations is

$$\frac{\partial m}{\partial t} + \frac{\partial (mv_j)}{\partial x_j} = \phi \quad (4)$$

In the above equations the following notation is used:

- i, j - indices, ($i, j = 1, 2$) where 1 stands for east coordinate, and 2 for west coordinate;
- t - time;
- u_i - components of the water velocity vector;
- v_i - components of the ice velocity vector;
- τ_{ij}^a - components of the wind stress vector over the sea;
- $\tilde{\tau}_{ij}^a$ - components of the wind stress vector over the ice;
- τ_{ij}^w - components of the water stress;
- τ_{ij}^b - components of the bottom stress;
- F_i - components of the force due to internal ice stress;
- ϵ_{ij} - Coriolis tensor;
- ζ - variation of the sea level or the ice around the undisturbed level;
- c - ice compactness;
- H - water depth;
- ρ_w - water density;
- A - lateral eddy viscosity, usually will be taken as $5 \cdot 10^4 \text{ m}^2/\text{s}$;
- m - ice concentration or mass per unit area;
- g - gravity acceleration.

Throughout **all** indexed expressions Einstein's summation convention will be applied.

Assuming that the **ice is not spread evenly over the whole sea surface**, the mass of ice can be **expressed through the ice compactness (c)**, ice thickness (h), and ice density (P):

$$m = \rho h c \quad (5)$$

A storm surge is a phenomenon of a relatively short duration, therefore thermodynamical sources and sinks **linked** to ϕ in equation (4) can be neglected. The equation of mass balance can be divided into two separate equations, i.e. a continuity equation for the ice compactness and an equation of thickness balance:

$$\frac{\partial c}{\partial t} + \frac{\partial (v_j c)}{\partial x_j} = 0 \quad (6)$$

$$\frac{\partial h}{\partial t} + v_j \frac{\partial h}{\partial x_j} = 0 \quad (7)$$

Both equations (6) and (7) will be applied along with equations (1) **through (3) to obtain the ice thickness and the ice compactness distributions**. It is reasonable to assume when the ice is not packed closely ($c < 1$) that the ice thickness is not changed due to the ice motion. If, on the other hand, due to internal ice stress, the ice compactness **will** grow beyond $c=1$, the excess of compactness will lead to a change of the ice thickness. In such a case **the new ice thickness distribution is computed through equation (7)**.

To derive a solution to equations (1) through (7) suitable boundary and initial conditions should be stated. Among all possible sets of the boundary conditions the **chosen one should lead to a unique solution to the**

above **system of equations**. Such a set of conditions is still undefined for the ice-ocean interaction; **therefore, we** shall assume (since the ice flow equations), that the specification of the normal and tangential velocities **along** the boundaries **is** sufficient to derive the unique solution (**Marchuk et al., 1972**). Usually at the open boundaries (i.e. water boundaries) the storm **surge velocity distribution is unknown**. To overcome this hindrance the conditions at the opening boundary are **specified** for the simplified hyperbolic problem in which the horizontal exchange of momentum is neglected. Simplified problems, **solved along the** open boundary, define the velocity distribution. This velocity is the new boundary condition when solution of the complete system of equations is sought.

2. Short discussion of certain terms in the equations of motion

The aim is to discuss **those terms in the equations of motion which still are not clarified with adequate precision**, due mainly to the lack of suitable experimental knowledge. The interaction of the atmosphere, ice, and water is generally expressed through the normal tangential stresses. The definition of tangential stress over the ocean

$$\tau_i^a = C_{10} \rho_a |W_i| W_i \quad (8)$$

includes the wind-drag coefficient C_{10} . Recently **Garrat (1977)** analyzed **almost all** measured data and found that C_{10} under a neutral atmospheric stability depends linearly on the wind velocity (W):

$$C_{10} = (0.75 + 0.067W) \cdot 10^{-3} \quad (9)$$

In (9) wind **velocity is expressed in m/s**.

In practice in storm surge computations (Henry and Heaps, 1976), the wind drag is usually set as constant and as large as $2.7 \cdot 10^{-3}$. Applying Garrat's expression one can see that this drag coefficient occurs at wind speeds close to 30 m/s, a speed which is too high even for average storm conditions. The large value of C_{10} was introduced into storm surge computations through comparison of the computed and observed sea level distributions in the coastal zone. Since the coastal effects are not always resolved properly, this may be the source of discrepancy. On the other hand measurements performed under strong wind conditions over the open ocean are quite rare. One can, therefore, argue that C_{10} should grow much faster with the wind speed due to the high roughness of the sea surface. Facing the necessity of choice of C_{10} as a constant value equal to $2.7 \cdot 10^{-3}$ and according to Garrat's expression (9) we take the former value in ensuing storm surge computations.

Definition of the wind stress over the pack ice,

$$\tilde{\tau}_i^a = \tilde{C}_{10} \rho_a |W_i| W_i \quad (10)$$

again leads to the same kind of problem. If one tries to scrutinize all data gathered during AIDJEX (Pritchard 1980) and the data dispersed in a few additional references, the dependence of \tilde{C}_{10} on wind will be probably close to the expression (9). Again the same flaw occurs, namely that the measurements were made over smooth ice which does not properly characterize the high roughness of the sea ice due to the hummocking processes- Leavitt (1980), McPhee (1980). In the ensuing computations the wind drag coefficient over the ice, C_{10} , will be assumed to be equal to the one over the sea, i.e. $2.7 \cdot 10^{-3}$.

Interaction of the water and ice in equations (1) through (7) is described by two forces - the pressure gradient and the water stress. The former is

fully defined if the sea level distribution is given; the latter we take as,

$$\tau_i^w = R_w |v_i - u_i| (v_i - u_i) \quad (11)$$

Water stress is sensitive both to the relative motion of the water and the ice, and to the magnitude of the coefficient R_w . The water drag coefficient is a function of the aerodynamic properties of the ice-water interface and the relative motion, its magnitude ranges from $3 \cdot 10^{-3}$ to $5.5 \cdot 10^{-3}$. For the pack ice drift in summer due to wind, McPhee (1980) estimated the water drag magnitude to be from $4 \cdot 10^{-3}$ to $5.5 \cdot 10^{-3}$. He also postulated that the ratio of the water drag coefficient to the wind drag coefficient is close to two ($R_w/C_{10} \approx 2$). The water drag coefficient is quite close to the above value. The drag coefficient under smooth first-year sea ice may be as small as $1.32 \cdot 10^{-3}$ (Langleben, 1982).

At the bottom of the sea a quadratic dependence of bottom stress on the velocity is also well recognized;

$$\tau_i^b = R |u_i| u_i \quad (12)$$

The bottom drag coefficient (R) is a function of the bottom roughness and the properties of the bottom boundary layer (Komar, 1976); R is usually taken in the range $(2 \div 4) \cdot 10^{-3}$.

The important problem to be clarified before the ice-water interaction can be studied is the formulation of a constitutive law which relates the stress (σ_{ij}) transmitted between floes to the variables in the problem

formulated by equations (1) through (7). Only the mechanical behavior of ice is considered. We shall assume that during the storm surge the ice **distribution will change** due only to the **ice** motion; the influence of the thermodynamic processes will be neglected.

Due to the internal ice stresses the force F_i (see equation 3) acts on the ice floes. The components of the force are given by the divergence of the stress tensor (σ_{ij}) ;

$$F_i = \frac{\partial \sigma_{ij}}{\partial x_j} \quad (13)$$

The stress-strain relationship is defined as follows;

$$\sigma_{ij} = 2\eta \epsilon_{ij} + (\lambda - \eta) \epsilon_{kk} \delta_{ij} - \frac{p}{\rho} \delta_{ij} \quad (14)$$

Here i, j are indices and they take the value 1 or 2. The strain-rate in (14) is expressed by the ice velocity;

$$\epsilon_{ij} = \frac{1}{2} \left(\frac{\partial v_i}{\partial x_j} + \frac{\partial v_j}{\partial x_i} \right) \quad (15)$$

Introducing (14) and (15) into (13) the components of the force due to the internal ice stress are derived

$$F_1 = \eta \Delta v_1 + \lambda \frac{\partial}{\partial x_1} \left(\frac{\partial v_1}{\partial x_1} + \dots \right); \quad (16a)$$

$$F_2 = \eta \Delta v_1 + \lambda \frac{\partial}{\partial x_2} \left(\frac{\partial v_1}{\partial x_1} + \frac{\partial v_2}{\partial x_2} \right) - \frac{1}{\rho} \frac{\partial p}{\partial x_2} \quad (16b)$$

In the ensuing computations, bulk (λ) and shear (η) viscosity coefficient are taken as equal, i.e. $\lambda = \eta$. The constitutive law has been applied a few times to investigate the under-ice tide propagation, but it

has **never** been used in storm surge models. In this law at least two empirical constants which express the mechanism of the floe interaction are unknown, i. e. **the viscosity coefficient (n) and pressure (p)**. Due to its discrete structure the **pack ice is able to transmit compressive** stresses only; the tensile stresses cannot propagate through the pack ice. It should be underlined that the ice **mechanics expressed by the constitutive law do not take into account each individual** ice-floe and its history. Sea ice cover is considered an aggregate of the ice floes, i. e. pack ice. The internal ice stress derived from the **constitutive law is**, therefore, a statistical average of the stresses between individual ice floes.

3. Constitutive laws to express internal ice stresses

Ice motion and ice compactness display close inter-relation, because nonuniform distribution of the ice velocity leads to variations in the ice compactness. Ice movement, practically unrestricted at a small compactness, is constrained at high compactness. The growth of compactness increases the internal stresses and **if a critical value of stress is reached, deformation processes like hummocking, ridging or breaking** will occur. This picture indicates that a simple frictional model of the ice flow interaction is unable to describe correctly the internal interaction over a wide range of compactness. From a certain value of compactness the frictional model should be aided by a **model** which is able to reproduce the high internal stresses in closely packed sea ice. Nonetheless, it is useful to consider the ice as a viscous fluid superposed over the water. A simple mechanism of the ice **flow** interaction is given by a linear viscous material, in that case the ice stress is proportional to the strain rate tensor (see **Campbell, 1965, and Glenn, 1970**).

If, further, the fluid is considered as noncompressible, the relation between strain and stress (14) simplifies to:

$$\sigma_{ij} = 2\varepsilon_{ij} \quad (17)$$

inserting (15) into the above expression, and calculating the divergence of the stress tensor by (13) the internal force becomes:

$$F_i = \eta \frac{\partial^2 v_i}{\partial x_j \partial x_j} \quad (18)$$

The magnitude of the kinematic viscosity coefficient (η) is difficult to evaluate. In the Arctic Ocean and in the Weddell Sea, Campbell (1965) and Ling et al. (1980) found the coefficients by tuning the computed pattern of the mean ice circulation to the observed pattern. The estimated values ranged from $5 \cdot 10^6$ m²/s to $5 \cdot 10^8$ m²/s. To evaluate the influence of viscosity on tidal waves a sequence of investigation was carried out by Kowalik (1981) in the Arctic Ocean. The viscosity coefficients found for the steady motions when applied to the tide led to the suppression of the tide and, therefore, are unsuitable to describe time-dependent motion.

Closer to the natural conditions is the assumption that the viscosity coefficient is a function of the ice compactness. Linear dependence proposed by Doronin (1970)

$$\eta = \alpha c; \quad \alpha = 5 \cdot 10^6 \text{ m}^2/\text{s}, \quad (19)$$

proved to be valuable in the prediction of the ice drift. However, since a long period was considered by Doronin it is not clear whether the success of the prediction was due to correct choice of ice mechanics or ice

thermodynamics. According to **Shirokov** (1977) the internal ice friction starts to play an important role when the ice compactness is close to 0.8 and one may argue that starting from this **value Doronin's** expression can be applied.

It is possible to approach a description of stresses between floes from a different point of view and to consider the elastic properties only. Internal pressure, due to the ice floe interactions, will be expressed as a function of the ice compactness. **Kheisin** (1971) postulated a linear dependence of the pressure on the compactness;

$$p = k_p \frac{\delta c}{c_0} \quad (20)$$

with constant coefficient of the ice compression (k_p). The internal ice pressure is only present when variations of compactness are positive ($\delta c > 0$); on the other hand, if $\delta c < 0$, $p=0$. According to **Kheisin (1971)** the magnitude of k_p in closely packed ice ($c = 1$) varies from $10^4 \text{ kg/m}\cdot\text{s}^2$ to $10^5 \text{ kg/m}\cdot\text{s}^2$. In a two-layered system: **ice-water**, a pressure signal is not only transmitted through the water with velocity of the long waves (\sqrt{gH}), but also an elastic wave propagates with velocity $\sqrt{\frac{k_p}{\rho}} = 10 \text{ m/s}$. In shallow water ($H < 10 \text{ m}$), the speed of elastic waves can exceed the speed of gravity waves.

A model of the ice drift with the ice **mechanics based on the elastic constitutive law**, has been developed and tested for the **Caspian Sea** by **Ovsienko** (1976, 1978). Internal ice pressure was set as a power function of the compactness

$$p = p_0 \left(\frac{c}{c_0} \right)^\kappa \theta \left(\frac{dc}{dt} \right) \quad (21)$$

where,

$$\theta \left(\frac{dc}{dt} \right) = \left. \begin{array}{l} 1, \quad \text{if } \frac{dc}{dt} > 0 \\ 0, \quad \text{if } \frac{dc}{dt} < 0 \end{array} \right\}$$

The magnitude of p is close to the coefficient of the ice compression in (20), exponent $\kappa = 4 \div 6$.

Models to include both viscous and elastic properties were introduced by **Rothrock (1975)** and **Kheisin and Ivchenko (1973)**. **Rothrock's constitutive law** contains pressure terms as a function of divergence of the ice velocity;

$$\left. \begin{aligned} \frac{p}{\rho} &= -A_p \frac{\partial v_i}{\partial x_i}, \quad \text{if } \frac{\partial v_i}{\partial x_i} < 0 \\ p &\equiv 0, \quad \text{if } \frac{\partial v_i}{\partial x_i} > 0 \end{aligned} \right\} \quad (22)$$

Analyzed **constitutive laws** contain rather simple mechanical properties of the ice, but they seem to describe the interaction of a storm-surge or tide with the pack ice in a quite satisfactory manner. For the long period processes, sophisticated models of the ice floe interaction, with both mechanical and **thermo-**dynamical properties have been proposed by Coon et al. (1974) and **Hibler (1979)**.

4. Numerical problems related to the **storm** surge modeling in the polar seas

A few numerical schemes were constructed to predict the time dependent water-ice interaction. **Hibler (1979)** investigated slow seasonal variations of the ice cover in the Arctic Ocean by an implicit numerical scheme.

Ovsienko (1976) employed particle-in-cell methods to predict the ice distribution and especially the position of an ice edge. We shall **apply** the scheme of Hansen (1962), which is explicit in time and staggered in **space, to** search for the solution of equations (1) through (7). The reason is that the explicit method has been employed in various oceanographical problems and its properties are quite well recognized (**Kagan, 1970**). It is of interest to understand how the ice cover will change the stability conditions of an explicit scheme.

Principal stability condition (Ramming and Kowalik, 1980)

$$T < \sqrt{\frac{l}{2gH}} \quad (23)$$

relates time step (T) to the distance (L) between grid points of a numerical scheme. If elastic properties of the ice cover are taken into account the inequality (23) must be modified accordingly, but the modification is necessary only in a very shallow basin ($l_i < 10$ m).

A significant difficulty of preserving numerical stability of the explicit scheme is created by internal friction, expressed by the lateral exchange of momentum. The ice kinematic viscosity coefficient, an analogue of kinematic eddy viscosity of water has high values up to $108 \text{ m}^2/\text{s}$. Kowalik (1981) demonstrated dependence of the stability condition on the magnitude of the horizontal viscosity. The general condition (23) should be assisted by two conditions related to the frictional forces:

$$T < (r_1 + 2A/L^2)/2f^2 \quad (24)$$

and

$$T < 1/(r_1 + 2A/L^2) \quad (25)$$

Coefficient r_1 is expressed as $r|u_i|/\rho_w H$, and in the deep ocean ($H \rightarrow \infty$), its value is negligible. Combining (24) and (25) for the deep ocean case, the range of variations of the horizontal viscosity is easily defined;

$$T(fL)^2 < A < \frac{1}{2T} \quad (26)$$

Viscosities defined beyond the range of inequality (26) will lead to the instability of the explicit numerical scheme.

5* Storm surges in ice-covered sea basins

Before starting the storm surge computation in the ice-covered Beaufort and Chukchi Seas one may investigate a similar process in a somewhat simple basin where complicated problems related to the open boundary conditions can be discarded. We take a square basin of 1000 km length with the depth variable along the x_1 (horizontal) direction from 50m (at $x_1=0$) to 30 m (at $x_1 = 1000$ km). At the initial moment wind starts to blow along the (x_2) vertical coordinate with the speed constant *in* time but variable in space. The speed varies linearly along the X_1 direction from 4 m/s at $x_1=0$, up to 20 m/s at $x_1=1000$ km. A series of experiments was carried out with the above distribution of wind to compare different distributions of the sea level and current related to the presence or the absence of the ice and to the various **constitutive laws of the ice mechanics**. Three cases of the ice behavior were tested:

- a) internal stress was neglected ($F_i=0$),
- b) internal stress was expressed through the horizontal exchange of momentum with a constant viscosity coefficient, and with the viscosity coefficient according to Doronin's expression (19), and,
- c). internal stress was given by the elastic constitutive law according to expression (21).

The ice leads to redistribution of the energy transmitted from air to sea. This is clearly seen both in the current and sea level distributions derived from the computations - Figure 1 to Figure 6. The computations with the various **constitutive laws** show that the influence of the internal ice stresses on the ice distribution, sea level and mean current is of secondary importance. The dominant features of the ice motion are well described by the ice model.

without internal ice stresses ($F_i=0$). Figures 1 and 2 display the sea level and the mean current at 2 hours and 90 hours from the onset of winds over the ice-free sea. Steady motion occurs after about 70-80 hours of the process. The asymmetry of the sea level distribution is due mainly to the strong wind torque. The horizontal grid distance is scaled as 25 cm/s, therefore the largest velocities are of the order of 30 cm/s. In Figures 3, 4, 5 and 6 the same situation is depicted when the sea surface is covered by ice. Ice with a high compactness ($c = 0.95$) covers the eastern portion of the sea and over the remaining are the ice compactness is quite small ($c = 0.1$) (Figure 4). A comparison of Figures 1 and 3 shows the variations of the sea level and current. Close to the southern edge of the ice field the change in the sea level is especially noticeable. Since ice is situated on the sea surface where wind acts and also because the ice is thinner than the water, the ice velocity (Figure 4) exceeds the water velocity (Figure 3). In case of steady motion represented by Figures 5 and 6 the motion of ice and water is completely adjusted to the wind stress distribution. In these figures one can find areas where the ice velocity is smaller than the water velocity, and therefore, the energy is transmitted from water to ice. Such situations occur where the water and ice motion is reverse to the wind direction. The current in that area is not related to the wind stress but to the water slope.

6. Storm Surges in the Beaufort and Chukchi Seas - Introduction

The importance of the storm surges and associated water and ice motion is related to the recent exploitation of the North Slope oil. The shore of the Beaufort Sea is generally of low relief; therefore, coastal plains can be inundated by the surge and waves. The knowledge of the sea level variation along the Alaskan Beaufort and Chukchi coasts is scant. Until now tide gauges were installed in this region for a short time only and the present set of data is

too small to estimate statistically valid distribution of the sea level variations. **Only** those surges which caused extensive flooding of the coastal communities were recorded. In the eastern Beaufort Sea in Tuktoyaktuk, Canada, a tide gauge was installed more than 20 years ago. Therefore some facts related to the storm surges in the Beaufort Sea can be inferred from this set of data. In Table 1, storm surges in excess of ± 0.9 m for the 11 year period (1962-73] are given after Henry (1974). Frequency of the major surges was not distributed uniformly in time and the highest sea level ever recorded at Tuktoyaktuk occurred on October 4, 1963. The same surge was observed at Barrow one day earlier. Sea level rose up to 3 m and this is historically known **as** the highest level ever observed at Barrow.

One can therefore conclude that sea level variations due to the storm surges are highly correlated along the Beaufort Sea coast. The storm in October 1963 caused damage of \$3 million to Barrow. Hume (1964) studied topography variation after the storm surge and concluded that the sediment transport during storm in the vicinity of Barrow was equivalent of 20 years normal transport. We shall simulate the surge of October 1963 by numerical modeling, and the relation **of the weather** pattern and **the sea level** variations will be studied.

Due **to** the lack of the sea level data the range of the surge was studied by examining associated events like the driftwood distribution. **In** such a way Reimnitz and Maurer (1978) found a 3 m surge along the coast of Alaskan Beaufort Sea. They tracked the driftwood distribution due **to the** storm surge **in the fall of 1970. The driftwood was stranded 20 m to 2000 m from the water line.** The storm occurred over the southern Beaufort Sea, with wind up to 40 m/s-50 m/s. During this storm the Tuktoyaktuk gauge was not in operation and the surge was estimated as 3m; even higher than the one recorded **in** October 1963. From Harrison Bay to MacKenzie Bay both **wind** and sea level were strongly correlated, and only in the

TABLE 1

Storm surges (in excess of 0.9 m) at Tuktoyaktuk (Canada) during summer 1962 to fall 1973.

Date	Surge Amplitude (m)	Date	Surge Amplitude (m)
July 28, 1962	1.37	Sept. 22, 1963	1.01
Aug. 29, 1962	1.04	Oct. 4, 1963	1.89
Aug. 31, 1962	1.43	Oct. 16, 1963	0.91
Sept. 4, 1962	1.83	Aug. 7, 1965	1.37
Oct. 13, 1962	-0.91	Nov. 12, 1965	0.94
Oct. 25, 1962	-1.01	July 18, 1966	0.91
Nov. 14, 1962	-1.16	Sept. 10, 1966	1.13
July 5, 1963	1.19	Oct. 4, 1966	-0.91
July 27, 1963	0.94	Oct. 15, 1966	-1.10
July 28, 1963	1.13	July 24, 1967	1.13
July 30, 1963	1*55	Aug. 13, 1967	1.07
Aug. 4, 1963	,0.91	Oct. 3, 1967	0.91
Aug. 10, 1963	1.01	Oct. 12, 1973	1.01
Aug. 17, 1963	1.37		

vicinity of Barrow was this surge not observed.

Hunkins (1965) was probably the first to measure an open sea surge in the **Chukchi** Sea, when Ice Island (T-3) was aground. In the spring and summer of 1961 for 7 weeks a tide gauge was installed on the Ice Island. A negative storm surge (i.e., sea level below mean sea level) recorded on 30 May 1961 was caused by the high pressure system - fig. 7. A positive surge of about 40 cm occurred on June 18 due to the passage of a low pressure system - fig. 8. Both pressure systems traveled from Siberia across **Chukchi** Sea into the Arctic Ocean. Matthews (1971) installed recorders at Point Barrow for 3 years, and was able to show seasonal variation of the surges, and the presence of negative surges. These surges can produce important effects in winter, causing fracture of shore-fast ice, and underwater structures previously in water under the ice may have to bear the full weight of an ice sheet.

During various measurements organized by OCSEAP in the Beaufort Sea the sea level records were taken at random both during the open ice season and from under ice (Matthews, personal comm.). Some of these data we shall use later in the testing and validation of the numerical model. The need to improve prediction of the storm flooding over the North **Slope** has been recognized long ago. Fathauer (1978) compiled a summary of storm surges and gave a thumb-rule procedure to forecast floods along the **Western** and Northern shores of Alaska. Wise et al. (1981) identified about 90 major storm surges and developed a forecast procedure which is based on frequency of the wind occurrence. Assuming that the wind frequency (f) is inversely proportional to the frequency interval (fi) for the storm surges,

$$F_i = K/f, \quad (27)$$

a constant (K) can be determined for any given location. In the vicinity of Barrow, with 5 storm surges recorded, and assuming a frequency interval of 125 years

for **12** foot surges with wind frequency of 0.013 for the related wind range (42-47 Kts), K equals 1.63. Although these relations are derived from the best **available data one has to be very careful in drawing conclusions from these results.** No one knows how often 12 foot surges occurred. The distribution of the **wind frequency is known better through various observations, but again the wind** during the storm peak is measured rarely. At the time of **storm** in October 1963 winds up to 20 m/s to 30 m/s were reported at Barrow. In the storm during fall of 1970 winds were 40 m/s - **50 m/s** along the **Beaufort Sea** coast. In actual fact wind and atmospheric pressure over the Arctic Ocean until **1979** were extrapolated from the coastal and a few ice drifting stations. When modeling the October 1963 storm surge we have found that the pressure maps are often misleading. The possibility to model storm surges **by applying realistic surface wind distribution was created only in 1979** through the Arctic Ocean Buoy Program carried out by Thorndike and Colony (1980). An array of buoys was placed on the ice in the Arctic Ocean to measure atmospheric pressure, air temperature and buoy position.

In one respect surges in the Beaufort and **Chukchi** Seas differ from those at the moderate latitudes. **The** whole area is ice-covered for 8 months in the year. **In** summer and early autumn only the southern part of the Beaufort and **Chukchi Seas** is ice-free and there the major storm surges are generated. One generally assumes that the ice cover diminishes the sea **level** variation and such behavior can be expected from the atmosphere-ice-water interaction described **by eqs. (1)-(4).** Sea level recorded under the ice in Tuktoyaktuk (Henry, **1975**) reveals the existence of mainly negative storm surges. The range of the positive sea level variations compared against summer-fall season is quite small. Therefore one can reasonably assume that the ice cover suppresses the positive surges. This conclusion is supported by the observations, but certain waves can also be amplified under the ice. The amplitude of the M4 component in Tuktoyaktuk is

about two times larger in winter than in summer - (Barber et. al, 1983). This is caused by fast ice which may lead to the essential difference between the water depth in summer and winter. A summary of the influence of the ice cover on various tidal constituents in Tuktoyaktuk is given in Table 2 (Barber et. al, 1983). Storm surges usually occur together with the astronomical tides and it is essential to understand how much the surge is altered by the tide. Various measurements taken along the coasts of the Beaufort and Chukchi Seas show that major surges would not be essentially altered by the tides (Huggett et. al, 1975). The maximum amplitude of the tides varies from 5 cm to 20 cm. In fig. 9 the distribution of M2 constituent (amplitude and phase) computed by Kowalik and Matthews (1982) is given. The amplitude of the tide is small relative to those in the major surges and consequently we shall neglect the tides in the numerical simulation of the major surges.

7. Numerical Modeling - Area, Grid and Boundary Conditions

Two efforts to model the storm surges in the Beaufort and Chukchi Seas ought to be mentioned. P. J. Schafer (1966) computed the surge distribution at Barrow by simulating the storm surge of October 3, 1963. It was truly a pioneering effort which allowed to elucidate the interaction of the coast and the atmospheric low.

Henry and Heaps (1976) applied numerical method to the storm surges in the Southern Beaufort Sea. The model was based on the vertically integrated equations of motion and continuity (1) and (2); but the influence of ice cover was neglected.

We shall study the storm surge generation and propagation by applying the full system of equations (1)-(4). By applying the storm surge model with equations of ice motion and continuity we hope to answer several questions. First, the influence of the pack ice on the sea level and current can be studied, secondly one can see whether the storm surge model is suitable to describe ice motion or at least the motion of the ice edge. To include ice in the storm surge model

TABLE 2

Summary of the Influence of Ice Cover on Various Tidal Constituents

Tidal Constit- uent	Frequency C.P.H.	Amplitude (ft.) Yearly	Amplitude (ft.) Winter 1962	Amplitude (ft.) Summer 1962	Amplitude (ft.) Winter 1963
M2	0.0805	0.420	0.360	0.533	0.370
S₂	<i>0.0833</i>	<i>0.176</i>	<i>0.145</i>	<i>0.243</i>	<i>0.158</i>
K₁	<i>0.0418</i>	<i>0.116</i>	<i>0.070</i>	0.123	<i>0.080</i>
O₁	0.0387	0.089	0.071	0.078	0.086
M4	0.1610	0.006	0.012	0.006	0.013
MS₄/MK₄	0.1639	0.003	0.008	0.005	0.010
MG	0.2415	0.002	0.005	0.002	0.006
2MS₆	0.2444	<i>0.003</i>	<i>0.008</i>	<i>0.004</i>	0.008

we assumed that variations of the pack ice distribution are due entirely to the wind and not due to the thermodynamical processes. The assumption is based on Wendler's (1973) analysis of an actual summer situation for a 5-day period in the Beaufort Sea. He was able to show that the ice conditions were strongly correlated to the wind direction.

The response of the sea level to the storm passage we shall consider in the domain depicted in fig. 10. Due to the large dimension of the area the spherical shape of the Earth cannot be neglected and we introduce a spherical system of coordinates to the system of equations (1)-(4). The grid intervals of the numerical lattice in Fig. 10 are 1/3 of a degree of latitude and 1 degree of longitude; i.e. at latitude 70°N the grid length is about 38 km. The open boundary follows the 74°N parallel from Banks Island to 180°W, then south along this meridian to the Siberian coast; the second open boundary is set in the Bering Strait. To derive unique solutions to equations (1)-(4) both initial and boundary conditions ought to be specified. On the open boundary (for the water) a radiating condition proposed by Reid and Bodine (1968) is selected. It allows for all waves propagating out of the domain to pass the boundary without restrictions. Velocity perpendicular to the boundary (say, along positive x_1 direction) is defined through the relationship between amplitude(ζ) and velocity (u_1) in the long wave - Lamb (1945);

$$\frac{\zeta}{H} = \frac{u_1}{\sqrt{gH}} \quad (28)$$

By changing u_1 to u_2 in (28) the velocity along the x_2 direction will also be defined. The radiating boundary condition has been extensively applied in the modeling of storm surges, from the time it was introduced by Reid and Bodine (1968),

Setting as the open boundary condition $\zeta = 0$ leads to different patterns

of the surge in the vicinity of an open boundary, **but the surge at the coast is usually quite similar to the case when sea level is defined by open radiating condition (28).** Usually sea **level** changes substantially at the shore **and over the shallow water area**; therefore, if the open boundary condition is set beyond the shelf it should only insignificantly influence the surge distribution at the coast. This conclusion can be readily applied to the Southern Beaufort Sea, where **the shelf is narrow and the largest depth is** about 4 km. In the Chukchi **Sea the depth is almost everywhere less than 200m** and even at large distances from the shore a strong sea level variation can be generated.

Open boundary conditions for the ice velocity and compactness are not easily specified. One set of conditions can be defined by assuming continuity of the ice velocity and compactness across the boundary and setting first **and** second derivatives equal to zero. This condition, though numerically feasible, assumes that the motion in the domain is defined completely by internal processes and is not **influenced by the motion from outside of the domain.** Such an approach is obvious for the storm surges, when the open boundary condition is set beyond the shelf, but whether it is right for the ice motion remains to be proven. Another set of boundary conditions can be taken from the measurements through the buoys deployed **in** the Arctic Ocean **if** the buoys are in the proximity of the boundary during simulated storm surge.

To start numerical computation with radiating boundary conditions or with any condition which is not related to the uniqueness theorem of the problem, one **has to check** if the model works "reasonably" well, i.e. whether the specific boundary conditions do not create sources or sinks. **Therefore, in** the first experiment a steady and uniform wind was applied over the **Chukchi** and Beaufort Seas. After about 3 days steady state was reached. When the integral of the sea level over the surface of the Chukchi and **Beaufort** Seas was estimated, **it was close to** zero, thus indicating the lack of sources and sinks.

8. Storm Surge of October 1983

8.1 Short analysis of the storm

Meteorological observations at the time of the storm were very scant. Surface pressure maps for the **six** hour intervals from the Canadian Meteorological Centre allowed reconstruction of the storm track - fig. 11. One has to understand that the numbers given on the maps are extrapolated from the few coastal stations. Our work was greatly facilitated by weather analysis of the storm performed by Schafer (1966].

The low pressure center travelled from Siberia (**00Z, October 3**) to the northern shores of Banks Island (**06Z, October 4**), where it stayed for about 24 hours. The low on its way was a source of unusually strong winds. Record high surges of about 3 m were reported along the Alaskan coast of the **Chukchi** Sea (Schafer, **1966**) and a very high surge of about 2 m was recorded in Tuktoyaktuk at the eastern coast of the Mackenzie Bay. In both cases the high surges were due to **NW** winds, and it is obvious **that the direction of the shoreline in both areas is quite similar**. An additional factor which might have influenced the sea **level** in the **Chukchi** Sea was the high velocity of the pressure center. The center **travelled** a distance of about 2100 **km** in 30 hours, with an average velocity of **about 19.5 m/s**. The velocity of the long free waves defined as $c = \sqrt{gH}$ is quite large in the **Beaufort Sea** due to the large depth, but in the **Chukchi**, the average depth is about 50m, therefore the velocity of the long wave is 22 m/s. Because the **velocity** of the atmospheric pressure center in the **Chukchi** Sea was close to the velocity of the free waves, the large sea level variations can be related to the resonance **effects (Lamb, 1945)**.

8.2 The results of numerical simulation

Every 6 hours starting October 3, 00Z till October 6, 00Z the wind distribution has been computed from the surface pressure maps. Between 6 hour

readings the wind velocity was interpolated linearly in time. A typical surface pressure map which served for the calculation of the wind velocity is given in fig. 12; it depicts the situation on October 3, 182. To compute geostrophic winds, the region was subdivided into lattices of 2 degree latitude and 10 degree longitude and atmospheric pressure was taken from the grid points. Based on the data gathered during the AIDJEX experiment (Albright 1980) we have applied the cross-isobar turning angle ($\alpha = 24^\circ$) and the ratio of the surface wind (W) to the geostrophic wind (G); $W/G = 0.6$, in computing surface wind distribution.

The results of storm surge simulations will be given as the distributions of sea level, current, ice velocity, ice compactness and wind velocity over the area of the Chukchi and Beaufort Seas. Usually two types of computation were attempted. First, the sea surface was assumed to be ice-free and only equations describing water motion were applied. In the second case, the actual ice distribution has been taken as the initial condition and the storm surge was computed by applying the complete set of equations of ice and water motion. By comparing two simulations one can conclude that even an ice cover of about 4/10 is practically equivalent to open water when storm surge generation or propagation is studied. The four sets of figures at hour 6, 1 day, 2 days and 3 days from the onset of computations, will be given to describe the propagation of the surge from the Siberian coast to Banks Island.

The situation on October 3, 062 is described in fig. 13 - fig. 19. The atmospheric pressure center was situated at that time to the East of Wrangel Island. Winds computed from the pressure distribution over rectangular 2" by 10° grids are constant (fig. 13). The velocity scale is defined by the horizontal distance between grid points and equals 5 m/s. We did not attempt to smooth the spatial distribution of the wind, but linear interpolation in time was necessary to preserve stability of the computations. Due to NW and W winds the sea

level (fig. 14, fig. 15) rose about **50 Cm** along the Alaskan coast of the **Chukchi** Sea and a smaller surge occurred in the Mackenzie Bay.

Velocity (fig. 16, fig. 17) defined as an average velocity from the surface to the bottom is stronger in the **Chukchi** Sea, obviously due to the small depth of **this** area. Ice compactness (fig. 18) 6 hours after onset of computation is actually very close to the initial distribution. **In the ice-free regions we** assumed a 2% ice cover for the continuous application of the equations of motion and continuity. Therefore the ice velocity is plotted everywhere in the area of computation including "ice-free" areas - fig. 19. The ice motion can be taken as an indicator of the motion at the sea surface.

The second set of figures describes the storm surge distribution on **October 4, 1963, 002**; fig. 20-fig. 26. A report of observations made at the Arctic Research Laboratory at Barrow (Schafer, 1966) pointed out that between 1300 and 1600 AST the storm reached its peak with winds of 45 mph and gustiness up to 65 mph. Water **level** was about 3m above normal sea **level**.

The wind computed from the surface pressure at Barrow shows **NW winds** up to **40 m/s** - fig. 20. The maximum of the set-up along Alaskan Beaufort Sea is about 2.5 m - fig. 21, fig. 22. It is obvious that sea level **rises** toward the South from Barrow. This tendency was confirmed by observation at **Wainwright**, where the sea level at the peak of the storm was as high as 3.5m (**Schafer, 1966**). On the other hand the sea **level** along the Beaufort Sea does not show any conspicuous variations. We shall later on describe sea level as a function of time at Barrow and at two locations, **one in the Chukchi** Sea and another in the Beaufort Sea at the distance of one grid (36 **km**) from Barrow. This will demonstrate the special nature of the geographical location of **Barrow between two water basins of different dynamics related to the shore** line geometry and depth distribution. The sea level in the **Chukchi** Sea (fig. 21, fig. 22) displays **the large sea level varia-**

tion at the open sea, while in the Beaufort Sea large variations are confined to the near-shore area. Strong currents (fig. 23, fig. 24) form a coastal jet with speeds up to 1 m/s. Both water and ice movement (fig. 26) changed the ice compactness along the southern coast of the Beaufort Sea to a value smaller than 0.25 - fig. 25.

On October 5, 00Z, the low pressure center was situated to the North from Banks island and only in the Mackenzie Bay area did the NW wind (fig. 27) set sea level about 2 m above the mean sea level - fig. 28 and fig. 29. Sea level in these figures displays a characteristic pattern which will often occur in major surges. Both in the Beaufort and Chukchi Seas the sea level contours, away from the shore, tend to develop the dome-like structures. According to the geostrophic flow pattern the velocity vectors tend to be parallel to the sea level contour lines. Two domes in the sea level structure divide the flow into two large gyres - fig. 30 and fig. 31. The division line runs from Point Barrow to the North. Ice velocity in fig. 33 also displays a similar pattern of circulation. Obviously, because of the negligible wind speed in the Chukchi Sea, the ice motion is induced there only by the water motion. Due to the easterly flow along the southern-coast of the Beaufort Sea the boundary between the ice and ice-free area has moved further toward the east and the ice compactness continued to diminish along the shore - fig. 32.

The final set of figures describes the storm surge 3 days after the start of computation; The center of the low pressure is not moving any longer. It stayed for about 24 hours to the north of Banks Island, producing quite low winds in the Southern Beaufort Sea so that the sea level subsided to the mean sea level - fig. 34, fig. 40.

To observe the propagation of the storm surge along the coast of the Beaufort Sea the temporal variations of the sea level at a few geographical locations are given

in fig. 41 - fig. 46. Both cases, i.e. with an ice cover and without one, are plotted, therefore the influence of the ice on the surge can be defined. Actually only at the peak of the surge is the difference noticeable. The largest difference at Barrow West (fig. 41) amounts to about 20-25 cm. The level at Barrow and at two other points, one in the Chukchi Sea (Barrow West) and another in the Beaufort Sea (Barrow East) each situated at distance of about 40 km from Barrow, is plotted in fig. 41, 42, 43. At the time when at Barrow West the sea level rose up to 3m, at Barrow East the level was close to the mean sea level. The sea level difference between these two points is obviously due to the special location of Barrow which is situated between two sea basins. In some other locations along the Beaufort Sea coast the computed maximum sea level was: 80 cm at Simpson Cove (fig. 44) and 50 cm at Demarcation Bay (fig. 45). The largest surge of about 2 m occurred on October 5, 00Z (fig. 46) at Tuktoyaktuk; this figure compares well with actual observations.

An example of the temporal variations of the wind velocity during 3 days of computations at the point $\lambda = 135^{\circ} 30' W$, $\phi = 70^{\circ} 30' N$ is given in fig. 47. As we mentioned before, velocity is linearly interpolated between 6-hr intervals.

9* Negative surges - open water season 1979

During the open water season of 1979 from May to November a tide gauge was deployed by OCSEAP in Harrison Bay. Due to ice conditions, the three tide gauges in Canada were not in operation during major storm. The storm surges occurred only in September and October and all major surges were negative. We shall reproduce two surges; a smaller one between September 12 and September 19 when sea level dropped about 30 cm and a negative surge of about 50 cm from September 26 to October 7. The latter storm we shall describe in detail. The storm started on September 26 and was due to an atmospheric high pressure system with the center situated between Point Barrow and the North Pole. The surface pressure

distribution over the Arctic Ocean during the storm surge **is** represented **by** the weather chart from Oct. 4, **1979**, 12Z (fig. 48) - Thorndike and Colony (1980). This is a typical weather situation which generates patterns of ice and surface water motion often observed through the ice drift and is responsible for the so-called Beaufort **Gyre**. The pressure systems during the storm of 1979 for about 10 days occupied nearly the same position. Basing on **geostrophical** wind computation E and NE winds from 7 m/s to 15 m/s, were found. Atmospheric pressure data used in calculation were stored at 3-hr intervals **on magnetic tape by Thorndike and Colony** (1980). Temporal variation of the wind speed (fig. 49) in Harrison **Bay has a time dependence** which is similar to the sea **level** variations (fig. 50). Measured sea level (continuous line) compares well with computed *values* (*broken line*), although due to **the M₂** constituent the recorded level is more **variable**. *In fig. 50* the results of computations for both surges are plotted but we will only examine sea level, current and ice motion associated with major surge. As before, **two** sets of experiments were run, i.e., with and without an ice cover. To describe the wind influence on the ice distribution we abandon the ice compactness charts **and** only plot the position of the ice edge at the start and **end of the storm as** observed by satellite. The ice edge **position on** October 7 computed by the model is also plotted in the same figure (fig. **51**). Both computed and observed positions of the ice edge along the Siberian coast show its movement towards the East. Initially ice cover along the Beaufort coast was negligible but the E and NE **wind piled** pack ice against the shore. It is obvious from the buoys drift (fig. 48) that the ice velocity beyond our domain had a strong southerly component along the Canadian islands toward the Beaufort Sea. **To introduce this component into the numerical model the ice velocity from the buoys was applied at the open boundary.** The storm surge computation spanned **12 days from 00Z, September 25 till 00Z October 7. Four sets of figures are**

given to represent the development of the storm surge after 12 hours, 4 days, 8 days **and 12** days (fig. 52- fig. 67).

As we have seen previously, the results for the ice-free and ice-covered sea **are very close, therefore we shall describe** only the ice-covered situation. Both the **Chukchi** and Beaufort Seas were practically ice free (fig. 51); a situation conducive to storm surge generation. For the period 26 September to 7 October the wind direction was practically constant, thus the flow and sea level pattern after a few days was quasi-steady. Throughout the whole period both current and sea **level** show consistent distribution related to the wind. Strong currents and sea level variations again occurred in the shallow coastal area. After about 3-4 days, along the shelf from Mackenzie Bay to Point Barrow a current, somewhat reminiscent of a "coastal jet" (**Csanady, 1974**) develops. In the vicinity of Barrow, due to the shape of the shore-line and probably due to the depth difference between the Beaufort and **Chukchi** Seas, the coastal *current* partly branches off into open **water and partly follows the coastal contour into the Chukchi Sea. This division line again splits the motion** into two **gyres** which are closely associated with the dome structure of **the sea level**. **Because** the direction **of** the current in the gyres is correlated to the sea **level** distribution it is obvious that only in the **initial** period of the wind action the current at the sea surface can be associated with the wind; after the initial period the sea level variations can change conspicuously the dynamics of the flow.

10. Storm surge, August 30 - September, 1981

At the end of August 1981 a low pressure center moved southward along the Canadian Islands from the high latitude region. For 2-3 days the low maintained strong **NW winds over the western Beaufort Sea** (fig. 68). According to the **Beaufort Weather and Ice Office (1981)** it was the second longest storm of the season with wind speeds up to 40 knots. **While the Western and Central Beaufort Sea**

were under the influence of the strong low, the winds over the **Chukchi** and Eastern Beaufort Sea were due to a shallow high with its center over Siberia.

In August and September, 1981, some 11 gauges were installed along the Beaufort coast both in the United States and Canada. A positive surge of about 60 cm was recorded in the Canadian Beaufort Sea, further westward the surge was mixed, it was negative at the beginning and changed to positive when winds changed their direction to **NW**. The storm occurred between August 30 and September 1, 1981, only, but to study the whole process we extended the computation for **10** days, from August 27, **00Z** to September 6, 00Z. Again, to compute the temporal and spatial distribution of the wind, the data compiled by **Thorndike** et al. (1982) were used; unfortunately the atmospheric pressure was stored for 12-hour intervals only. For comparison with computed sea levels the eight tide gauges along the **Beaufort** coast were used (fig. 69). The measured levels compare well with computed sea level, with the ice included into the model or with an ice-free surface (fig. 70- fig. 77). During the peak of the surge, in four cases the observed level exceeds the computed level, in four other cases the reverse situation occurred. Surge maximum was observed on 30, 31 August and October 1; i.e. on day 4, 5, 6 from the start of computation. Needless to say, the sea level is "repeating" the temporal variation of the wind speed (fig. 78). At the peak of the storm between August 30 and October 1 both sea level and wind show two maxima and the minimum occurred on August 31. We were unable to resolve very accurately this feature due to the long time intervals (12-hour) between consecutive wind computation. The low temporal resolution of the wind is also possibly associated with the time difference (up to 12 hours) between calculated and recorded sea level. We shall not discuss the ice motion and ice compactness during this storm because ice conditions did not change distinctly from the initial distribution (fig. 79).

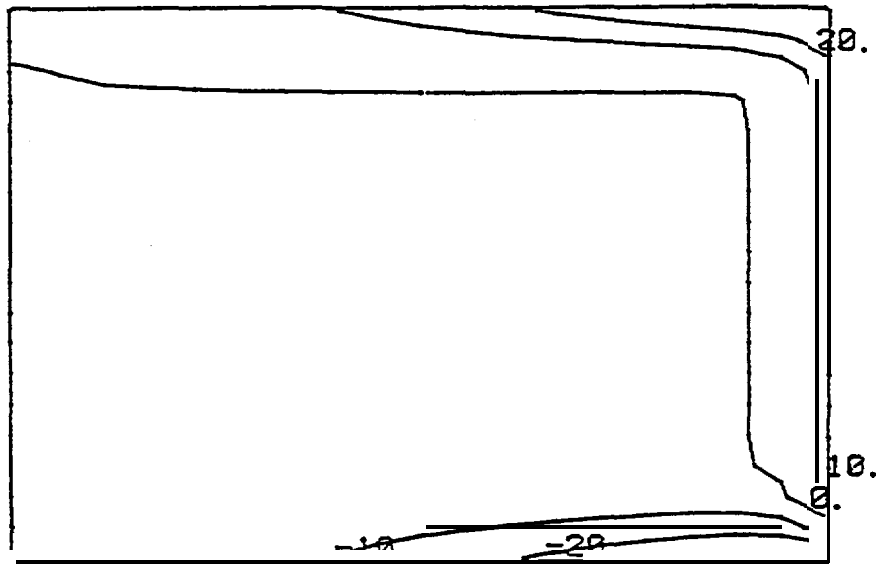
At the peak of the storm the patterns of the wind, sea level and velocity are plotted in fig. 80, fig. 81, fig. 82. It is interesting to observe again the dome structure in the sea level chart. With negative values at the center of the dome in the Beaufort Sea and positive values in the **Chukchi** Sea, the associated **gyres** display counter-clockwise motion in the Beaufort Sea and clockwise motion in the **Chukchi** Sea. As we found from the previous computation usually two **gyres** are generated, but the rotation in the **gyres** will depend on the type of pressure center (low or **high**), **geographical position of the center and its direction of travel.**

REFERENCES

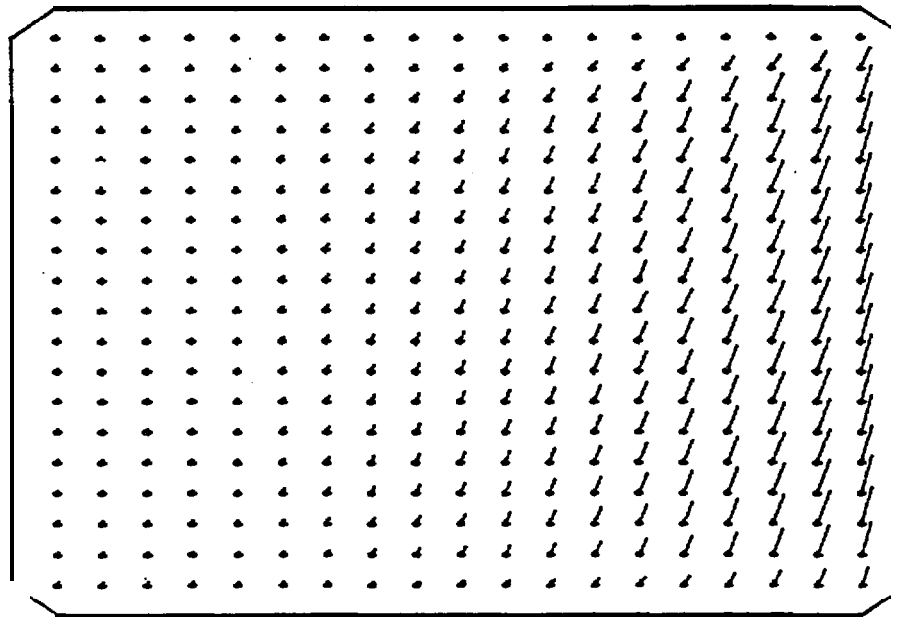
- Albright, M.**, 1980. **Geostrophic** wind calculations for **AIDJEX**. Sea Ice Processes and Models, Ed. by R. S. Pritchard, Univ. of Washington Press, Seattle and London, 474 pp.
- Barber, F. G., Taylor, J. D., **Bolduc, P. A., Murty, T. S.**, 1983. Influence of the ice cover on resonance phenomena in Tuktoyaktuk **Harbour, Proc. of 34th Alaska Science Conference, Whitehorse, CANADA.**
- Beaufort Weather and Ice Office 1981 Report. Atmospheric Environment Service, Western **Region, Arctic Weather Center**, 172 p.
- Campbell, W. J., 1965. The wind-driven circulation of ice **and water** in a Polar Ocean. Journ. **Geoph. Research.** 70, 14, pp. 3279-3301.
- Csanady, T. T.**, 1974. **Barotropic** currents over the continental shelf. Journ. **Phys. Ocean.** 4, 3, p. 357-371.
- Coon, M. D., Maykut, G. A., Pritchard, R. S., Rothrock, D. A., and Thorndike, A. S., 1974. Modeling the pack ice as an elastic-plastic material. **AIDJEX Bulletin**, 24pp. 1-105.
- Doronin, Yu. D.**, 1970. On the method of calculate compactness and drift ice. Trudy Arctic-Antarctic Inst., Leningrad, 291, 5-17.
- Fathauer, T. F.**, 1978. A forecast procedure for coastal floods in Alaska, NOAA technical memorandum **NWS AR-23**, 27 p.
- Garrat, J. R.**, 1977. Review of drag coefficients over oceans and continents. Month. **Weath. Rev.** 7, 105, pp. 915-929.
- Glen, J. W.**, 1970. Thoughts on a viscous model for sea ice. **AIDJEX Bulletin**, 2, pp. 18-27.
- Hansen, **W.**, 1962. **Hydrodynamical** methods applied to the oceanographical problems. **Proc. Symp. Math.-Hydrodyn. Meth.** Phys. Oceanography. Mitt. Inst. **Meeresk.**, Univ. Hamburg, 1, pp. 25-34.
- Henry, R. F., 1974. Storm surges in the Southern **Beaufort** Sea. Interim Report, Dec. 1974, Beaufort Sea Project, Institute of Ocean Sciences, Patricia Bay, Sidney, B. C., Canada, 14p.
- Henry, R. F., 1975. Storm surges. Beaufort Sea Technical Report #19. Institute of Ocean Sciences, Sidney, B. C., Canada, 41 p.
- Henry, R. F., and N. S. Heaps, 1976. Storm surge in the southern Beaufort Sea. **Journ. Fisher Res. Board of Canada** 33(10), **2362-2376.**
- Hibler III, W. D.**, 1979. **A dynamic-thermodynamic** sea ice model. **J. Phys. Oceanogr.**, 9, pp. 815-846.

- Huggett, W. S., Woodward, M. J., Stephenson, F., Hermiston, F. V., Douglas, A., 1975. Near bottom currents and offshore tides. Beaufort Sea Proj. Tech. Rept. #16, Inst. of Ocean Sciences, Sidney, B.C., Canada, 38 p.
- Hume, J. D., 1964. Shoreline changes near Barrow, Alaska, caused by the storm of October 3, 1963. Report of the 15th Alaskan Science Conference, Fairbanks.
- Hunkins, K. L., 1965. Tide and storm surge observations in the Chukchi Sea. *Limn. Oceanogr.* **10**, pp. 29-39.
- Johannessen, O. M., 1970. Note on some vertical current profiles below ice floes in the Gulf of St. Lawrence and near the North Pole, *J. Geoph. Res.* **75**, 2857-2862.
- Kagan, B. A., 1970. On the features of some finite-difference schemes used at numerical integration of tidal dynamics equations, *Izv. Atmospheric and Oceanic Physics*, **6**, **7**, pp. 704-717.
- Kheisin, D. E., 1971. On the excitation of ice compression forces at the hydrodynamic stage of drift of close ice pack. *Trudy ANII* v. 303, pp. 89-97.
- Kheisin, D. E., and Ivchenko, V. O., 1973. A numerical model of tidal ice drift with allowance for the interaction between floes. *Izv. Atmospheric and Oceanic Physics*, **9**, **4**, pp. 420-429.
- Komar, P. D., 1976. Boundary layer flow under steady unidirectional currents. In *Marine Sediment Transport and Environmental Management*. John Wiley and Sons Publ. Ed. O. J. Stanley and D. J. P. Swift., pp. 91-106.
- Kowalik, Z., 1981. A study of M_2 in the ice-covered Arctic Ocean. *Modeling, Identification and Control* v. 2. N. 4, 201-223.
- Kowalik, Z., Matthews, J. B., 1982. The M_2 tide in the Beaufort and Chukchi Seas. *Jour. Phys. Ocean.* **12**, **7**, pp. 743-746.
- Lamb, H., 1945. *Hydrodynamics*. New York. Dover Publ. 738 p.
- Langleben, M. P., 1982. Water drag coefficient of the first-year sea-ice. *Jour. Geophysical Research*. v. 87, **NC1**, 573-578.
- Leavitt, E., 1980. Surface-based air stress measurements made during AIDJEX. In *Proceedings of the AIDJEX Symposium*, Univ. of Washington Press, pp. 419-429.
- Ling, C. H., Rasmussen, L. A., and Campbell, W. J., 1980. A continuum sea ice model for a global climate model. In *Proceedings of the AIDJEX Symposium*, University of Washington Press, pp. 187-196.
- Marchuk, G., Gordev, R., Kagan, B., et al., 1972. Numerical method to solve tidal dynamics equation and results of its testing. *Novosibirsk: Comput. Centre.*, pp. 78.

- Matthews, J. B., 1971. Long period gravity waves and storm surges on the Arctic Ocean continental shelf. **Proc. Joint Oceanogr. Assembly, Tokyo**, p. 332.
- McPhee, M. G., 1980. An analysis of pack ice drift in summer. In Proceedings of the AIDJEX Symposium. **University of Washington Press**, pp. 62-75.
- Ovsienko, S. N., 1976. On the numerical modelling of the ice drift. **Izv. Atmospheric and Oceanic Physics**. T.12,N.11, pp. 1201-1206.
- Ovsienko, S. N., 1978. Numerical model of the ice drift due to the wind in Caspian Sea. Trudy Gi drometeorol ogiceskogo Naucno-Issl edov. **Centra SSSR**, "Leningrad, 194, p. 53-58.
- Pritchard, R. S. (editor), 1980. **Sea Ice Processes and Models. Proceedings of the AIDJEX Symposium**. University of Washington Press, pp. 474.
- Ramming, H. G., and Kowalik, Z., 1980. Numerical modelling of marine hydrodynamics. **ELSEVIER. Amsterdam - New York**, pp.148-154.
- Reid, R. O., and B. R. Bodine, 1968. Numerical model for storm surges in Galveston Bay. **J. Waterway and Harbour Div., 94 (HWI)**, p. 33-57.
- Reimnitz, F., and D. K. Maurer, 1979. Effect of storm surge on the Beaufort Sea coast, northern Alaska. **Arctic 32**, pp. 229-344.
- Rothrock, D. A., 1970. The kinematics and mechanical behaviour of pack ice: the state of subject. **AIDJEX Bulletin**, 2, pp. 1-10.
- Rothrock, D. A., 1975. The mechanical behaviour of pack ice. **Annual Review of Earth and Planetary Sciences**, 3, pp. 317-342.
- Schafer, D. J., 1966. Computation of a storm surge at Barrow, Alaska. **Archiv für Meteorologi c, Geophysik and Bioklimatologie**, Ser. A, 15, N. 3-4, pp. 372-393.
- Shirokov, K. P., 1977. Influence of compactness on the wind-driven ice drift. **Sbornik Rabot Leningradskoi CMO** 9, pp. 46-53.
- Thorndike, A. S., Colony, R., 1980. Arctic Ocean Buoy Program. **Data Report**. Polar Science Center, University of Washington, Seattle, 131 p.
- Thorndike, A. S., Colony, R., **Munöz**, E. A., 1982. Arctic Ocean Buoy Program Data Report. Polar Science Center, University of Washington, Seattle, 137 p.
- Wendler, G., 1973. Sea ice observation by means of satellite. **Journ. Geoph. Res.**, 78, 9, pp. 1427-1448.
- Wise, J. L., **Comiskey**, A. L., Becker, R. 1981. Storm surge climatology and forecasting in Alaska. Arctic Environment Information and Data Center, Anchorage. 26 p.

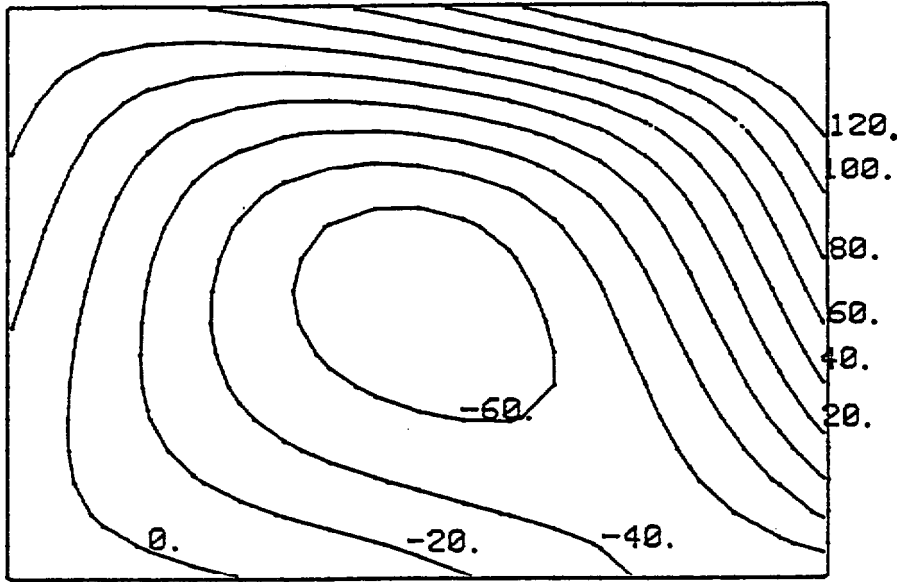


SEA LEVEL HOUR 2

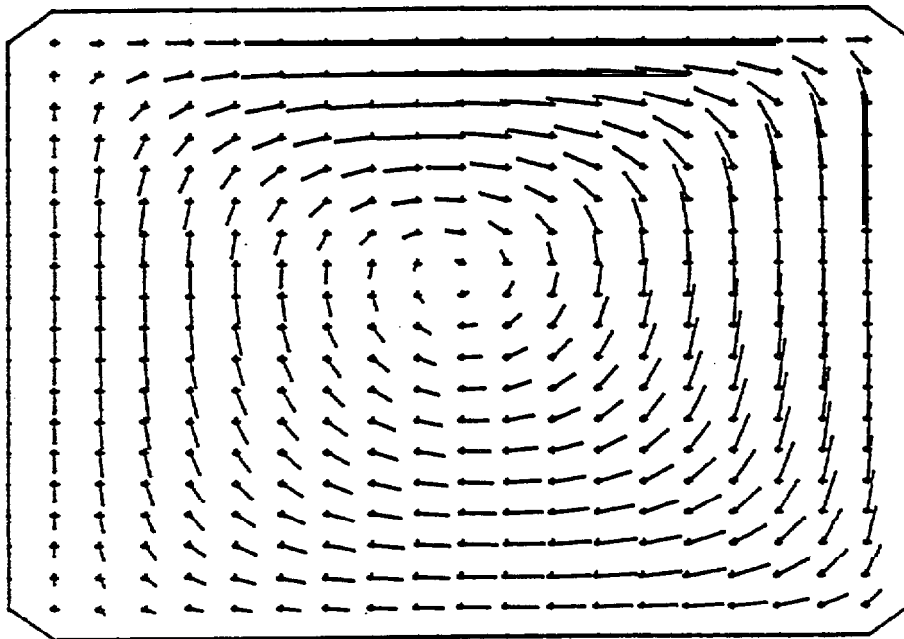


VELOCITY HOUR 2

Figure 1.—Windblows along the vertical coordinate only. Wind speed is constant in time but **varies** along the horizontal direction from 4 m/s (at $x_1 = 0$) to 20 m/s (at $x_1 = 1,000$ km). Sea level variation is expressed in centimeters. For velocity, the grid distance along the horizontal direction is scaled to 25 cm/s. In this experiment, velocity vectors are not identified by arrows; therefore, direction of the flow is away from the grid point. Ice compactness is measured in relative units from 0 to 1.

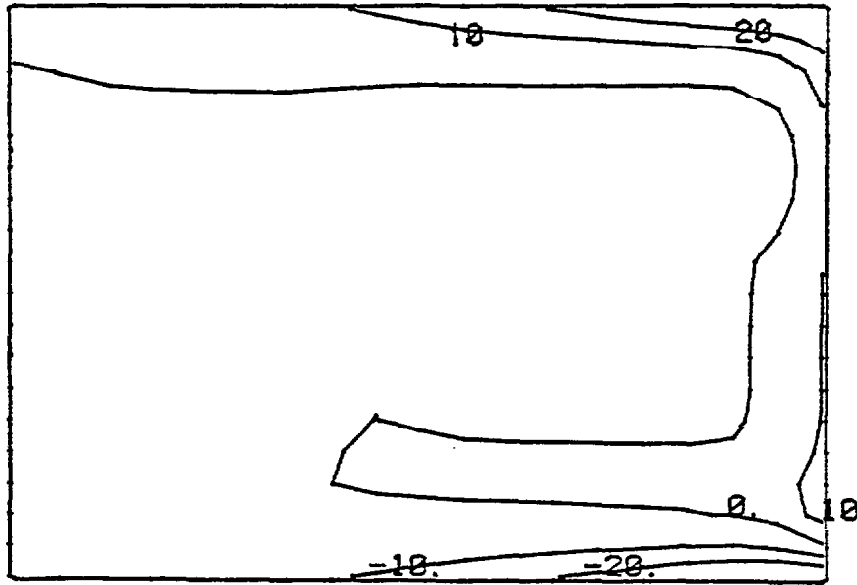


SEA LEVEL HOUR 90

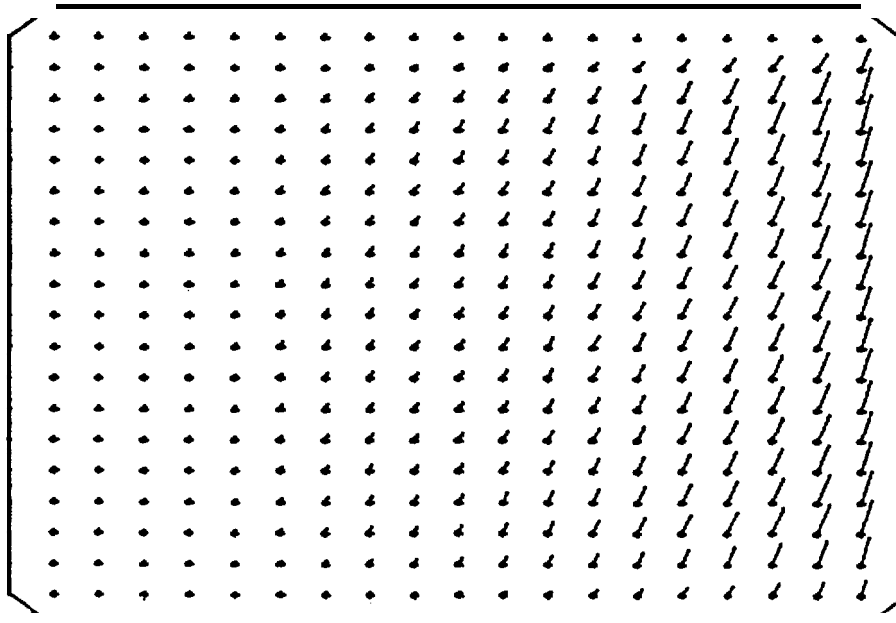


VELOCITY HOUR 90

Figure 2. --(See caption for Fig. 1.)

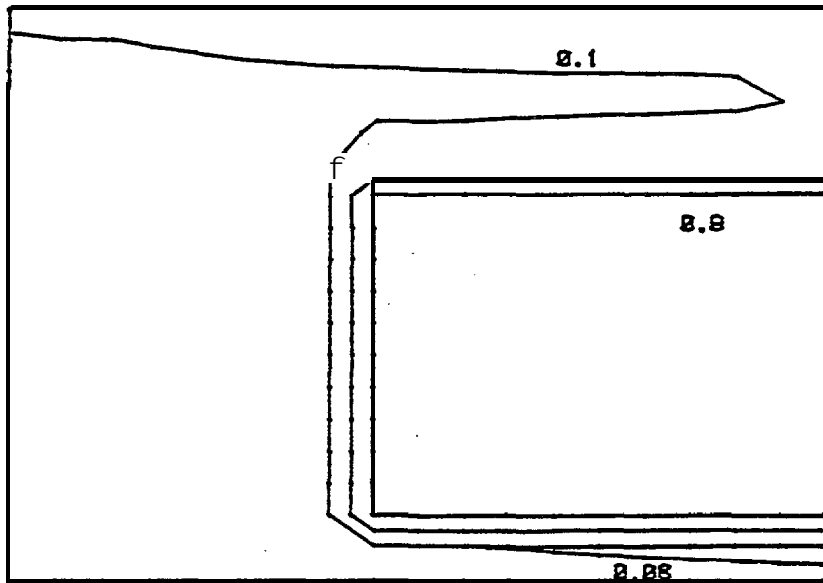


SEA LEVEL HOUR 2

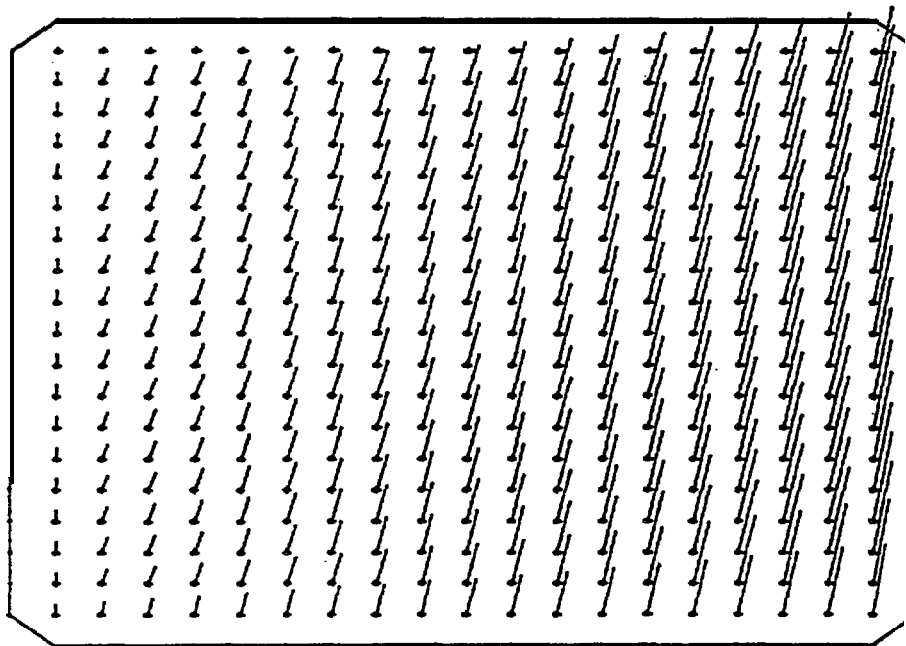


VELOCITY HOUR 2

Figure 3.--(See caption for Fig. 1.)

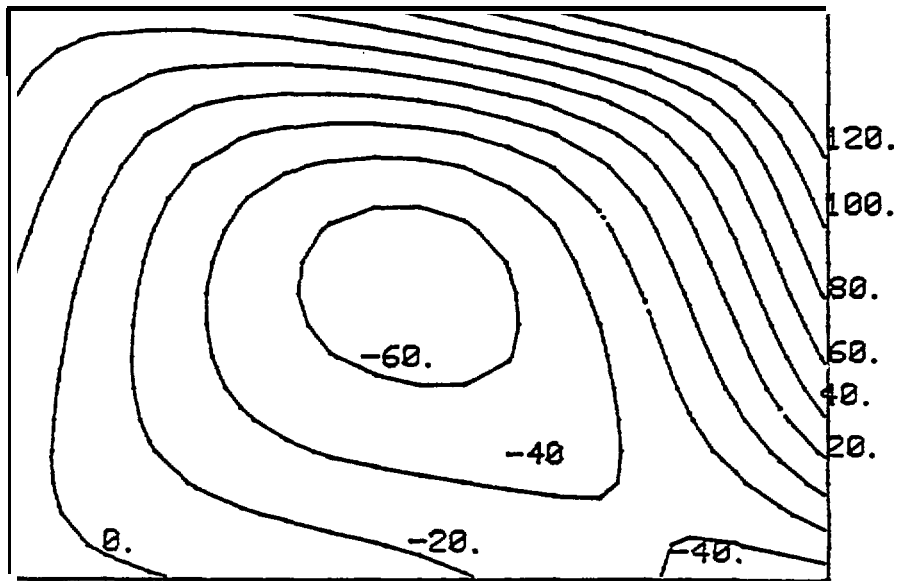


ICE COMPACTNESS HOUR 2

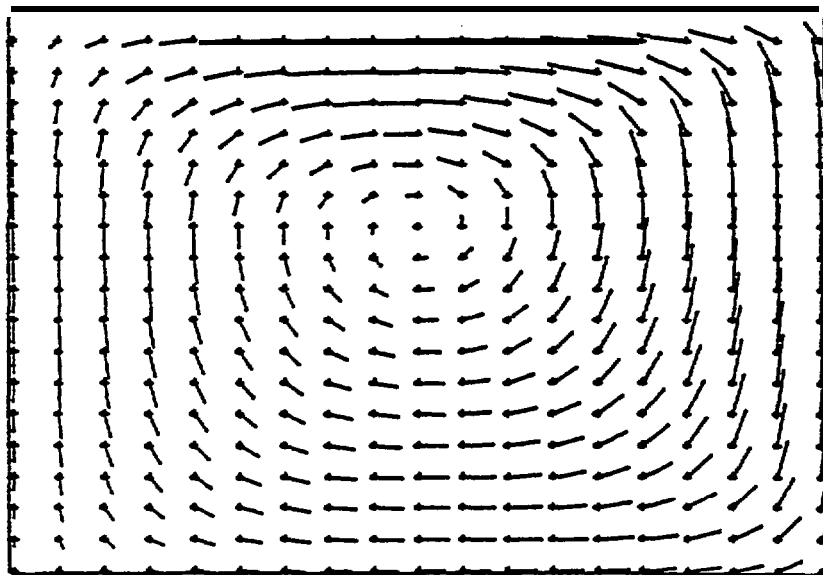


ICE VELOCITY HOUR 2

Figure 4.--(See caption for Fig. 1.)

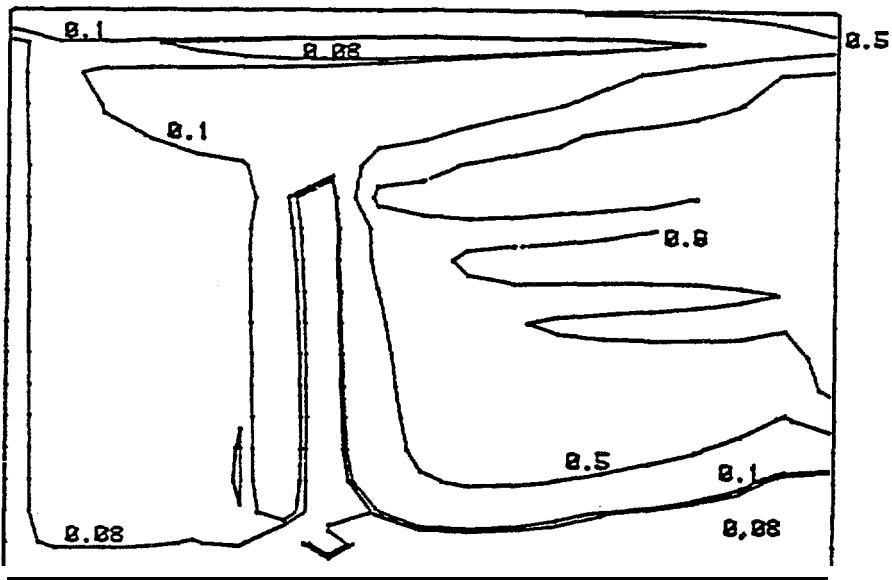


SEA LEVEL HOUR 90

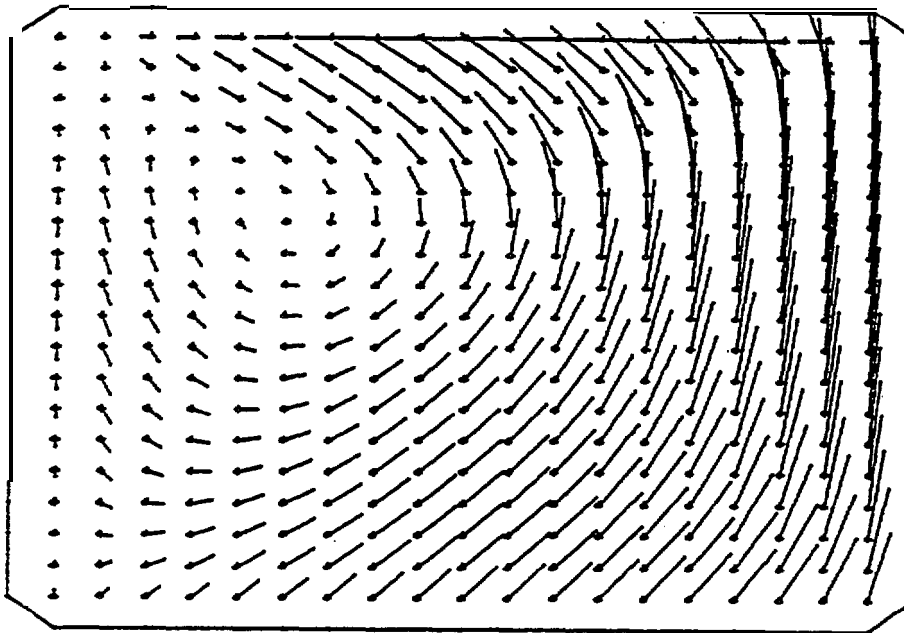


VELOCITY HOUR 90

Figure 5.--(See caption for Fig. 1.)



ICE COMPACTNESS HOUR 90



ICE VELOCITY HOUR 90

Figure 6. --(See caption for Fig. 1.)

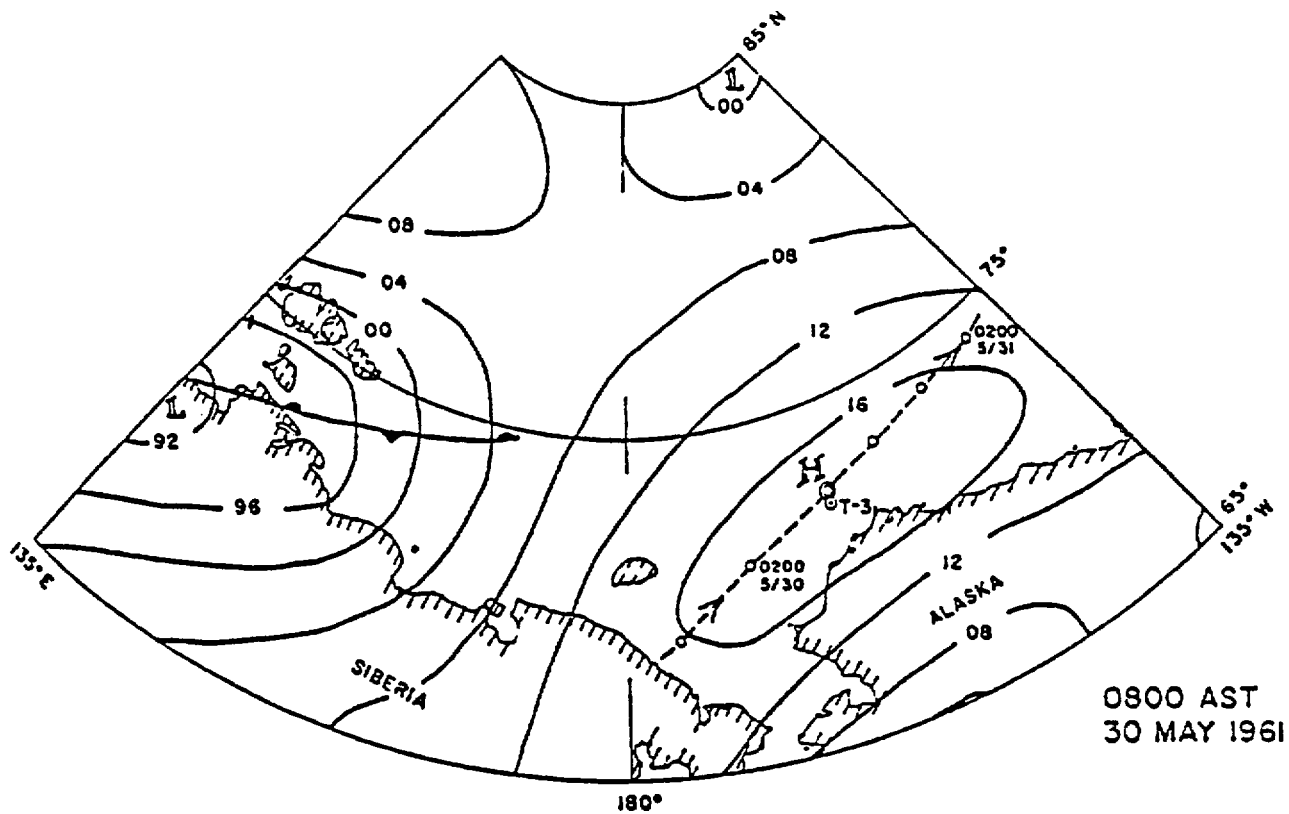


Figure 7. --Surface weather chart for 0800 AST, 30 May 1961, at approximately the time of the closest passage to T-3 of the high. Pressure in millibars. Dashed line represents the track of the high. Open circles represent positions of the **high**-pressure center at 6-h intervals. From Hunkins (1965).

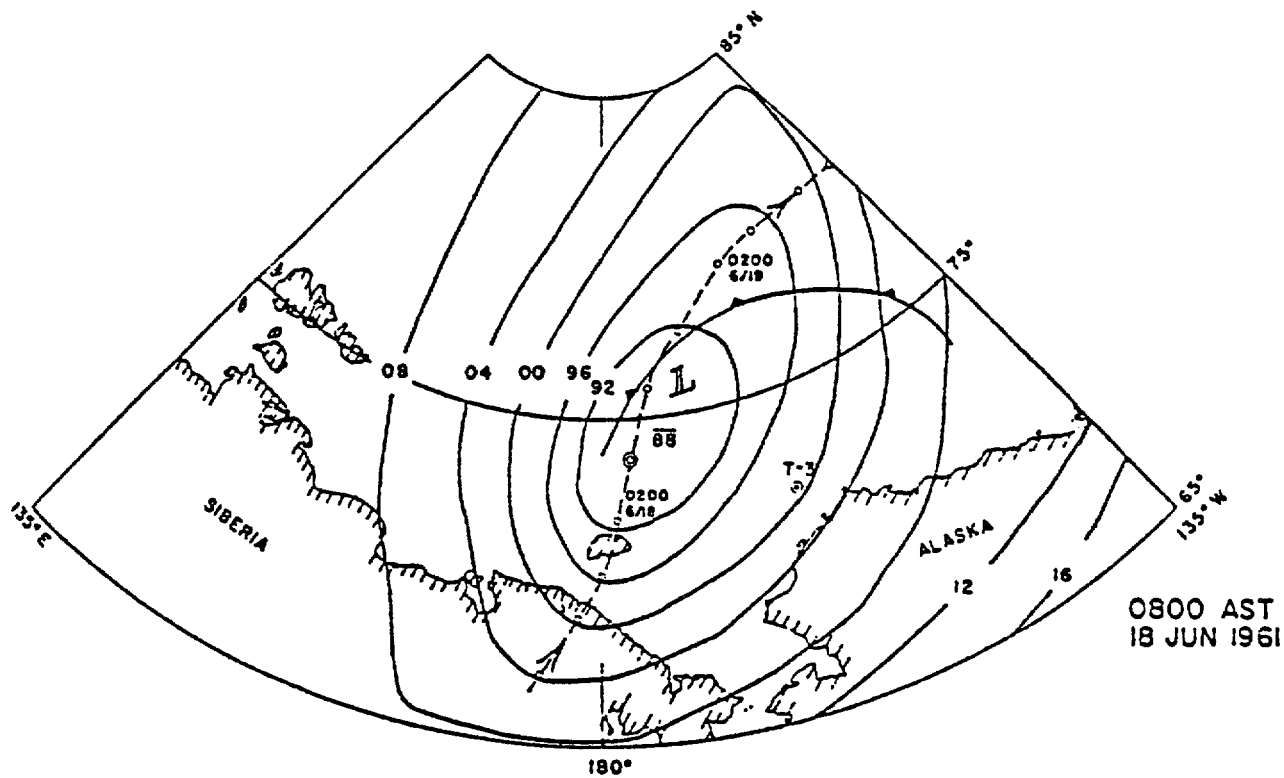


Figure 8. --Surface weather chart for 0800 AST, 18 June 1961. Pressure in millibars. Dashed line represents storm track. Open circles represent positions of the low-pressure system at 6-h intervals. From Hunkins (1965).

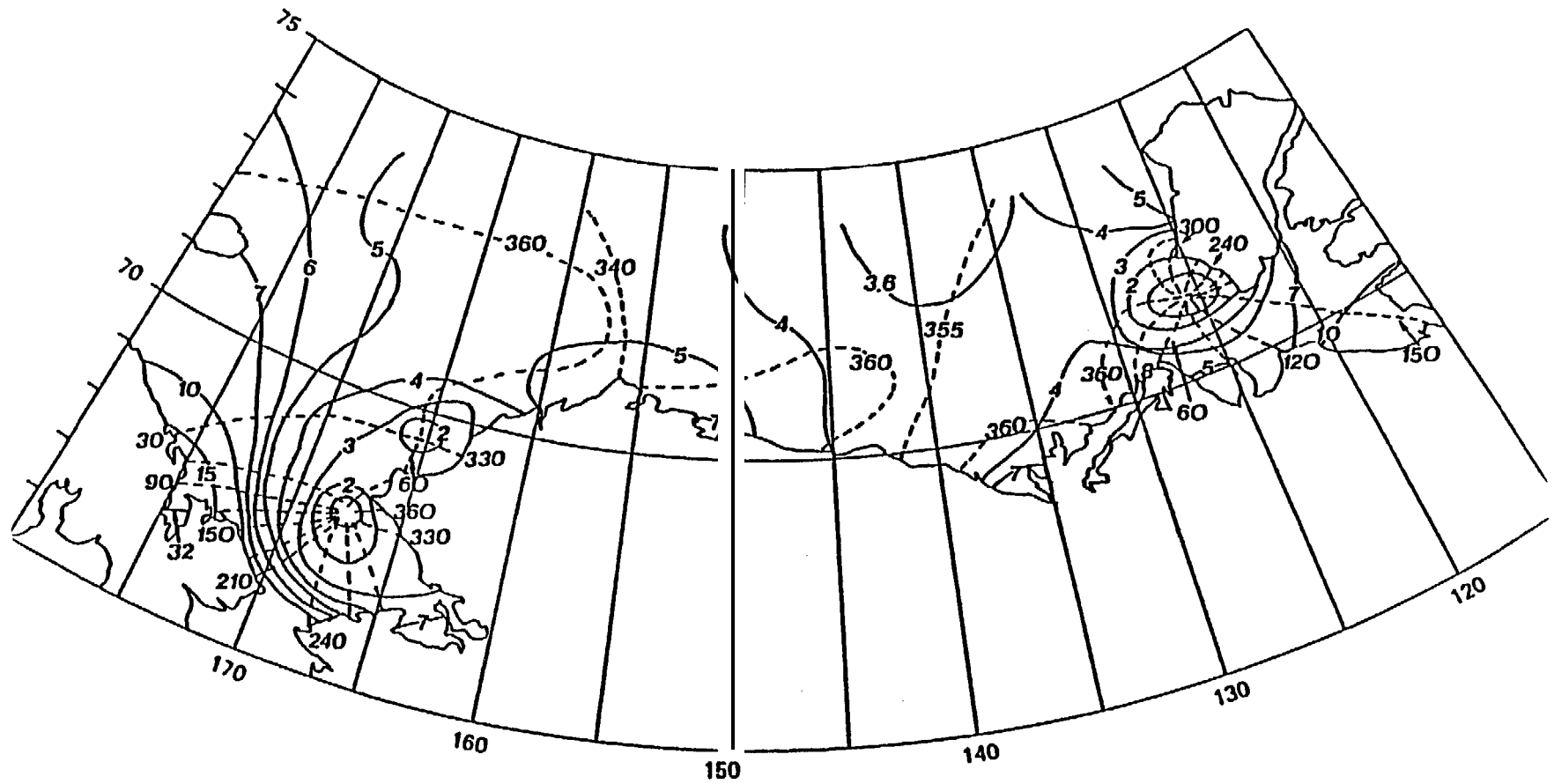


Figure 9. --Co-tidal (broken) and co-range (continuous) lines of the M_2 tide. Phase angles in degrees are referred to Greenwich (solar time); amplitudes are given in centimeters. From Kowalik and Matthews (1982).

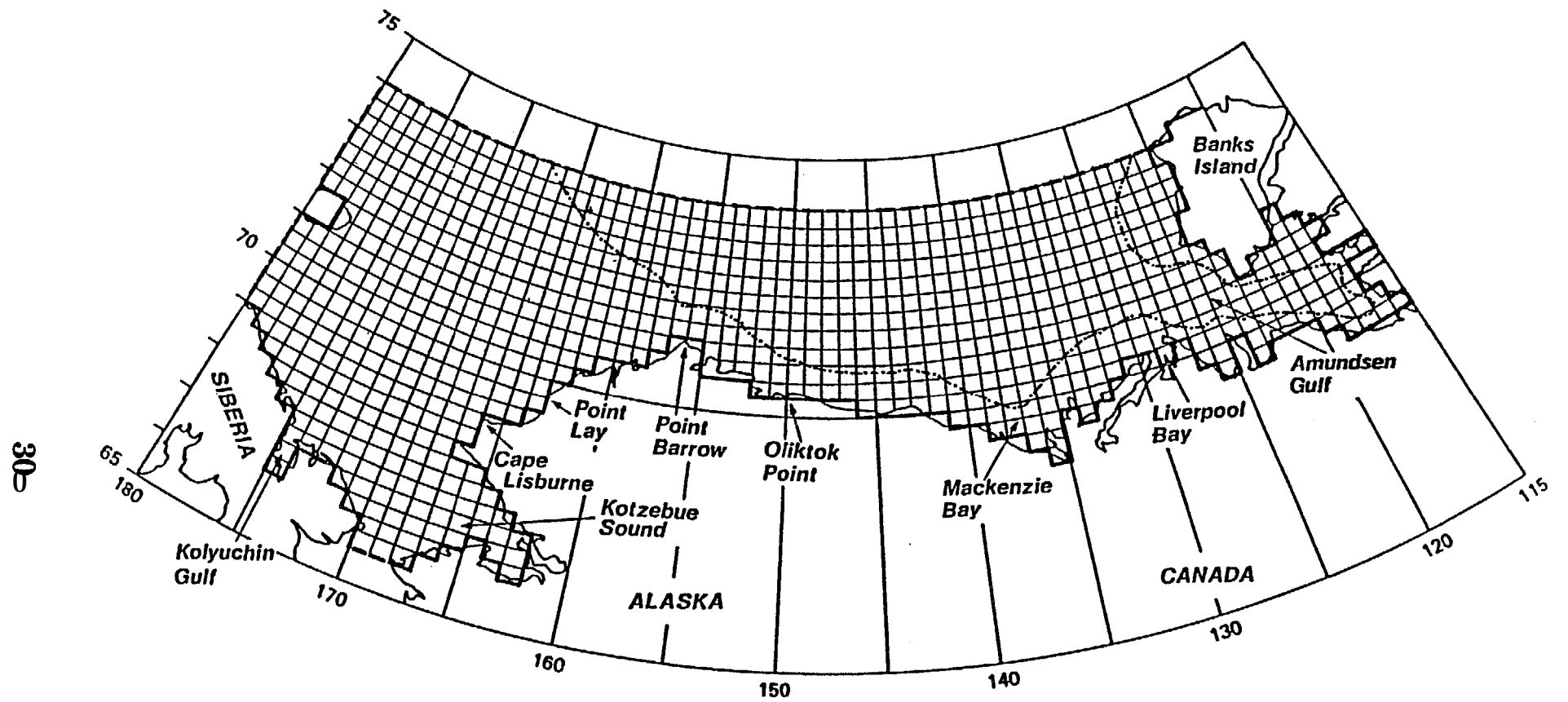


Figure 10. --Grid net for the numerical computation of the M_2 tide in the Beaufort and Chukchi seas. Dashed line represents open boundary, solid line is land boundary, dotted line is 200-m depth contour.

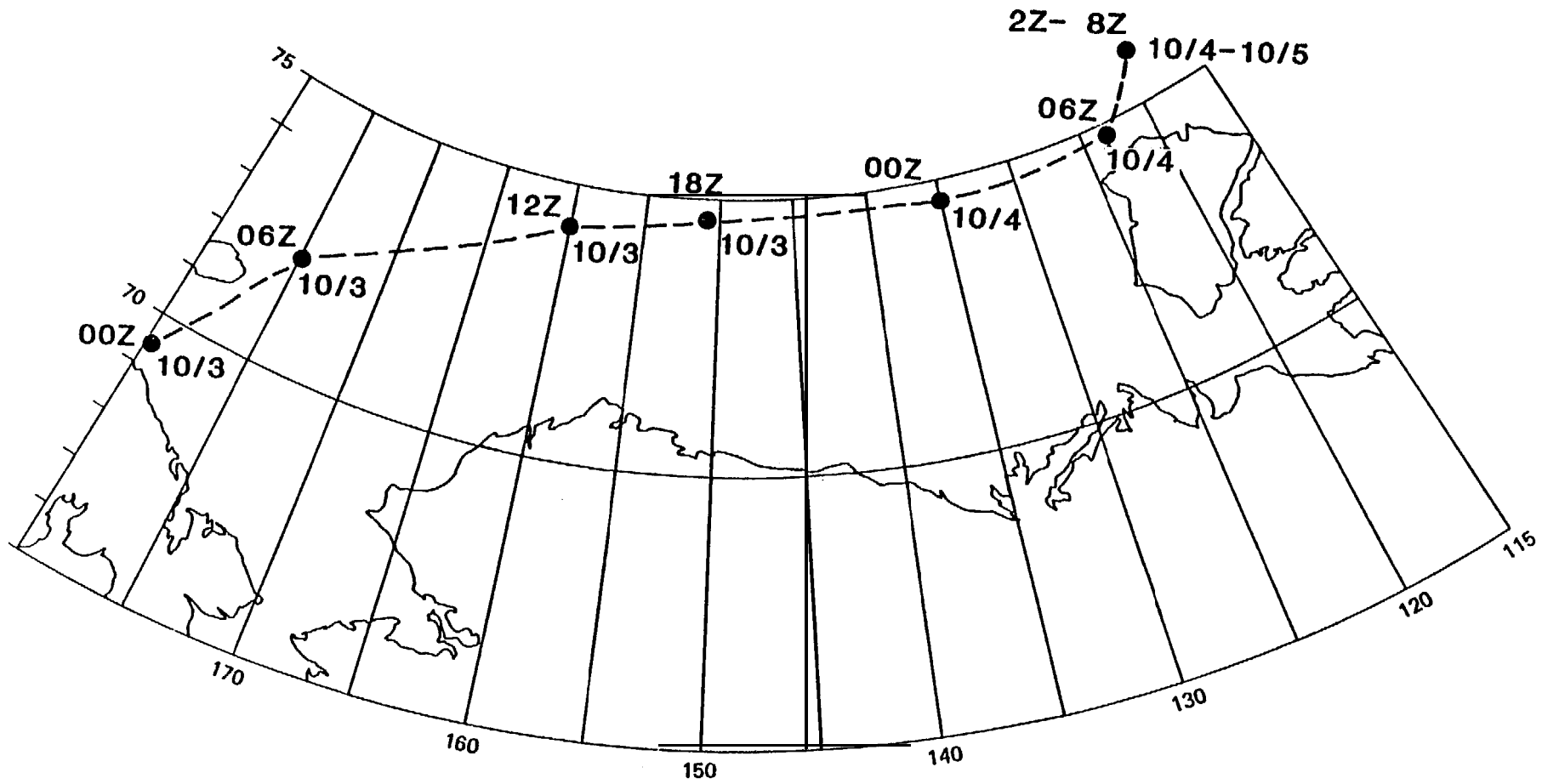


Figure 11.--Positions of the low pressure system from October 3, 00z, to October 5, 18z.

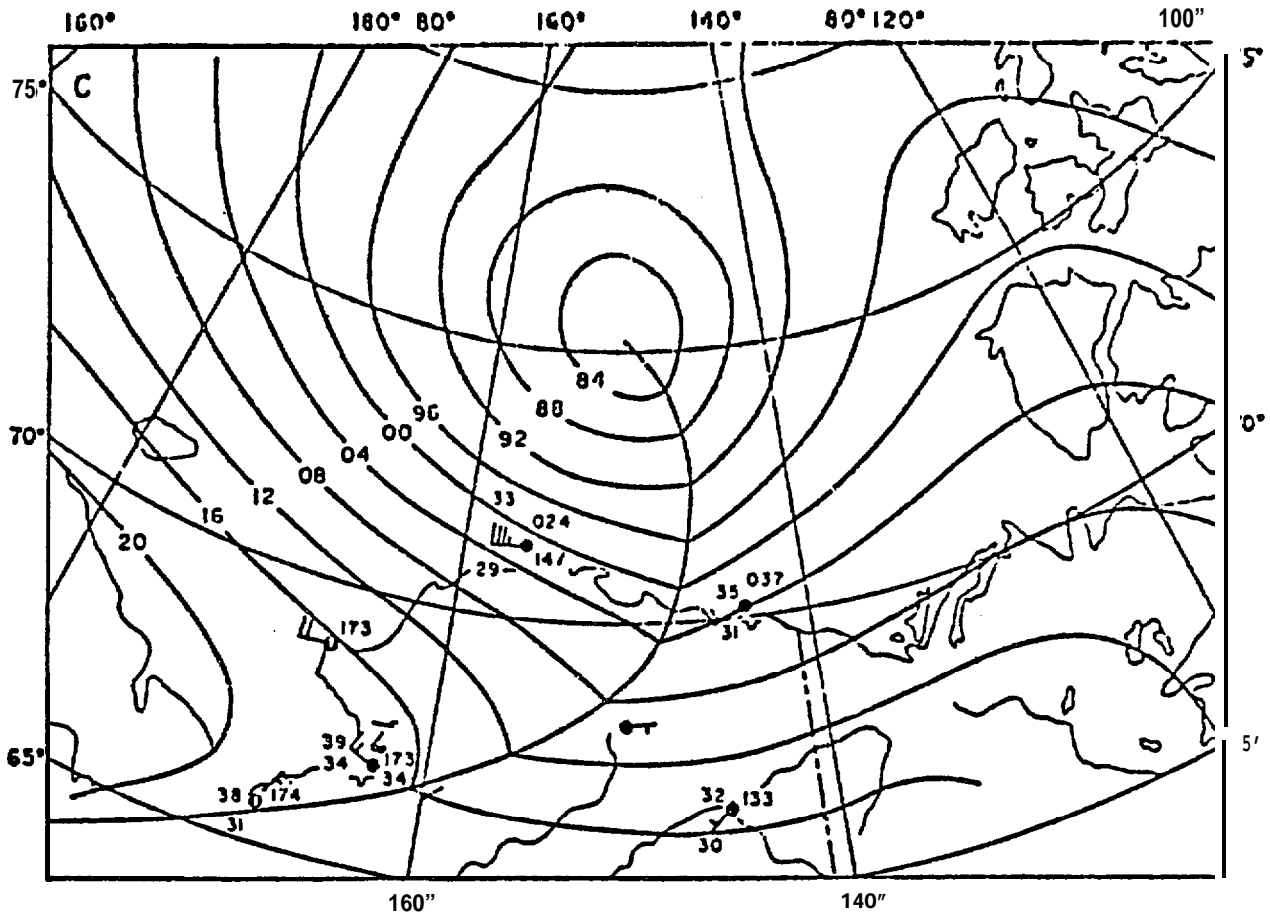


Figure 12. --Synoptic weather chart, 3 October 1963, 18Z. Pressure in millibars. From Schafer (1966).

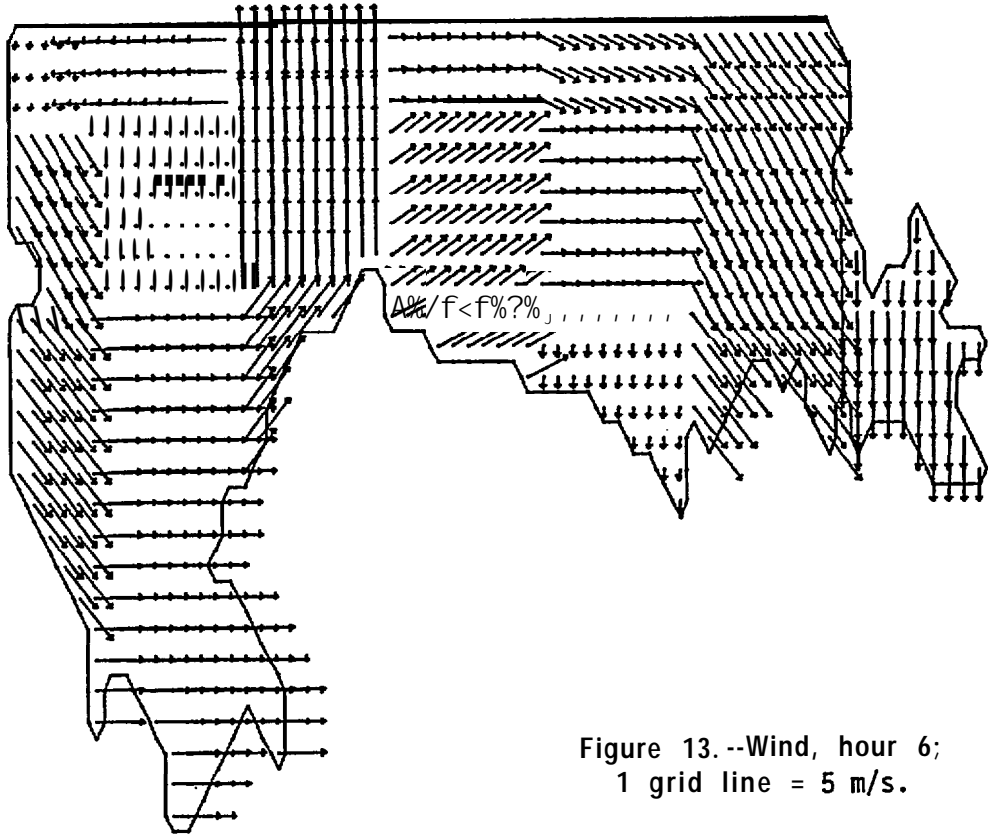


Figure 13.--Wind, hour 6;
1 grid line = 5 m/s.

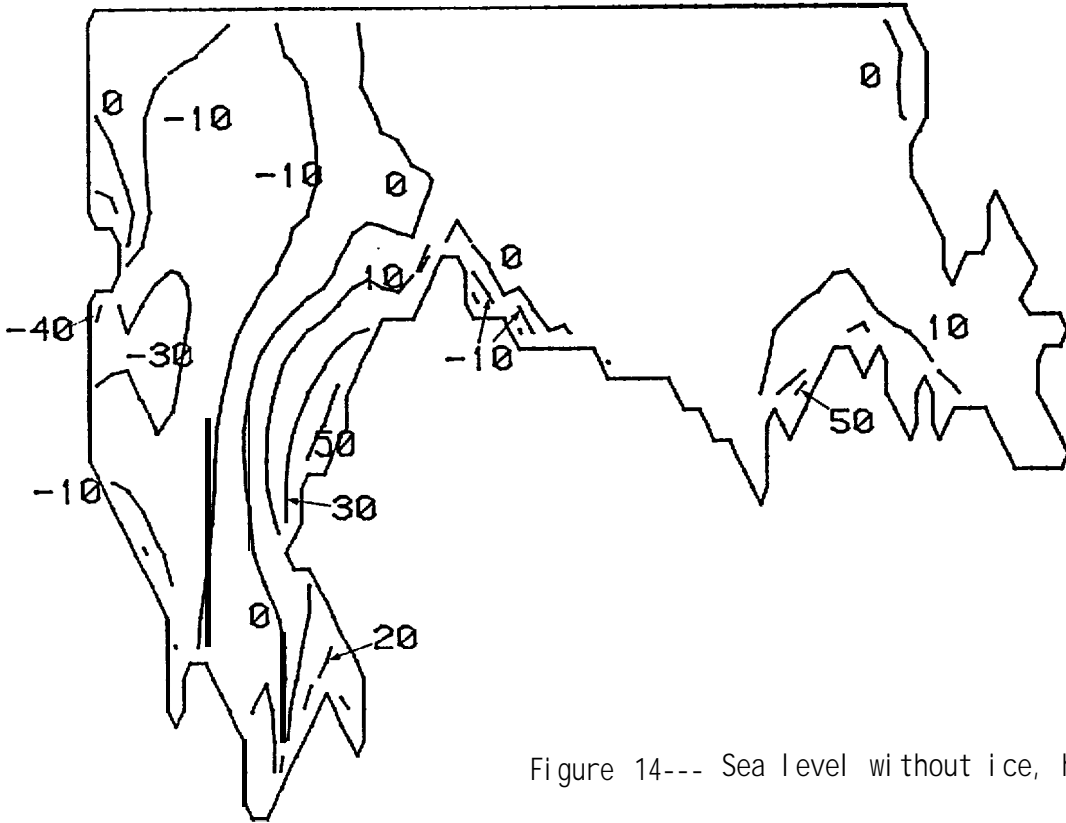


Figure 14--- Sea level without ice, hour 6.

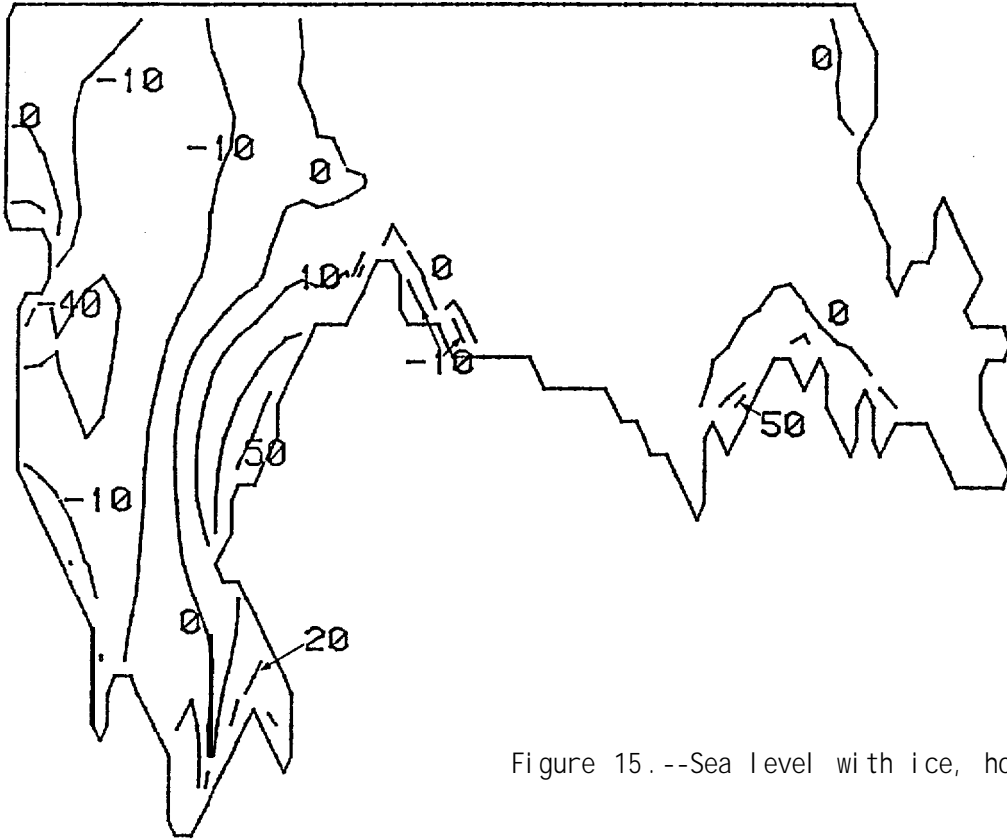


Figure 15.--Sea level with ice, hour 6.

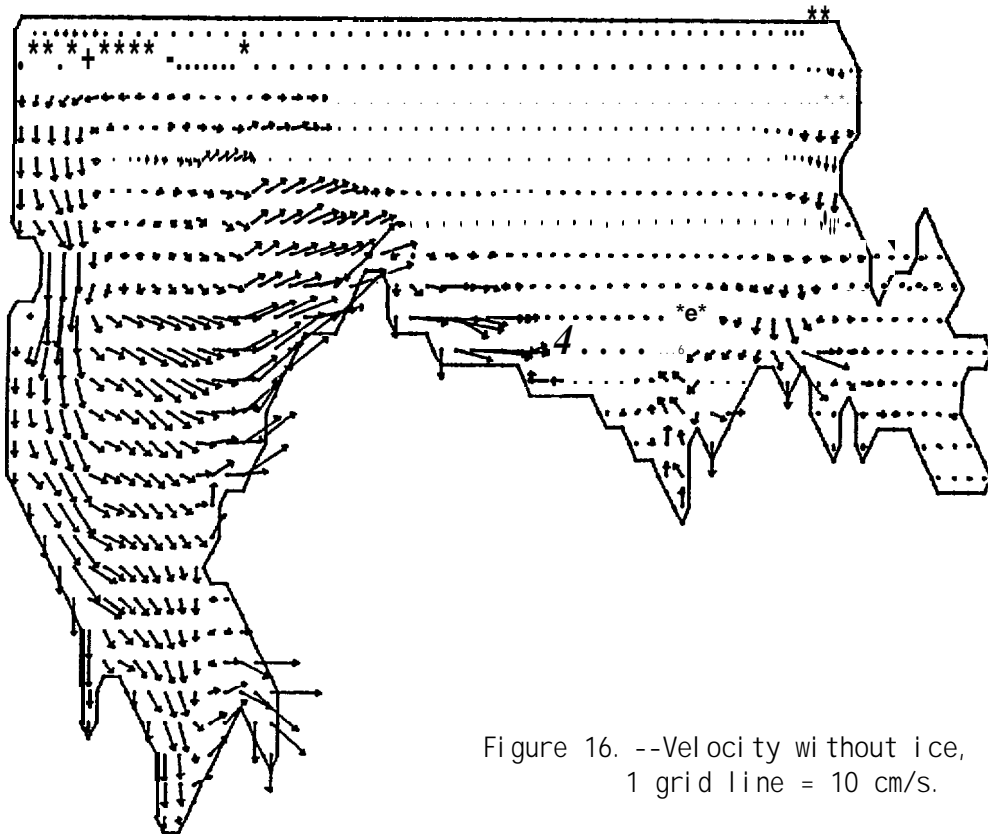


Figure 16.--Velocity without ice, hour 6;
1 grid line = 10 cm/s.

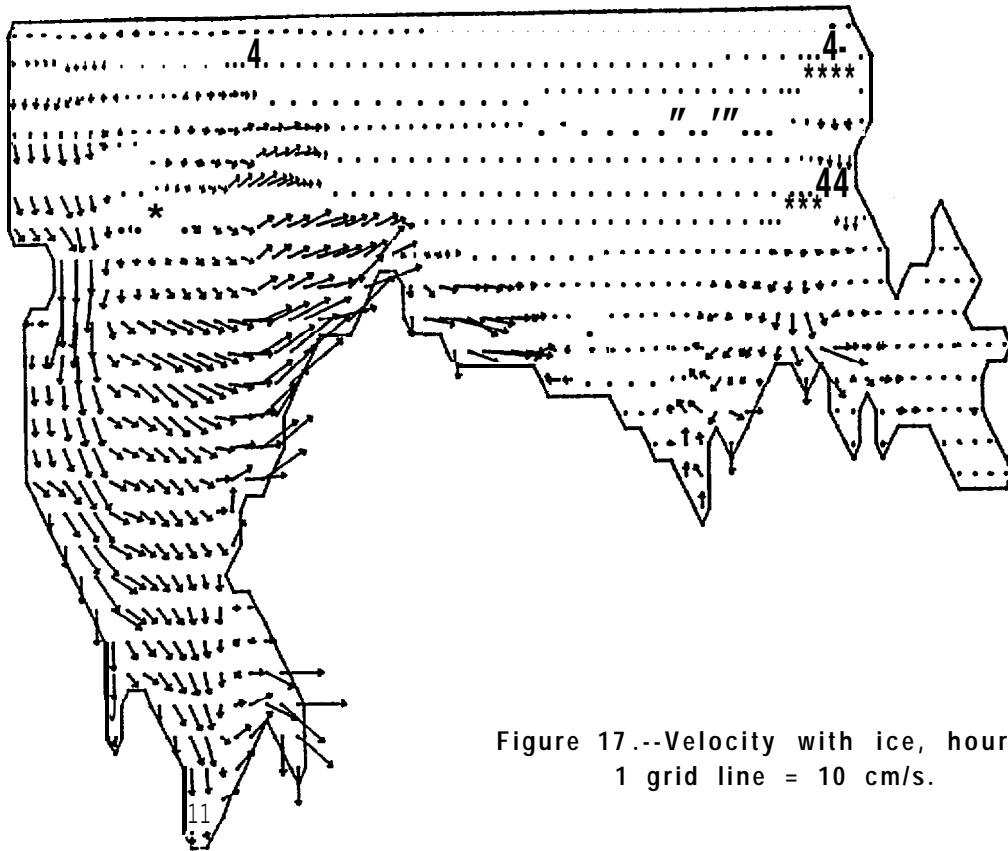


Figure 17.--Velocity with ice, hour 6;
1 grid line = 10 cm/s.

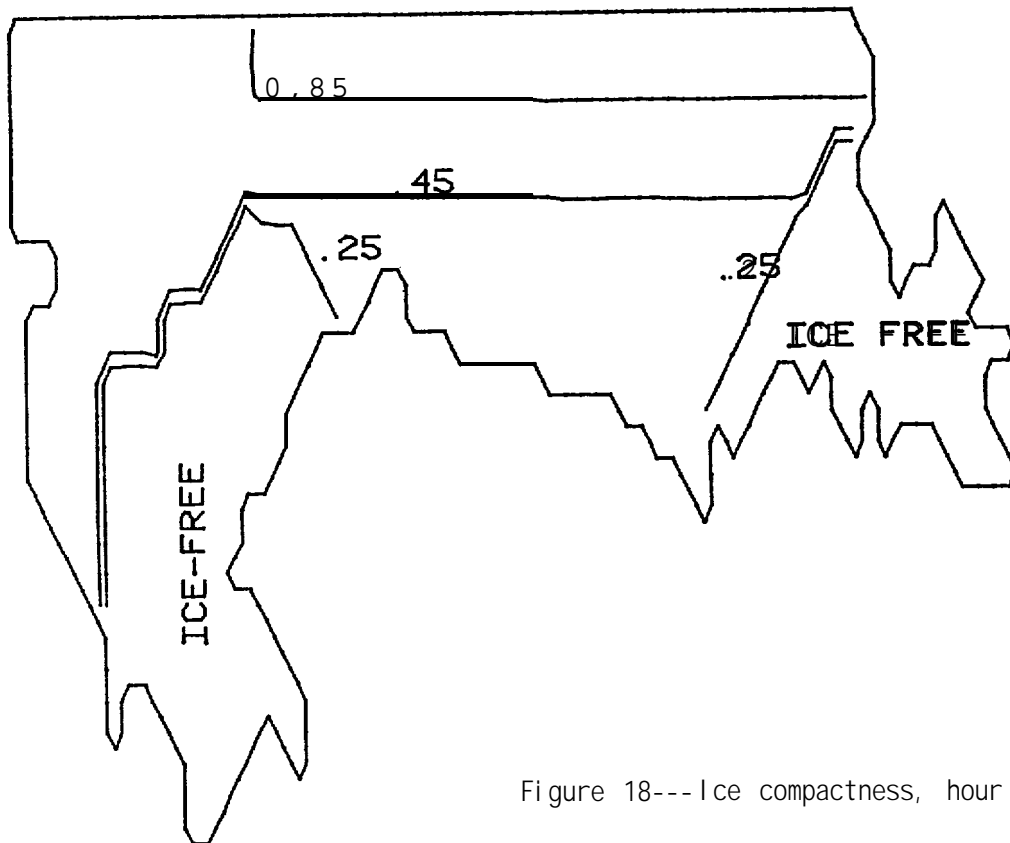


Figure 18---Ice compactness, hour 6.

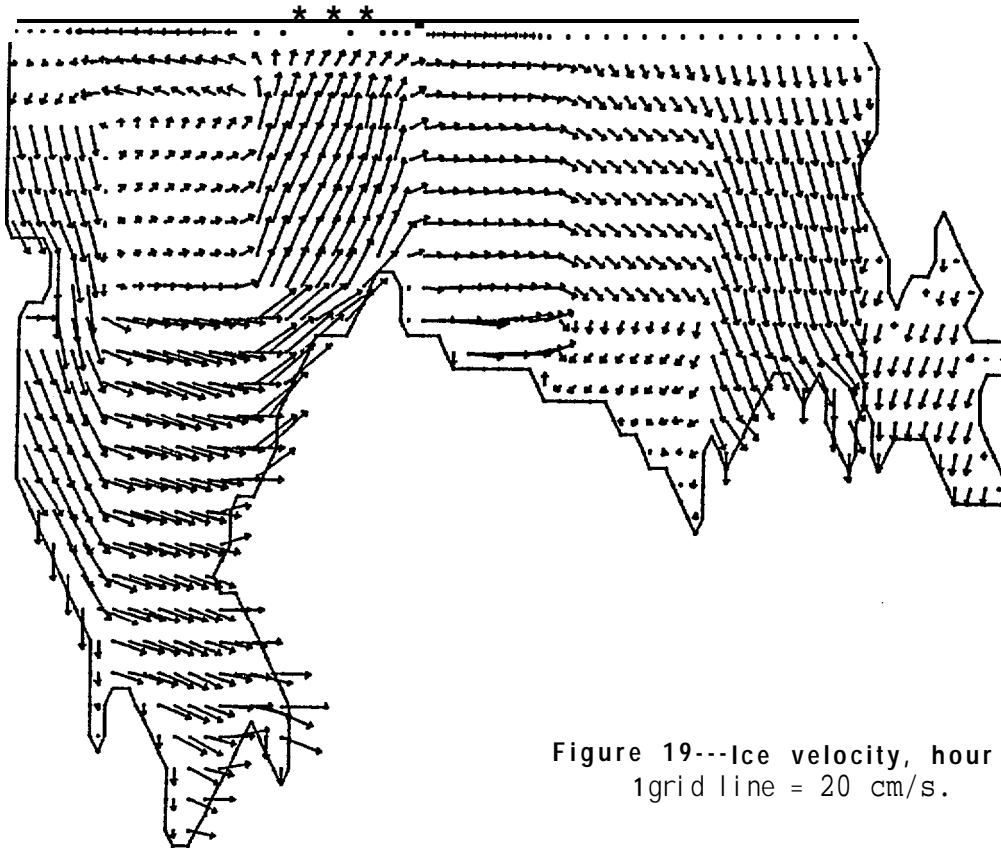


Figure 19---Ice velocity, hour 6;
1grid line = 20 cm/s.

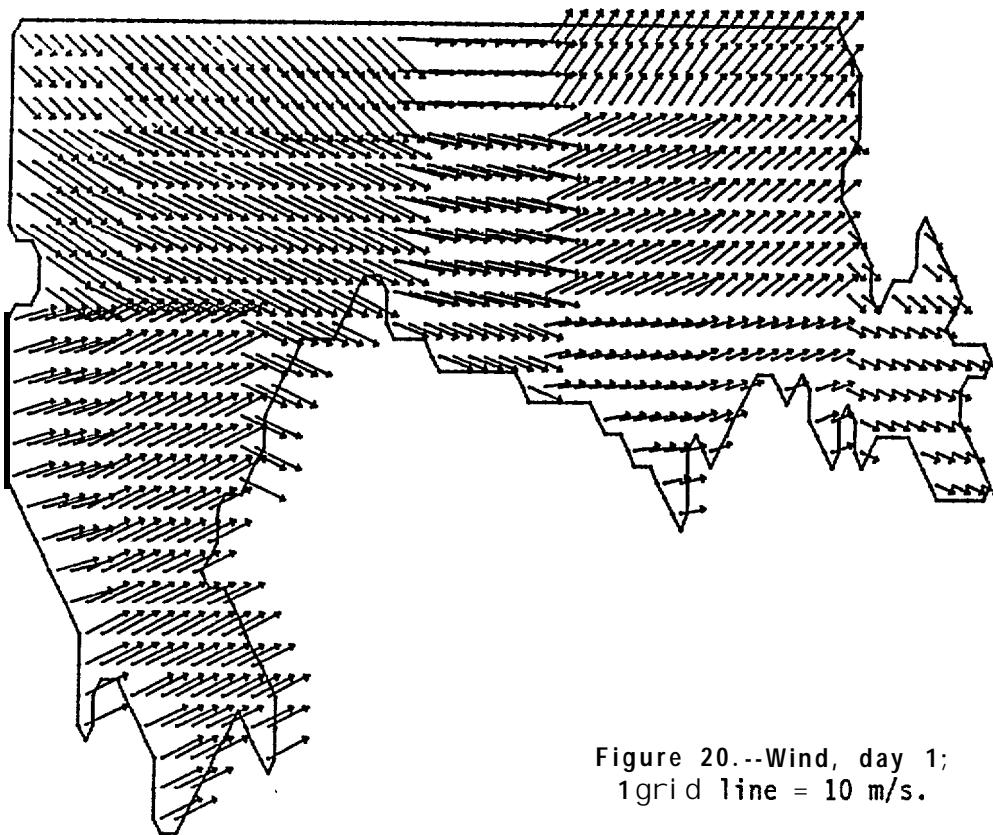


Figure 20.--Wind, day 1;
1grid line = 10 m/s.

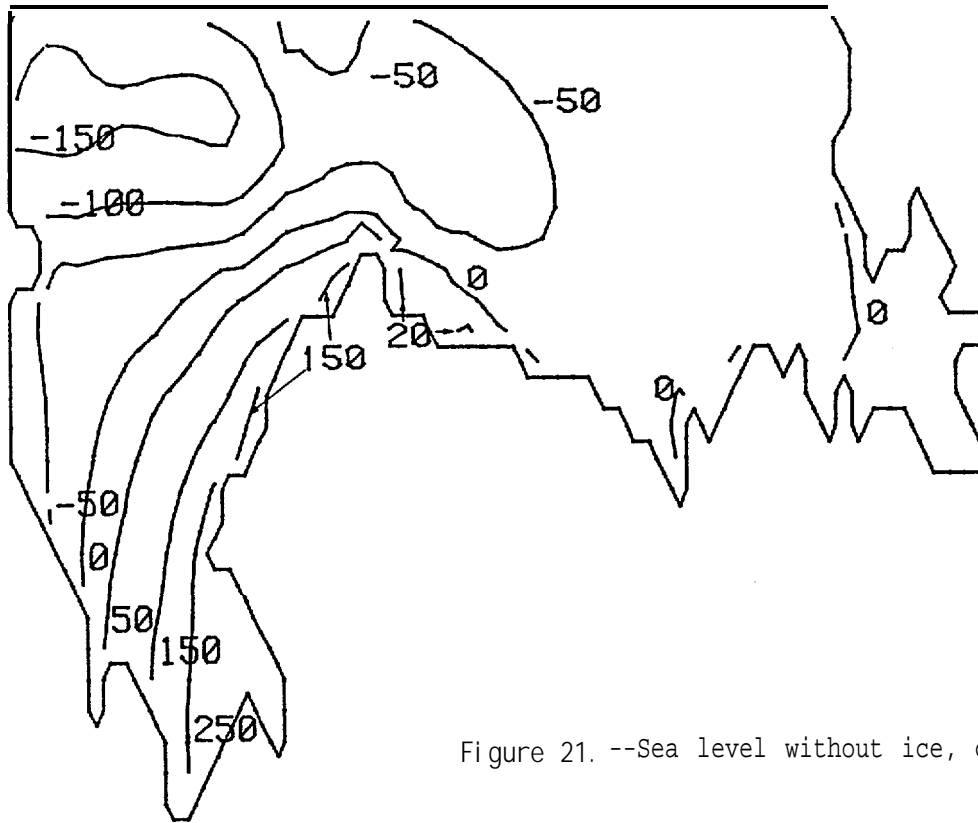


Figure 21. --Sea level without ice, day 1.

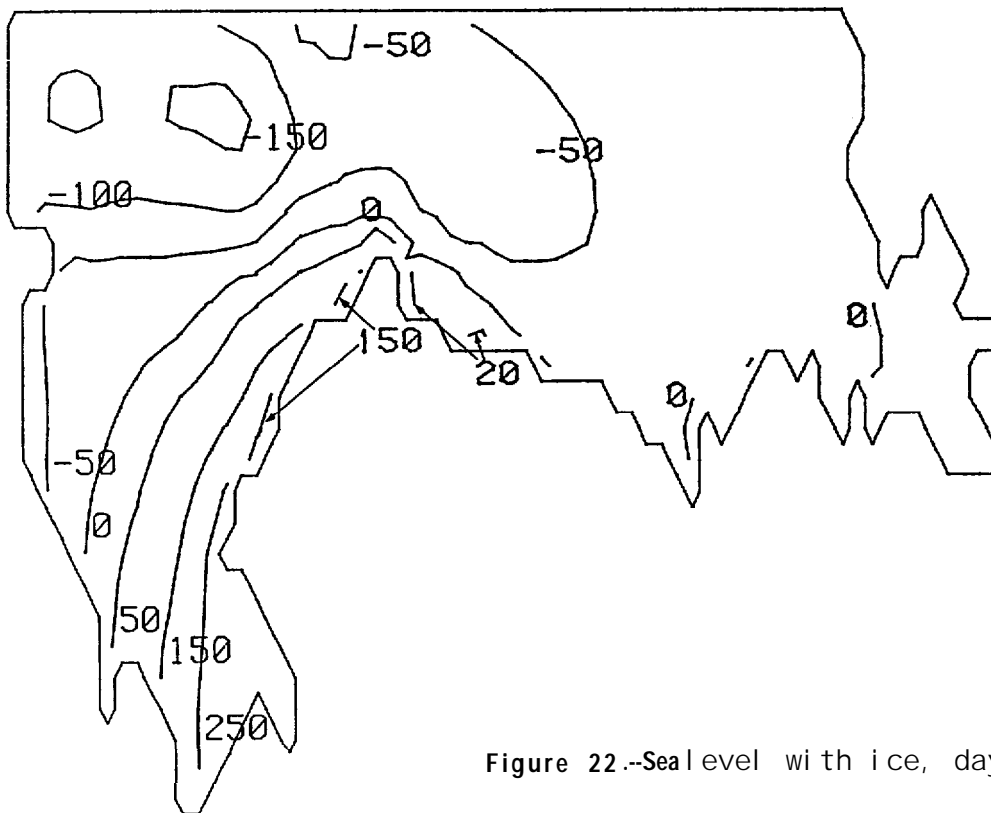


Figure 22.--Sea level with ice, day 1.

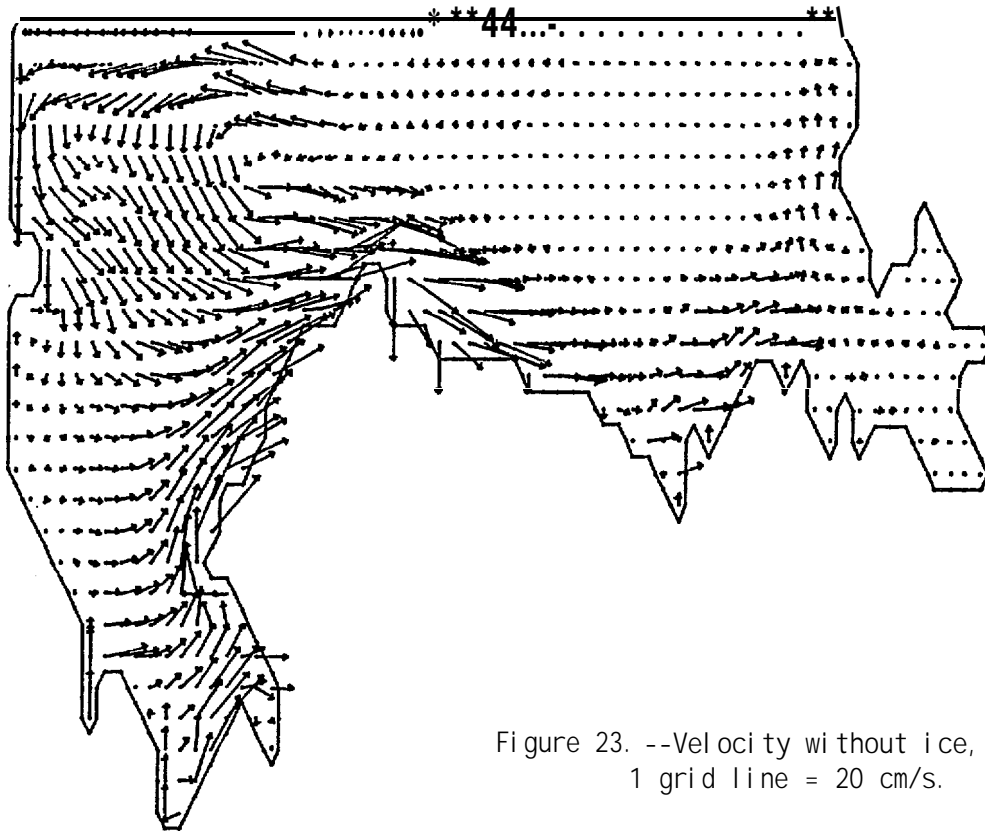


Figure 23. --Velocity without ice, day 1;
1 grid line = 20 cm/s.

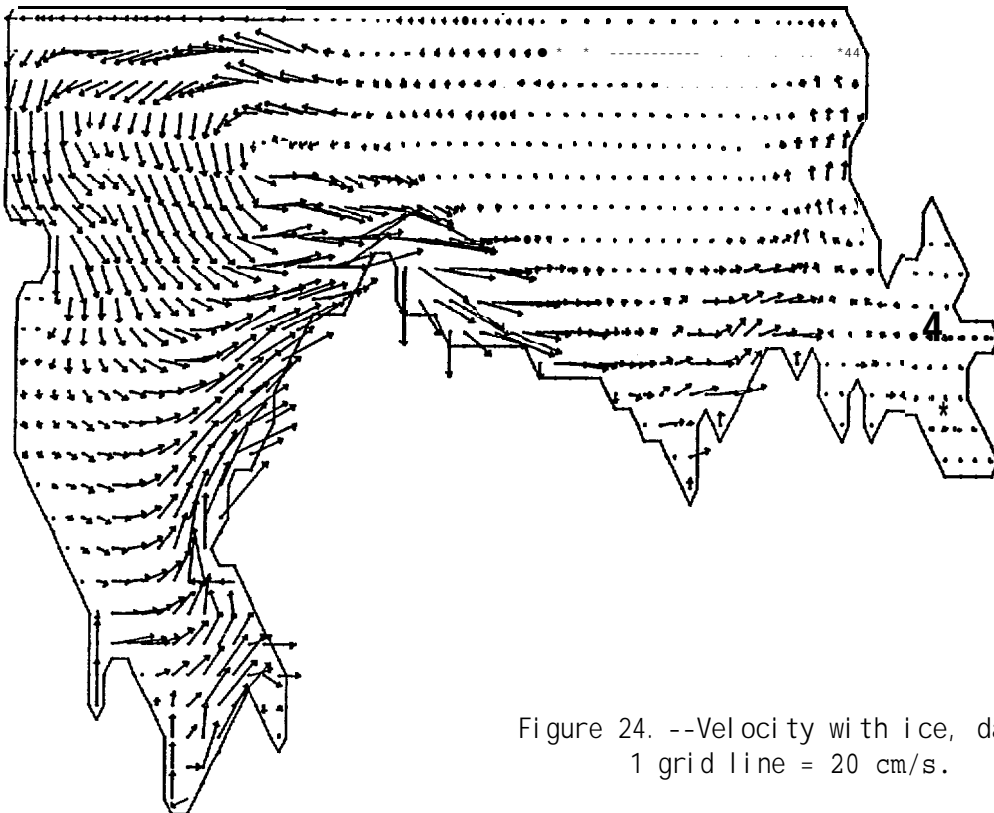


Figure 24. --Velocity with ice, day 1;
1 grid line = 20 cm/s.

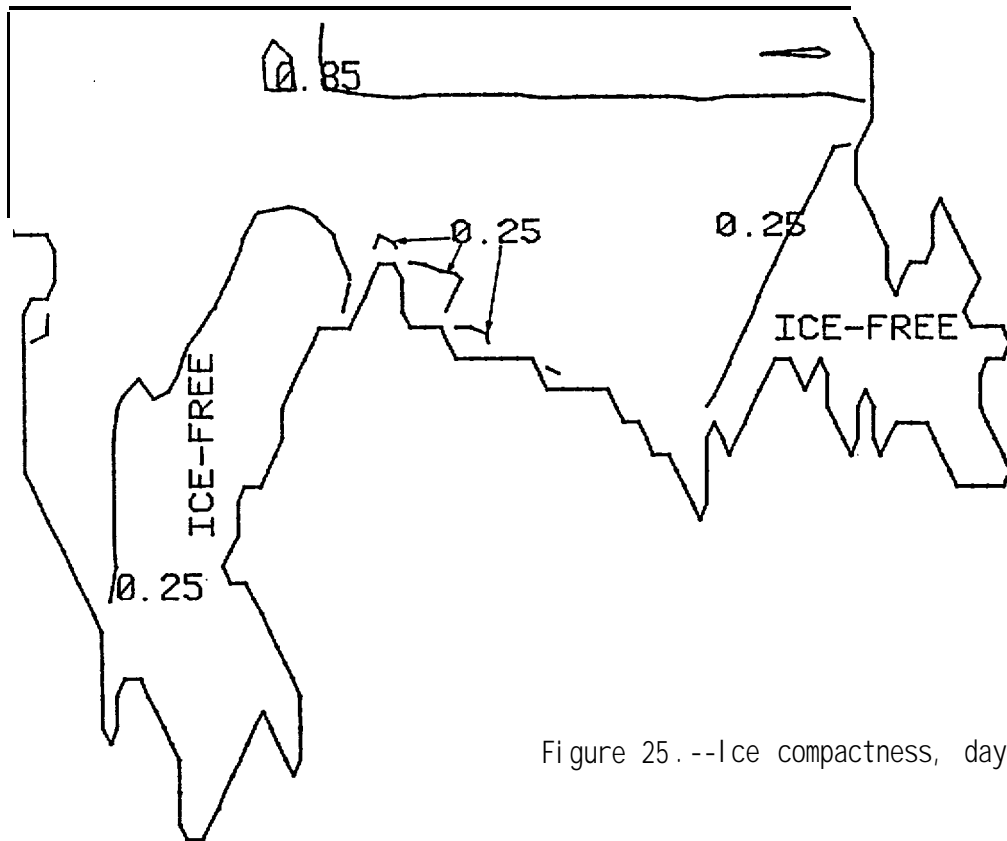


Figure 25.--Ice compactness, day 1.

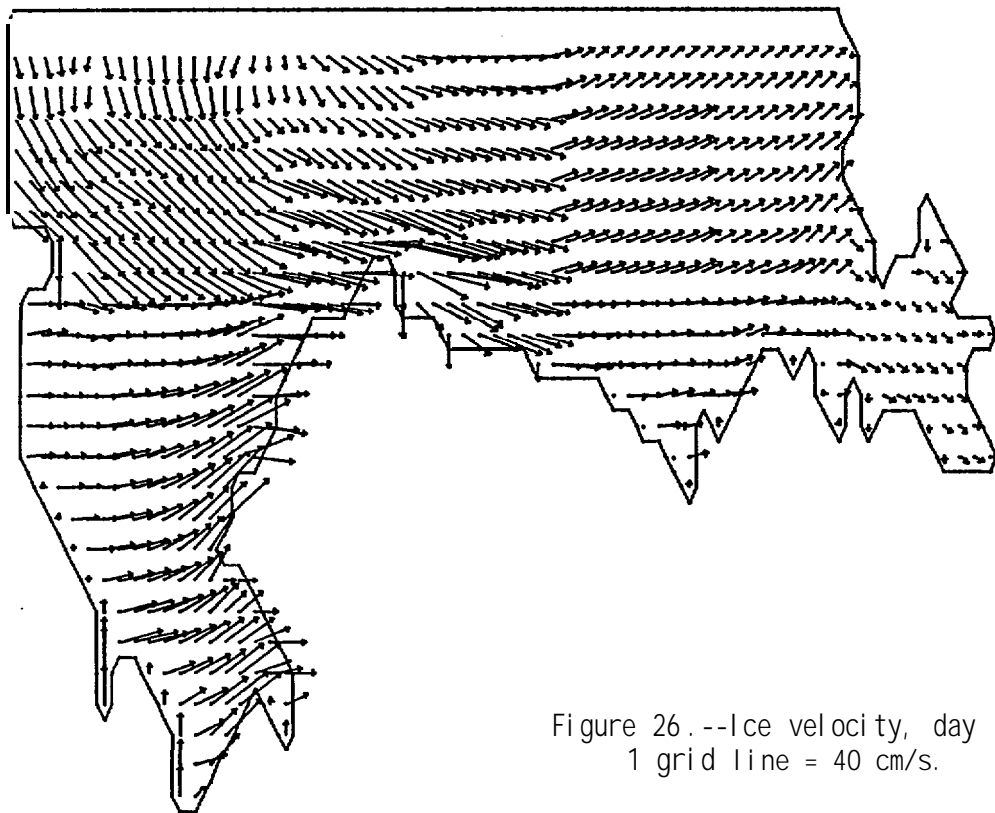


Figure 26.--Ice velocity, day 1;
1 grid line = 40 cm/s.

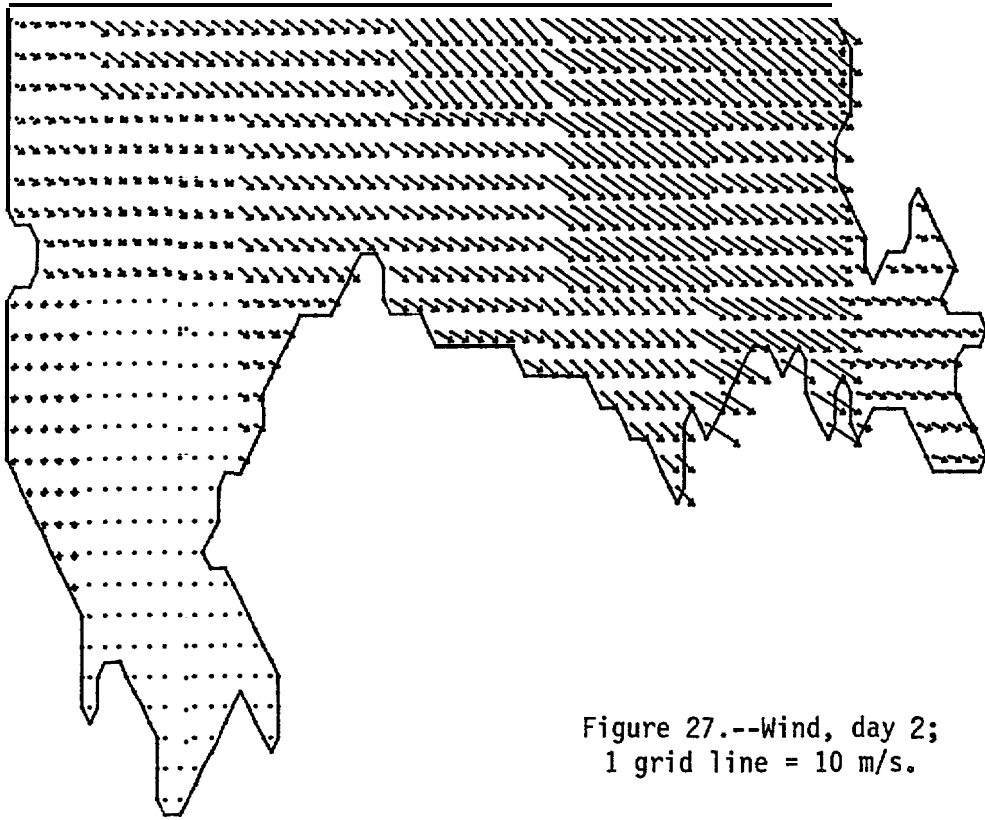


Figure 27.--Wind, day 2;
1 grid line = 10 m/s.

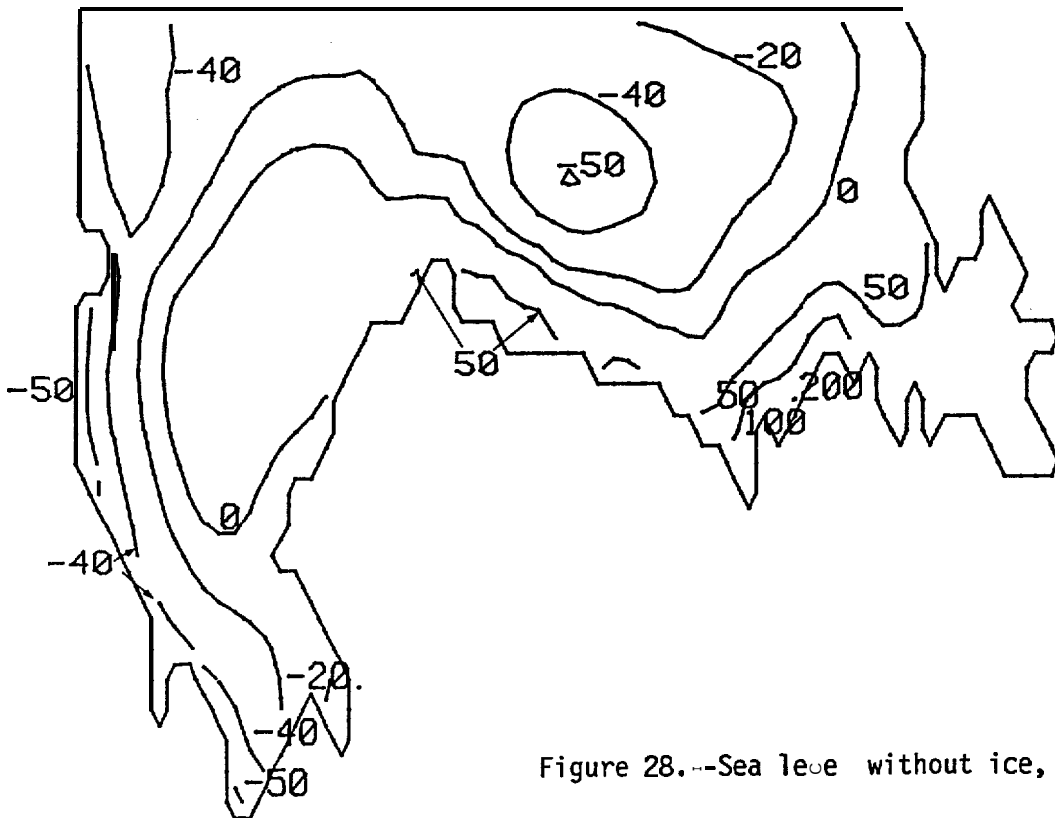


Figure 28.--Sea level without ice, day 2.

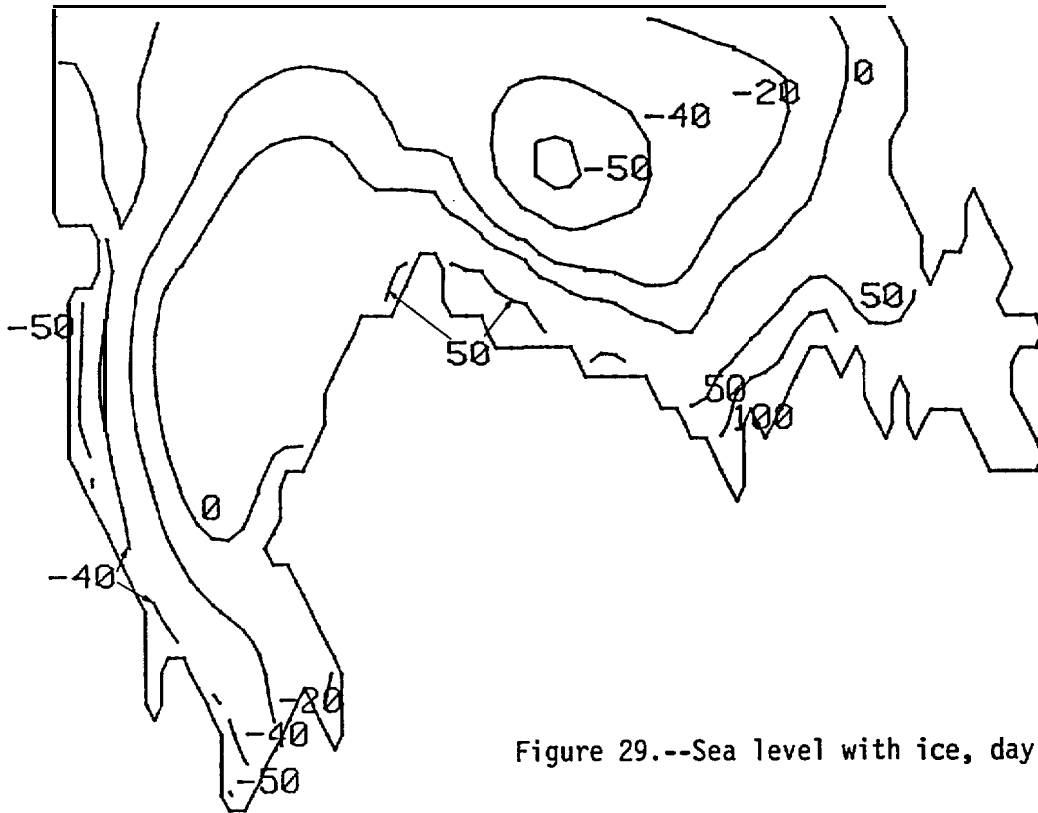


Figure 29.--Sea level with ice, day 2.

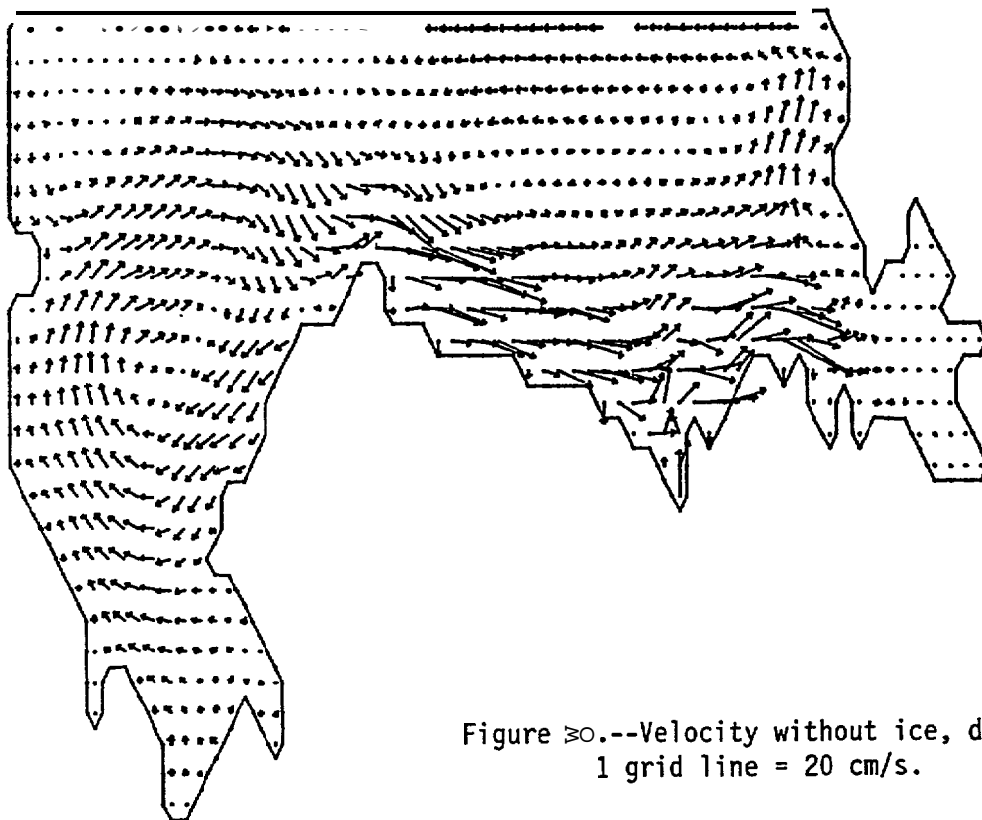


Figure 30.--Velocity without ice, day 2;
1 grid line = 20 cm/s.

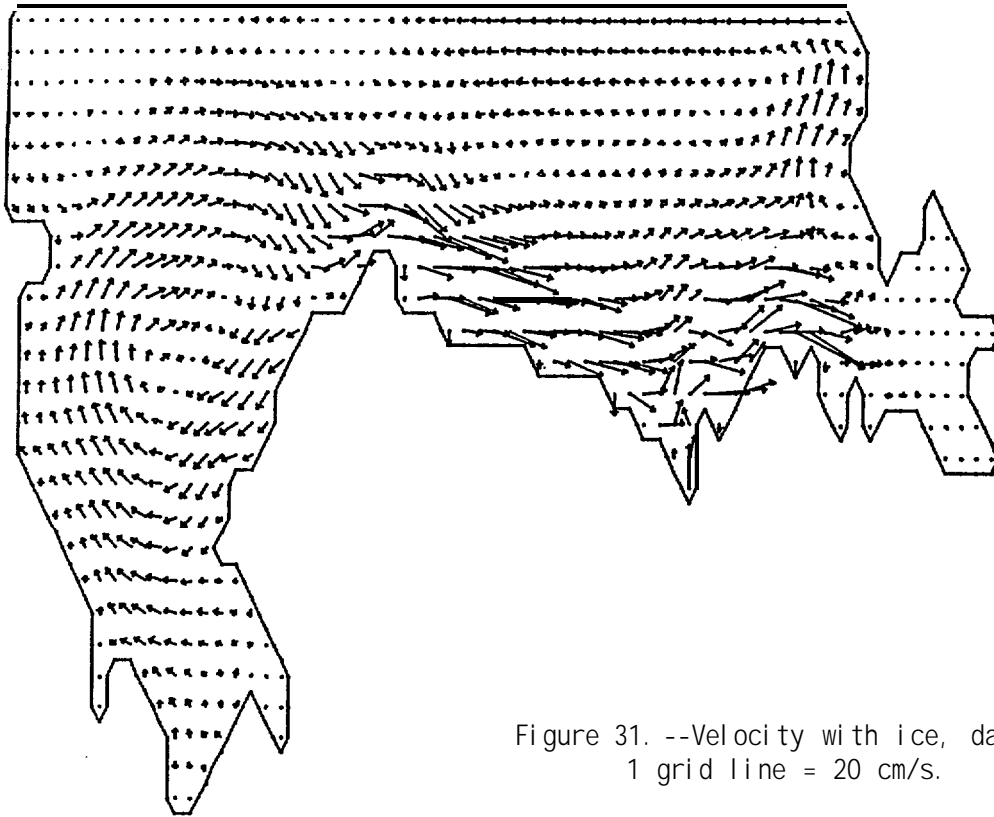


Figure 31. --Velocity with ice, day 2;
1 grid line = 20 cm/s.

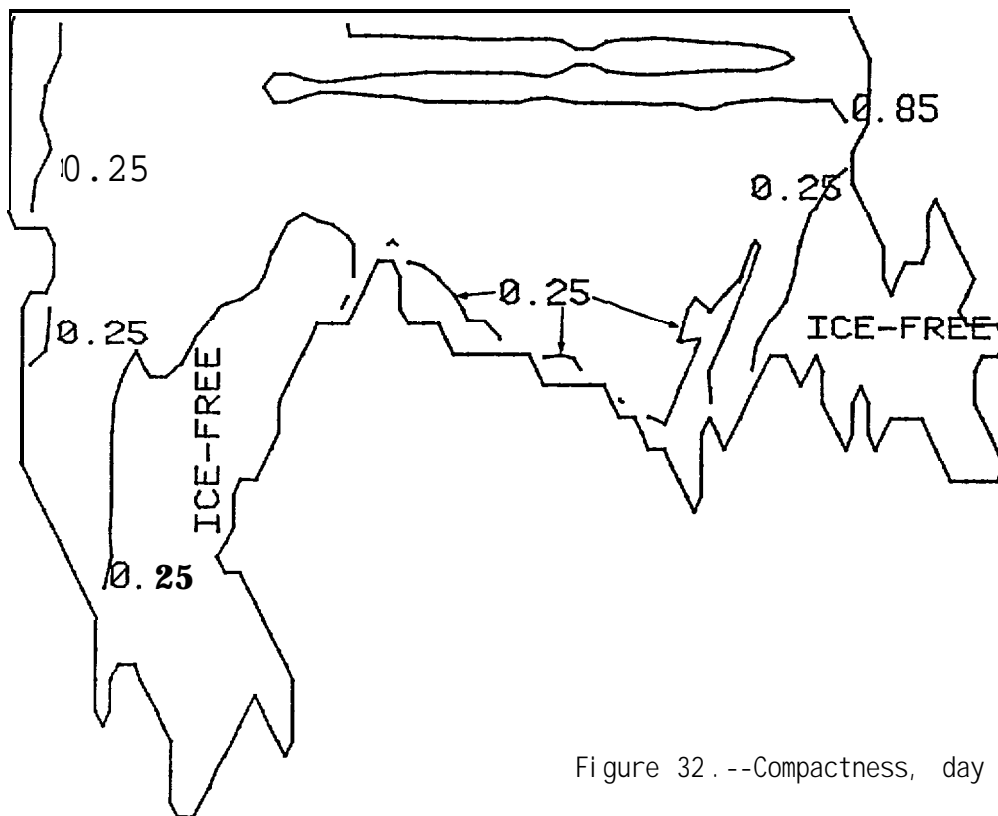


Figure 32. --Compactness, day 2.

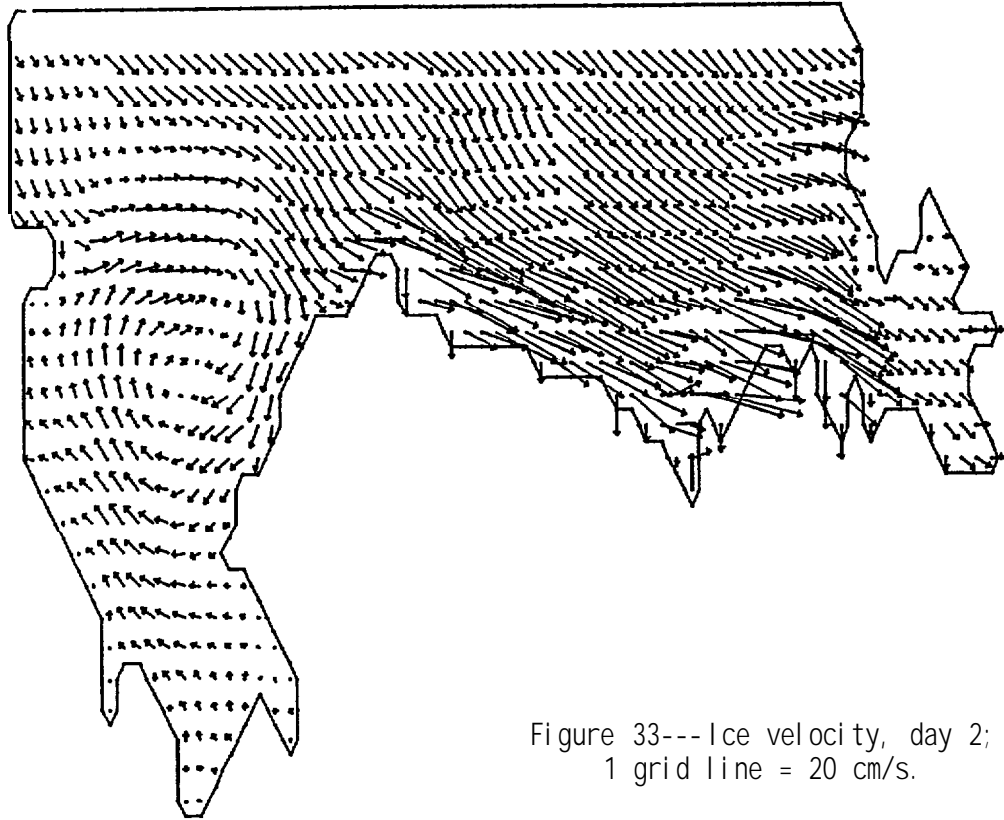


Figure 33---Ice velocity, day 2;
1 grid line = 20 cm/s.

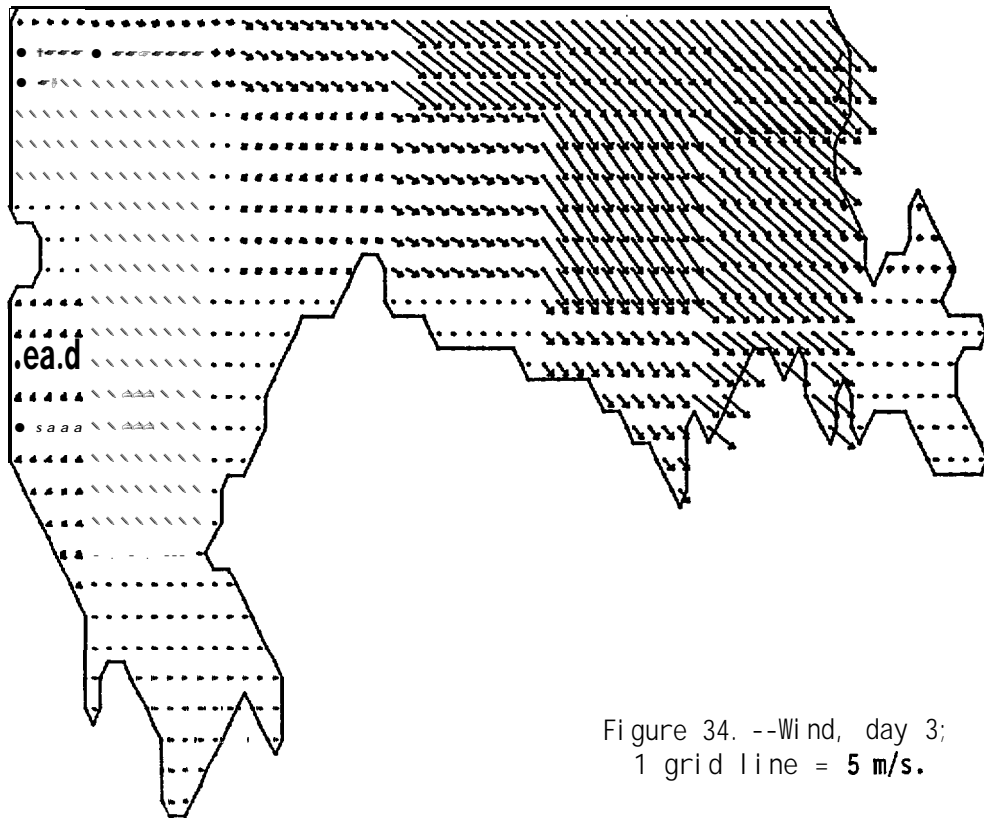


Figure 34. --Wind, day 3;
1 grid line = 5 m/s.

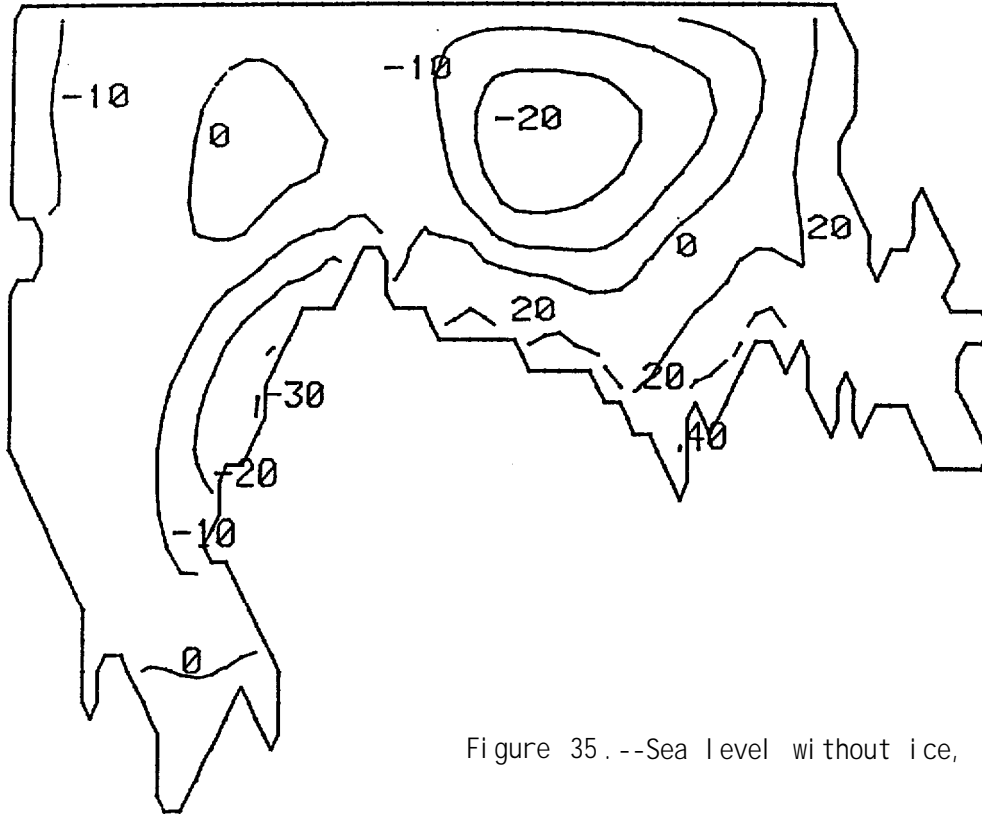


Figure 35.--Sea Level without ice, day 3.

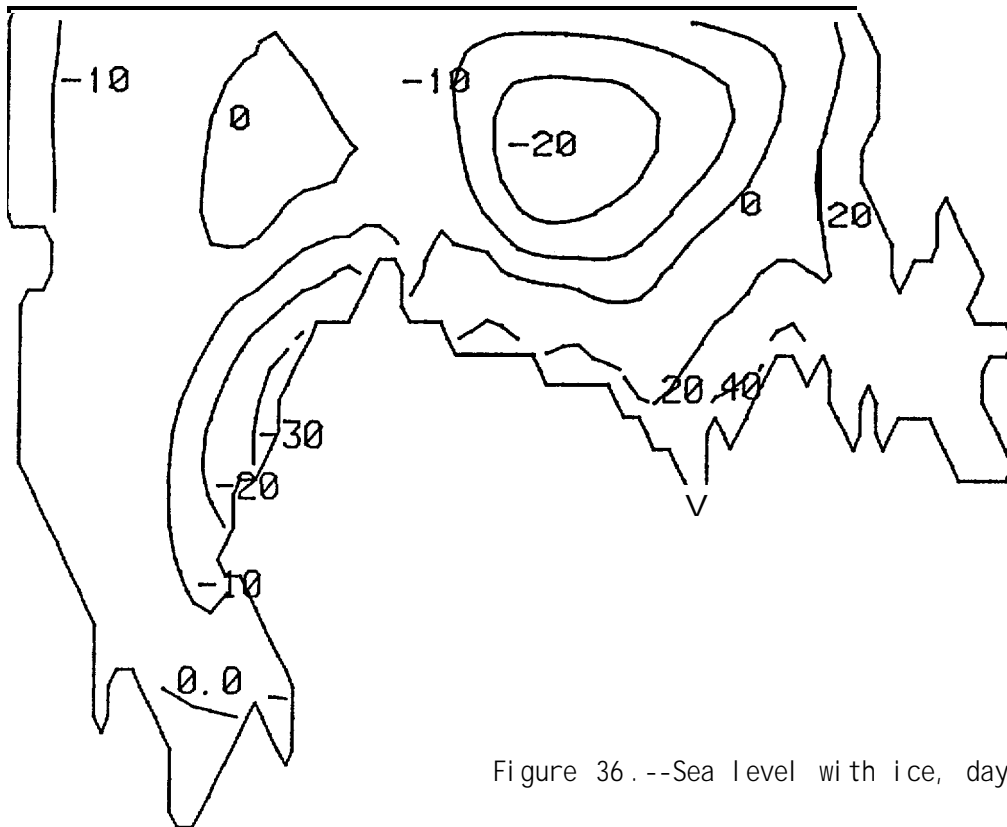


Figure 36.--Sea Level with ice, day 3.

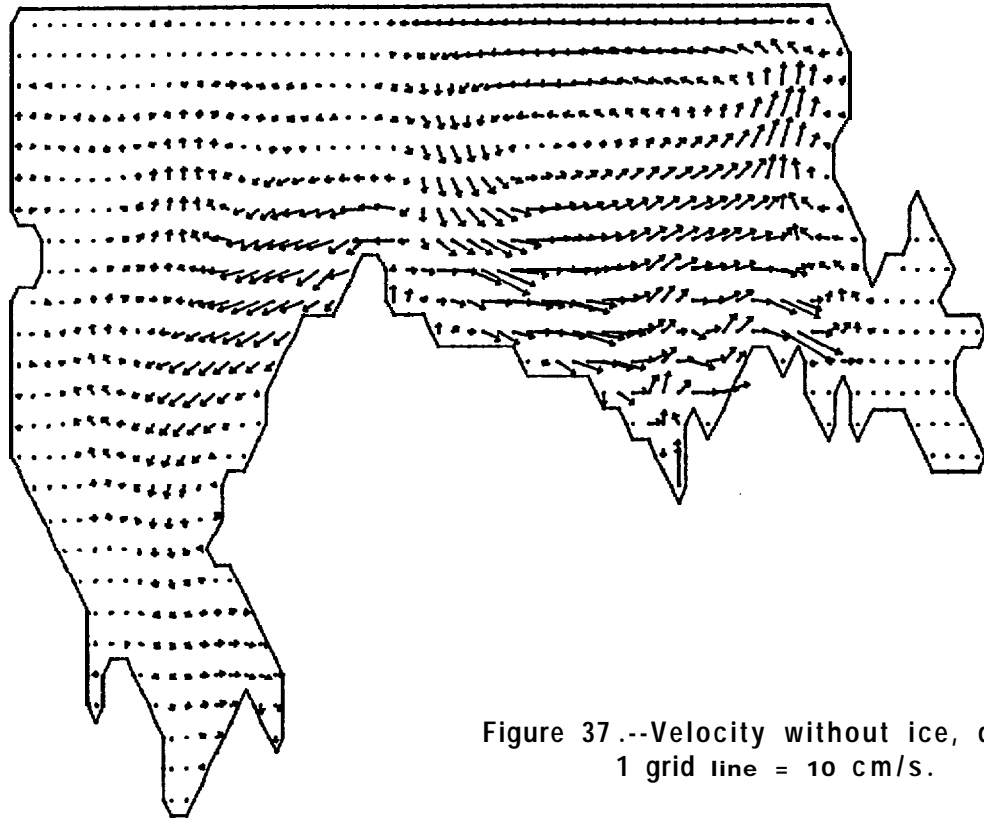


Figure 37.--Velocity without ice, day 3;
1 grid line = 10 cm/s.

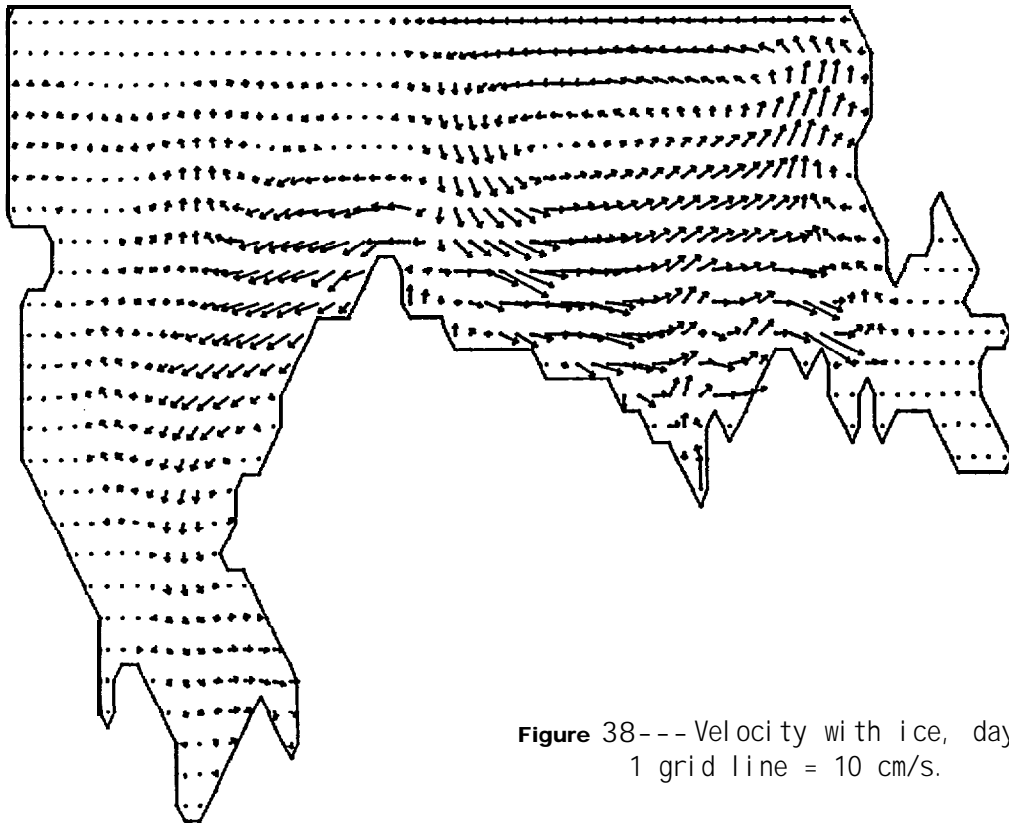


Figure 38--- Velocity with ice, day 3;
1 grid line = 10 cm/s.

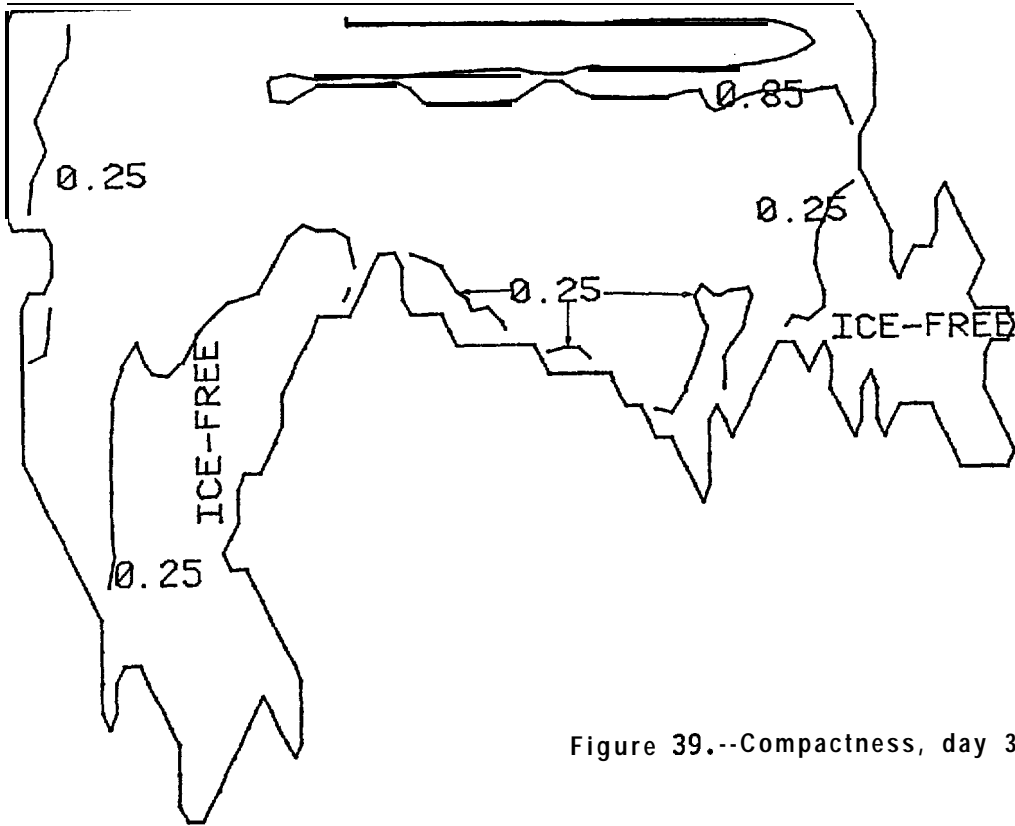


Figure 39.--Compactness, day 3.

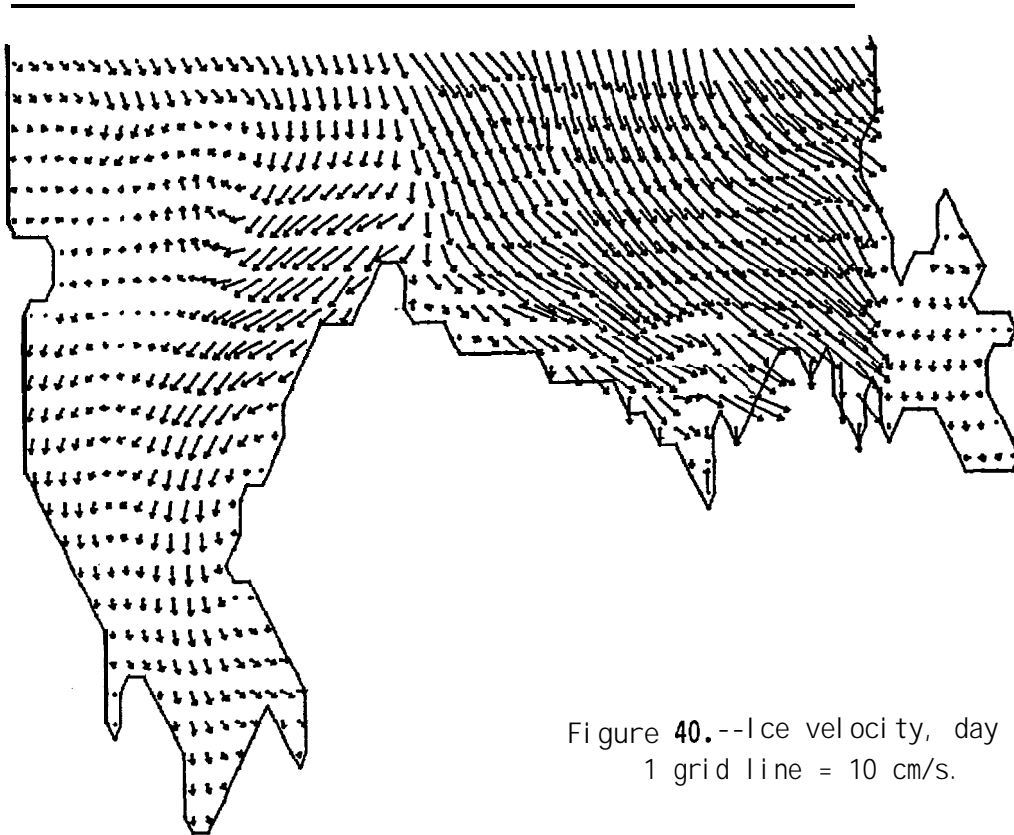


Figure 40.--Ice velocity, day 3;
1 grid line = 10 cm/s.

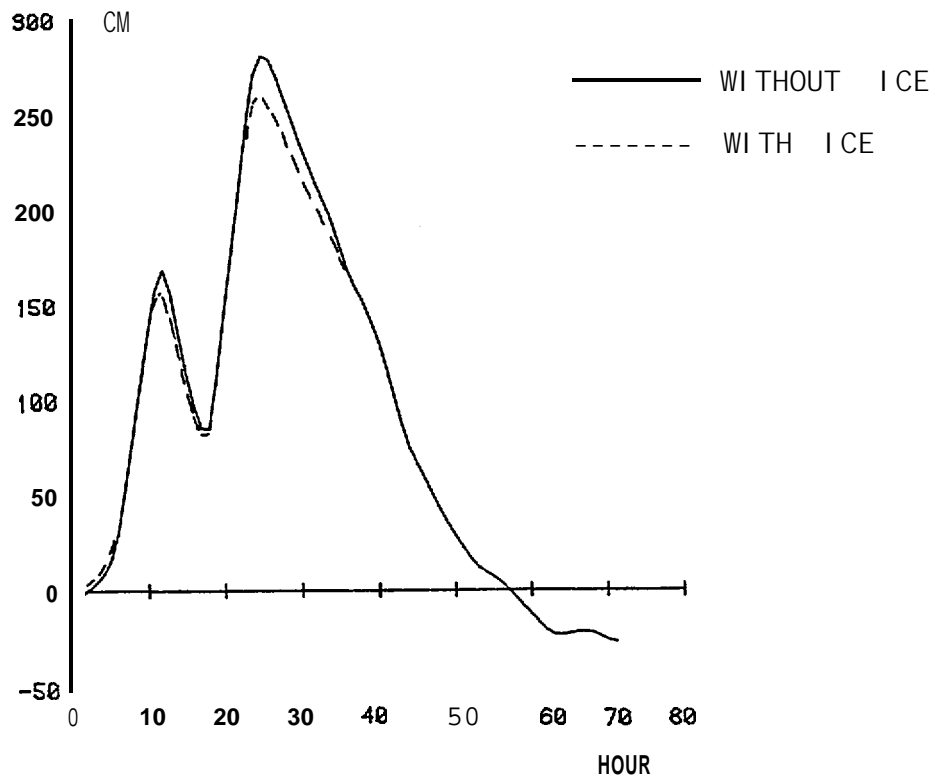


Figure 41. --Sea level variation, Pt. Barrow west.

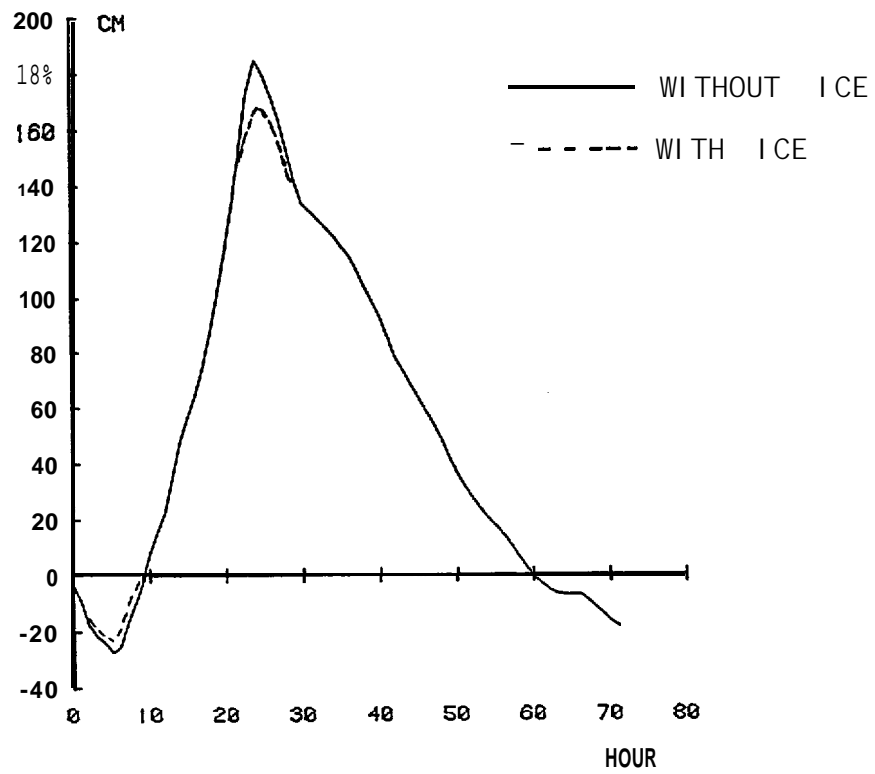


Figure 42. --Sea level variation, Pt. Barrow.

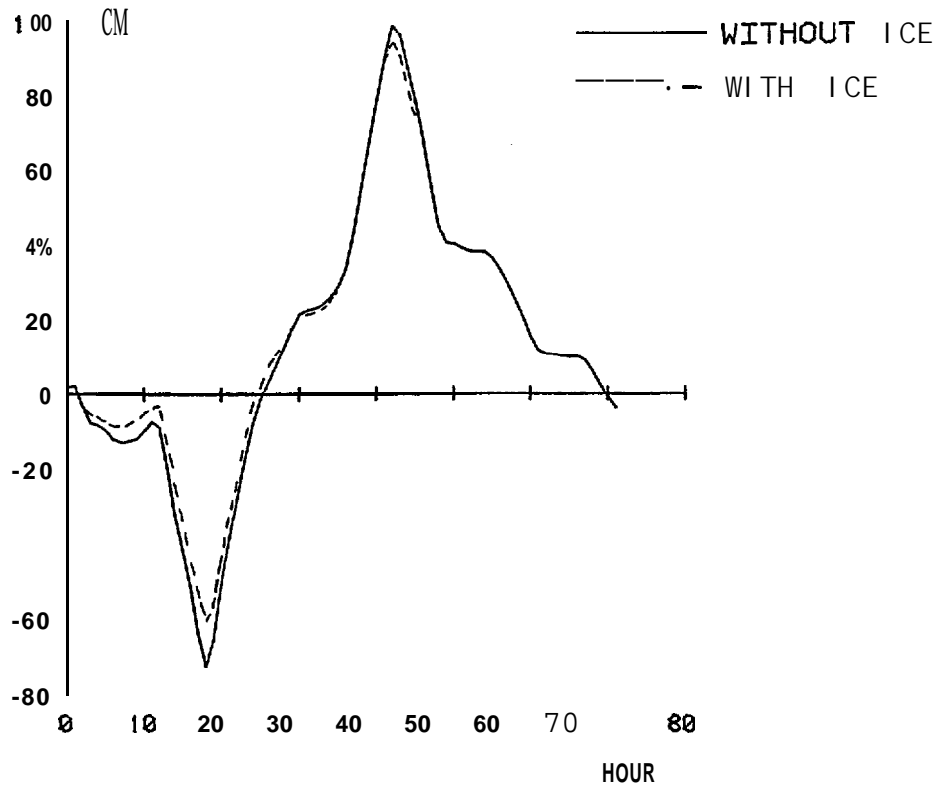


Figure 43.--Sea level variation, Pt. Barrow east.

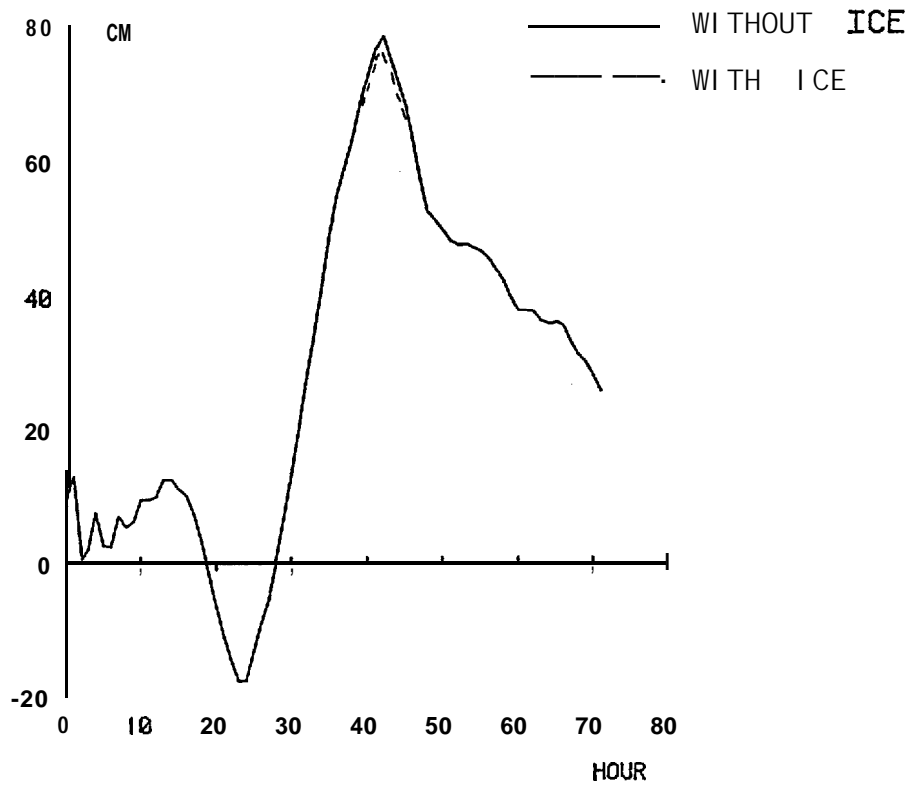


Figure 44.--Sea level variation, Simpson Cove.

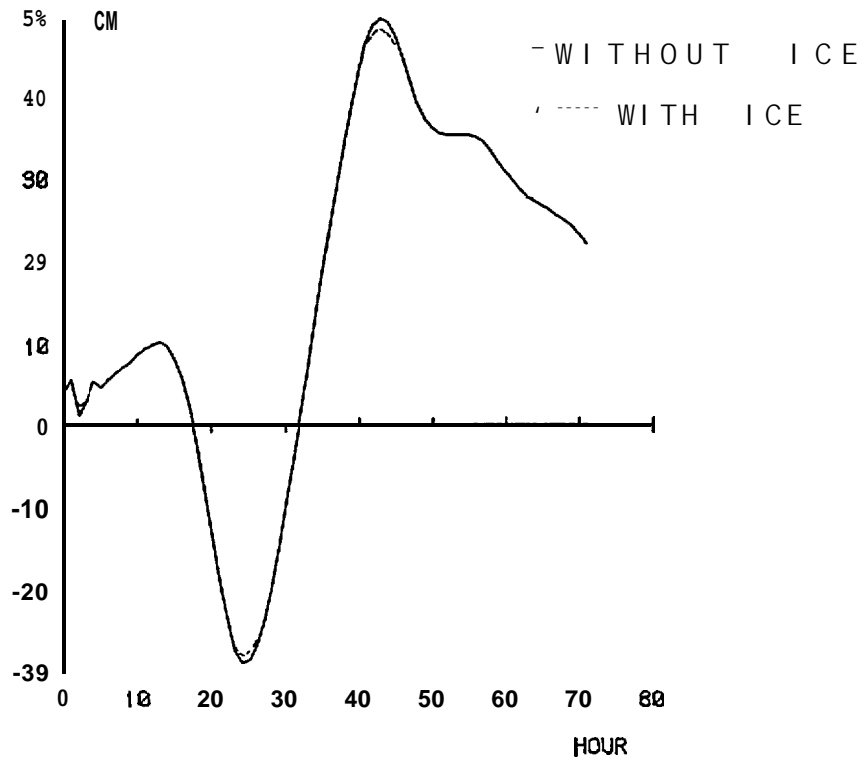


Figure 45.--Sea level variation, Demarcation Bay.

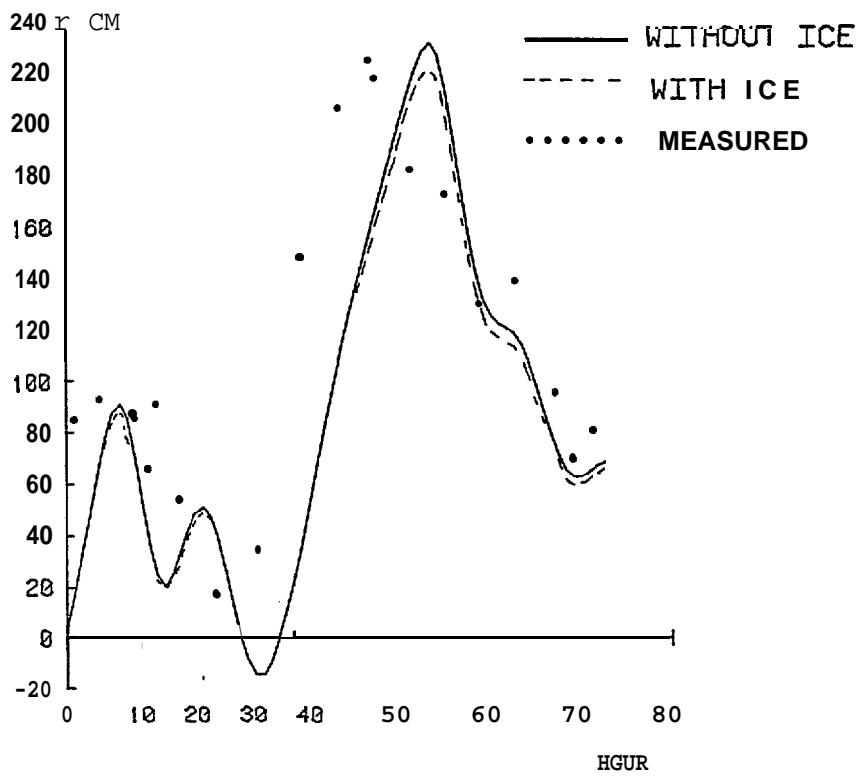


Figure 46.--Sea level variation, Tuktoyaktuk.

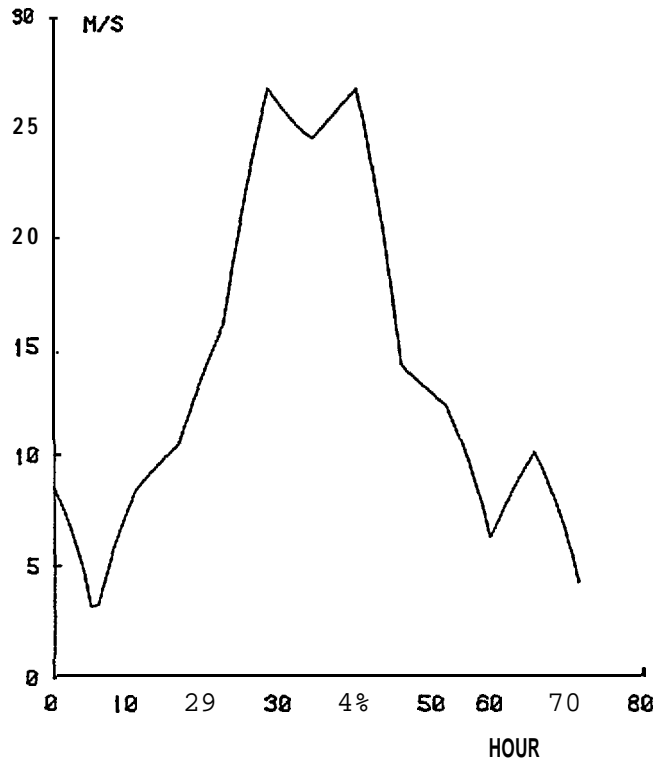


Figure 47---Wind velocity at 70°30'N,135°30'W. Speed is linearly interpolated between 6-h intervals.

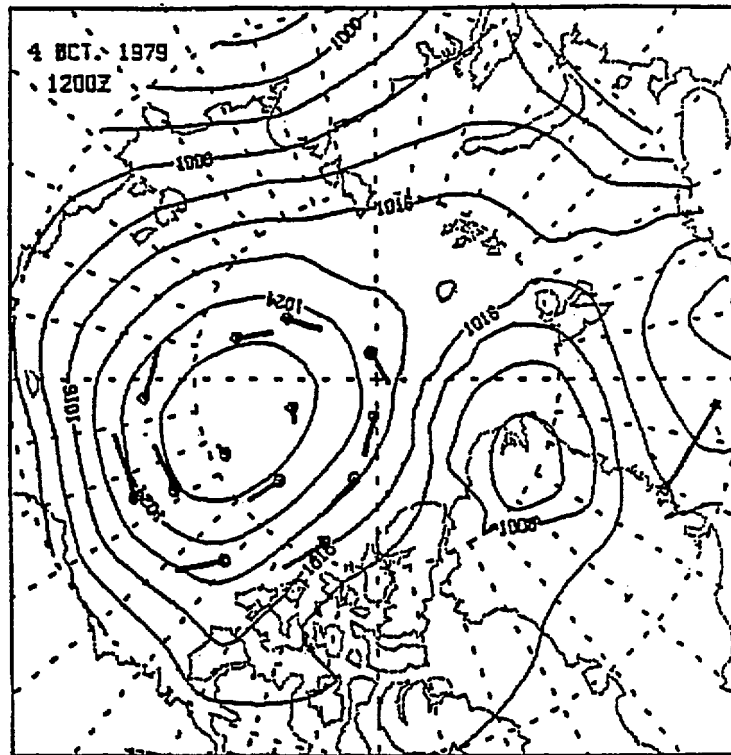


Figure 48.--Weather chart for 4 October 1979, 12Z. Pressure in millibars. Ice motion is described by the vectors originating at the open circles. From Thorndike and Colony (1980).

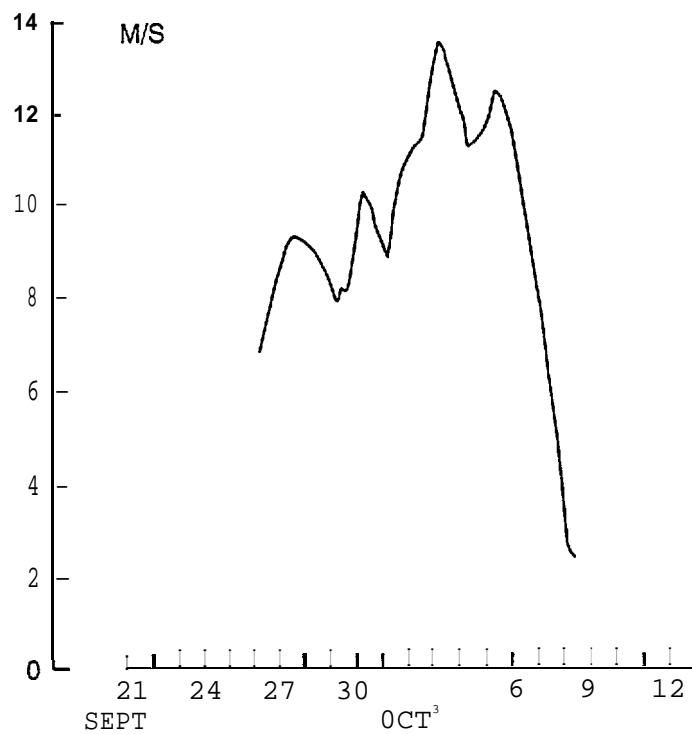


Figure 49---Wind speed in Harrison Bay (70°30'N, 151°W) during storm from September 26 to October 7, 1979.

322

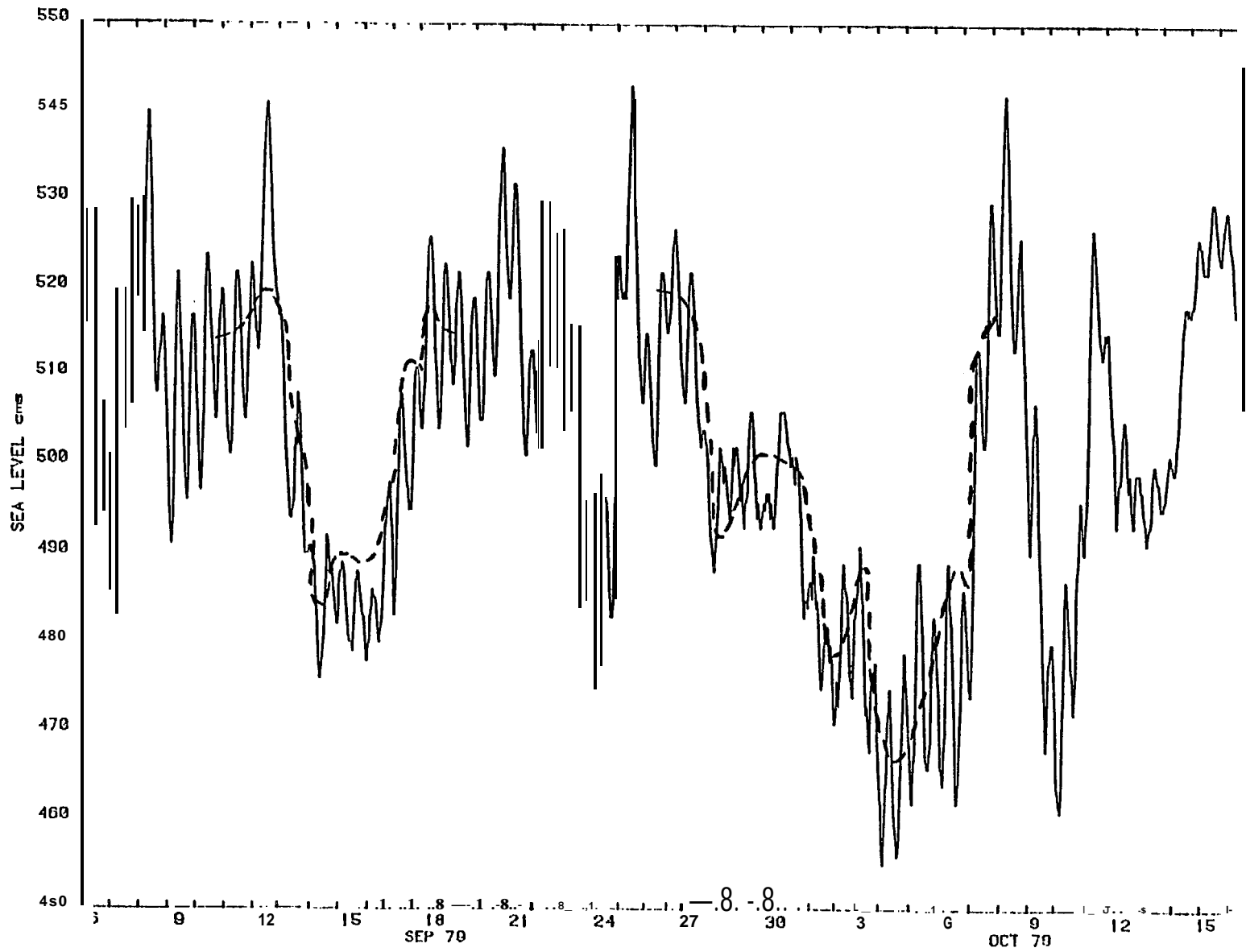


Figure 50.--Sea level in Harrison Bay. Solid line represents measured sea level, dashed line represents computed level.

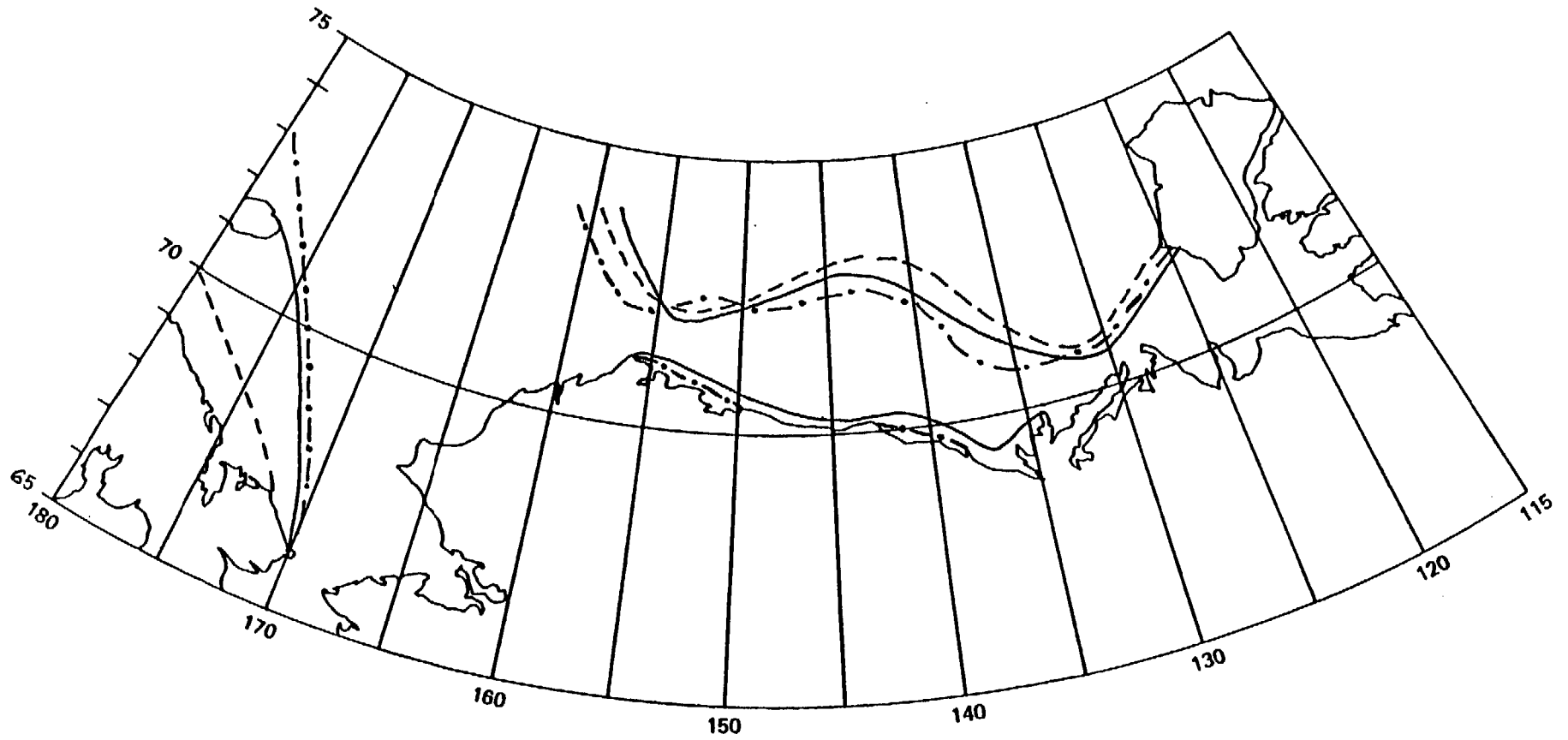


Figure 51.--Ice edge position on September 26 (dashed line) and on October 7 (measured represented by solid line, and computed by dash-dot line).

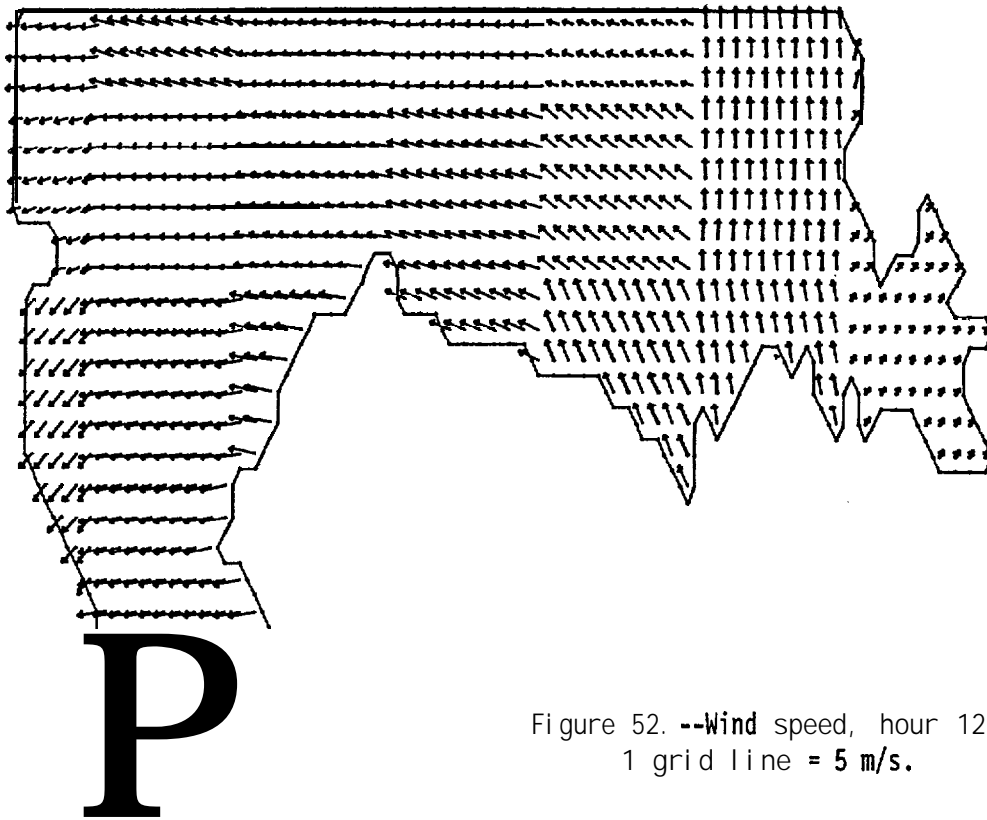


Figure 52. --Wind speed, hour 12;
1 grid line = 5 m/s.

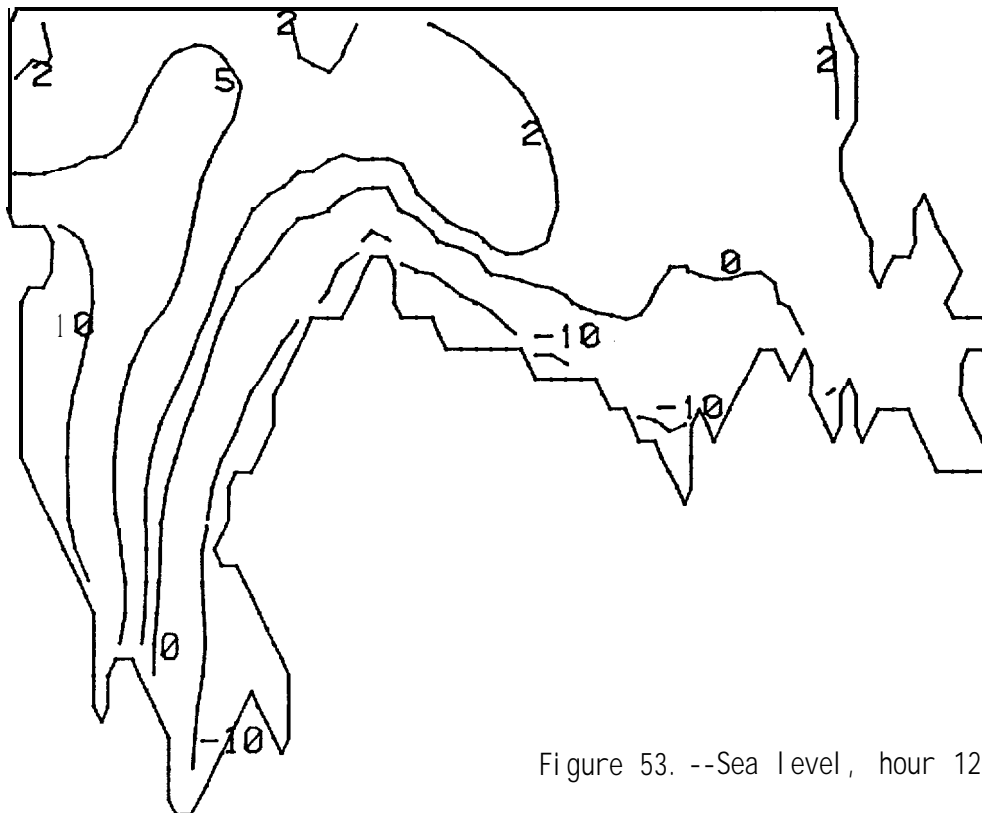


Figure 53. --Sea level, hour 12.

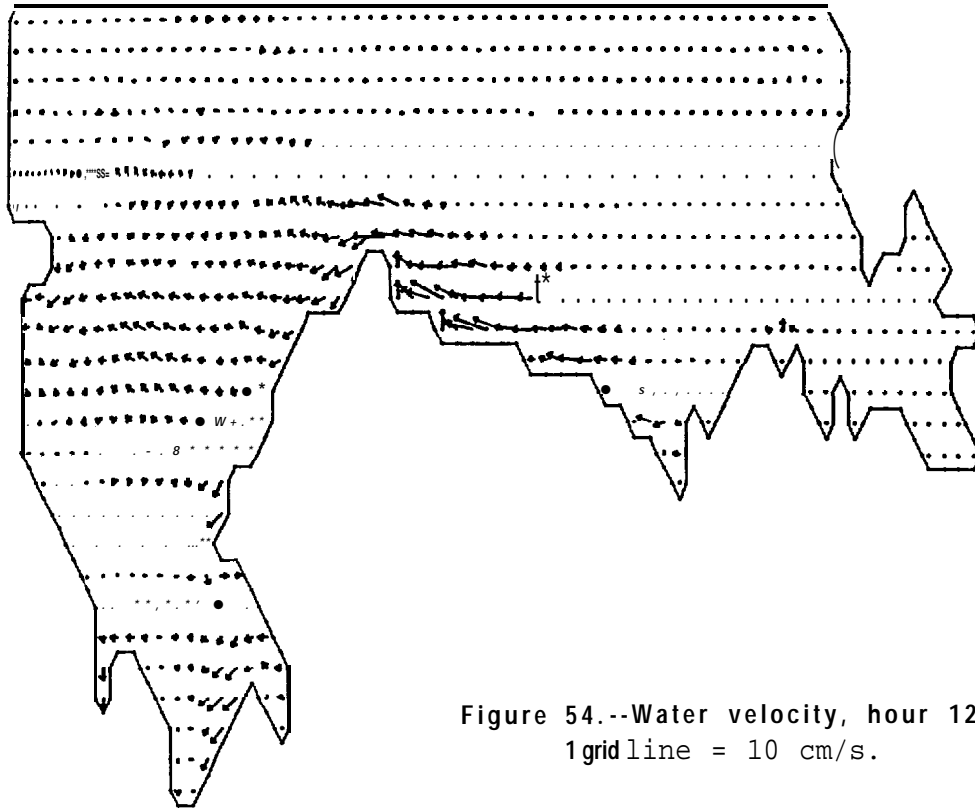


Figure 54.--Water velocity, hour 12;
1 grid line = 10 cm/s.

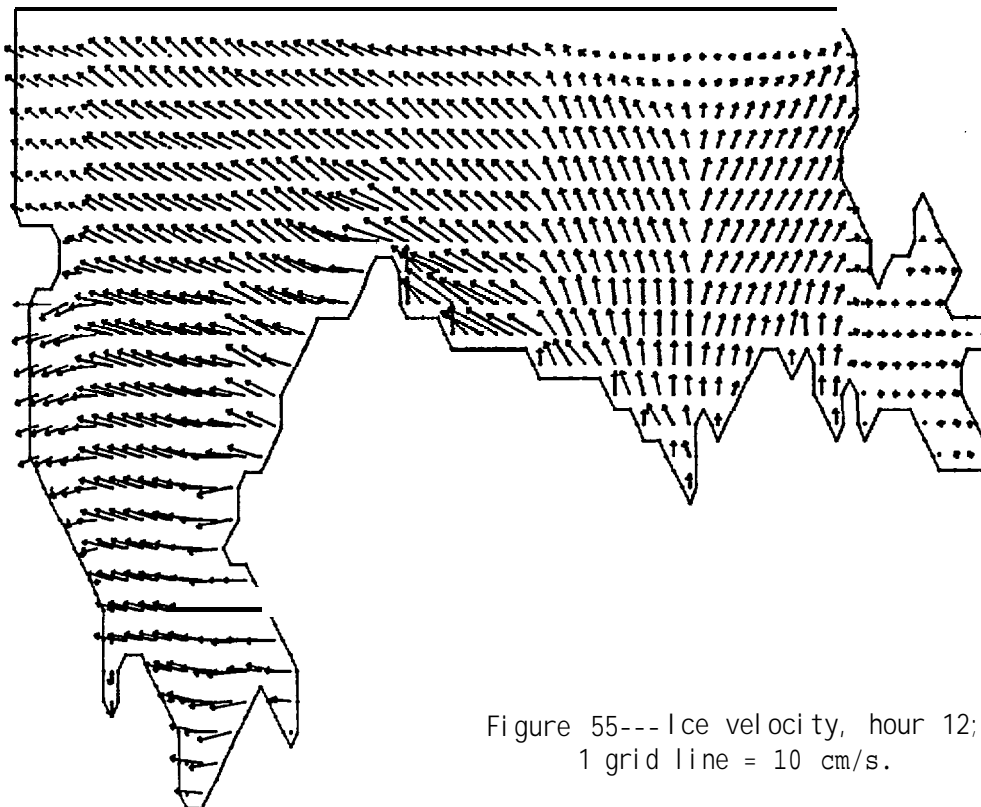


Figure 55---Ice velocity, hour 12;
1 grid line = 10 cm/s.

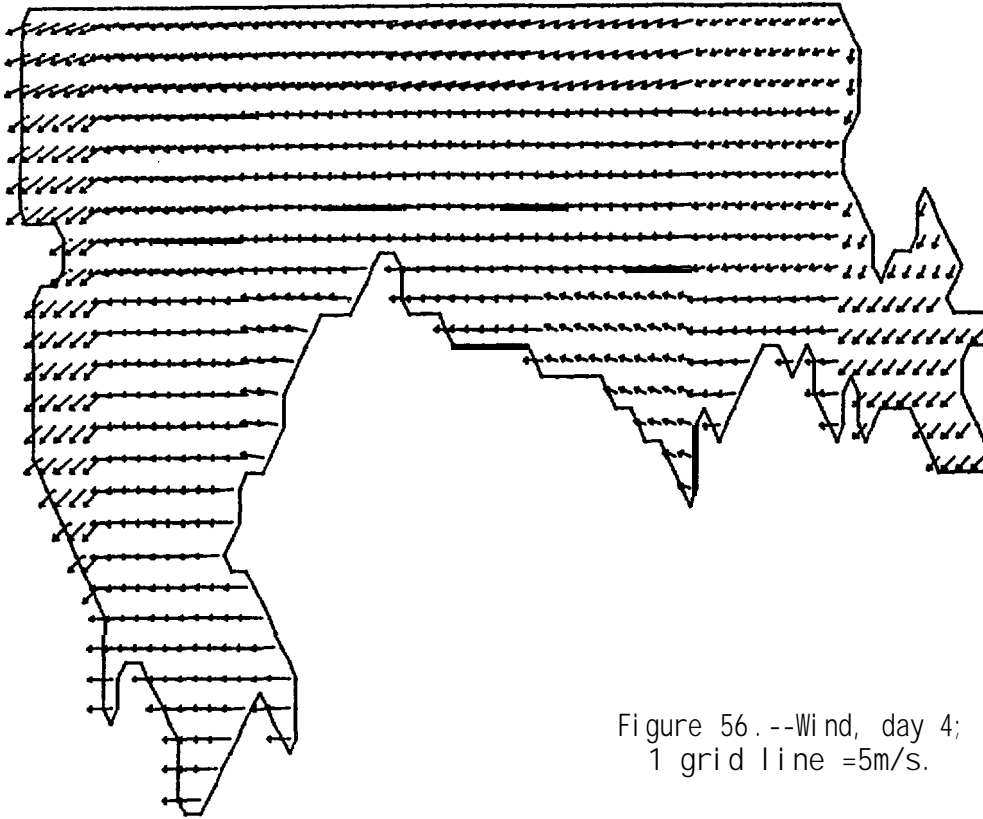


Figure 56. --Wind, day 4;
1 grid line = 5m/s.

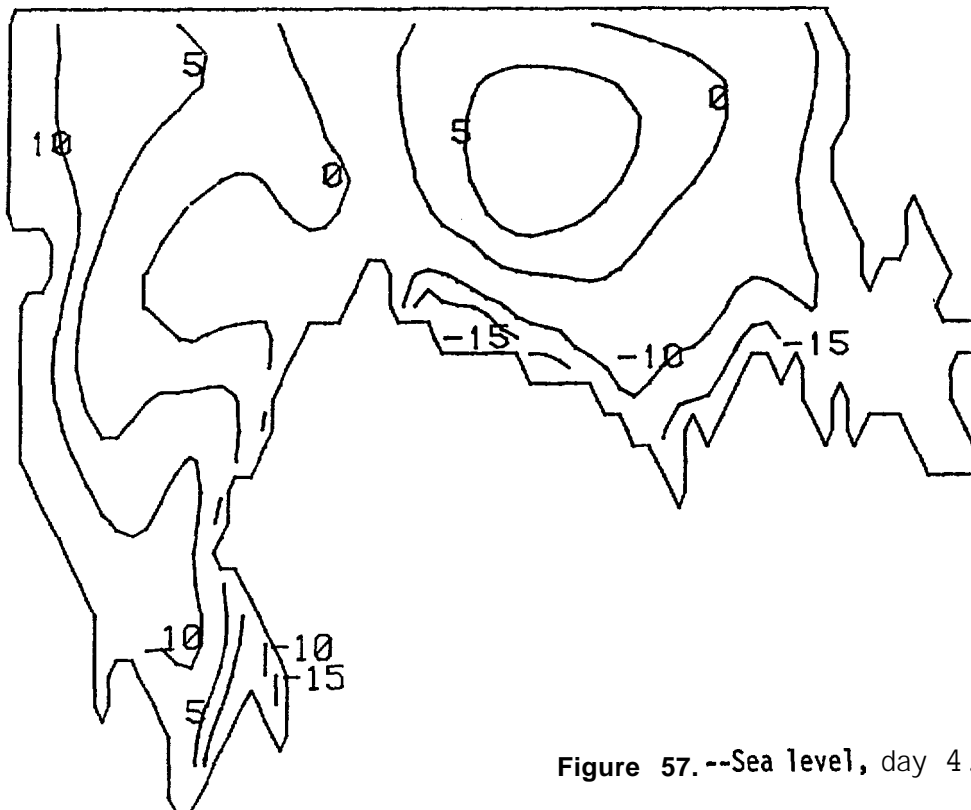


Figure 57. --Sea level, day 4.

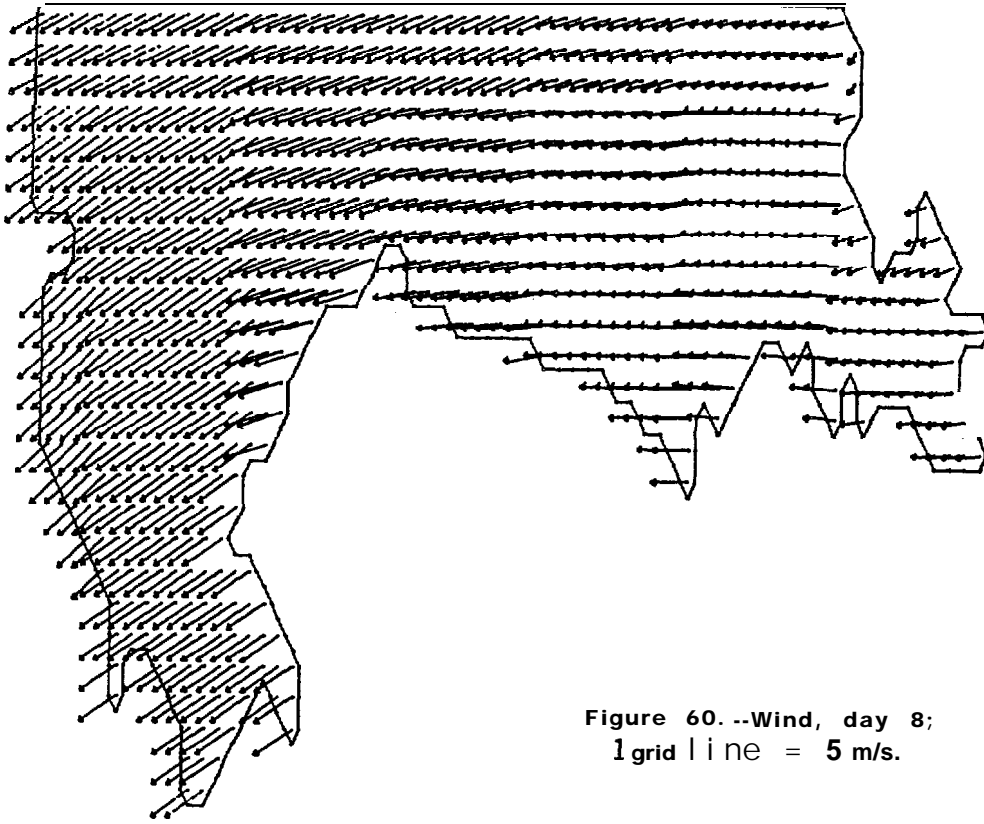


Figure 60.--Wind, day 8;
1 grid line = 5 m/s.

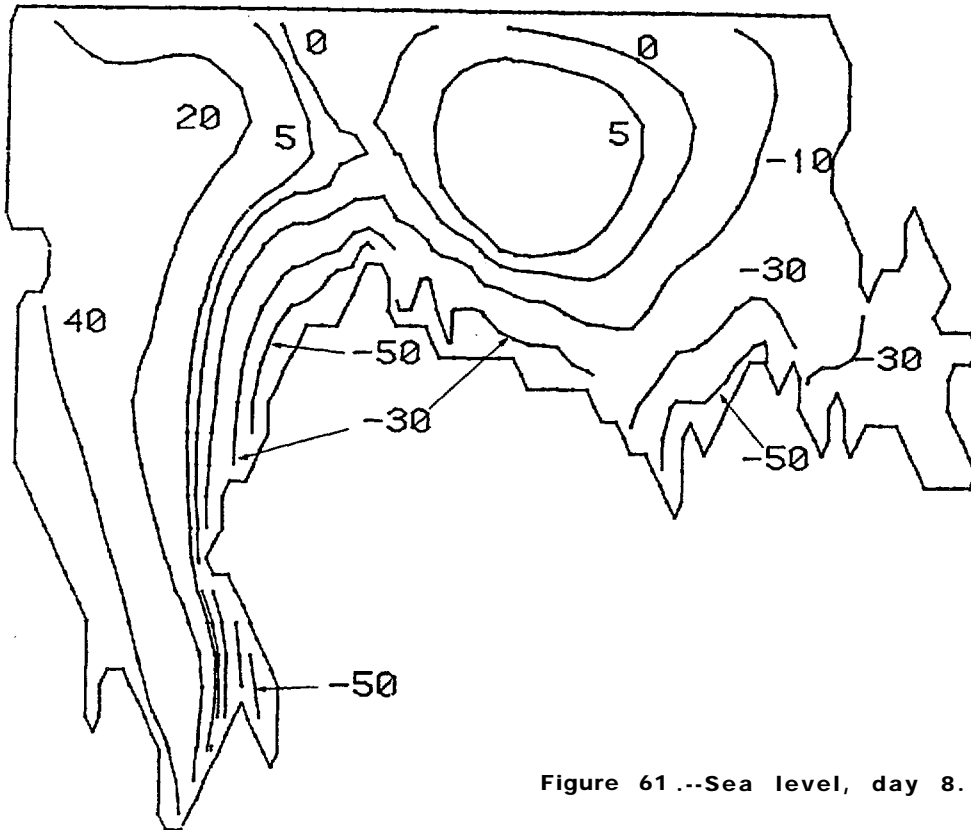


Figure 61.--Sea level, day 8.

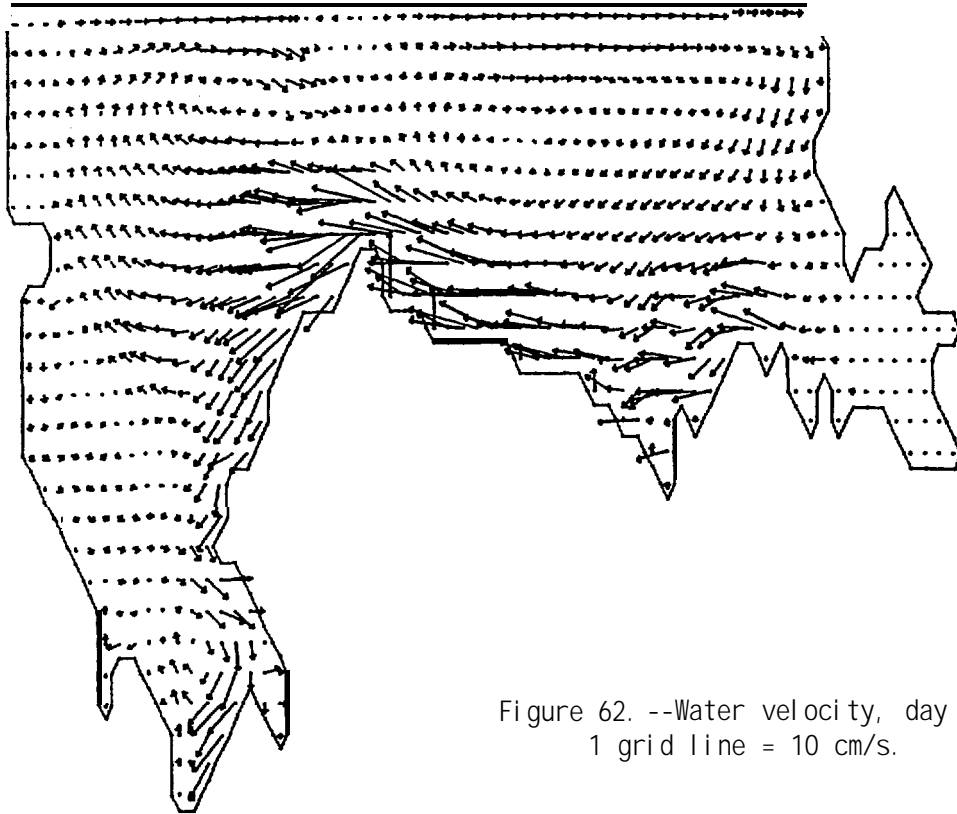


Figure 62. --Water velocity, day 8;
1 grid line = 10 cm/s.

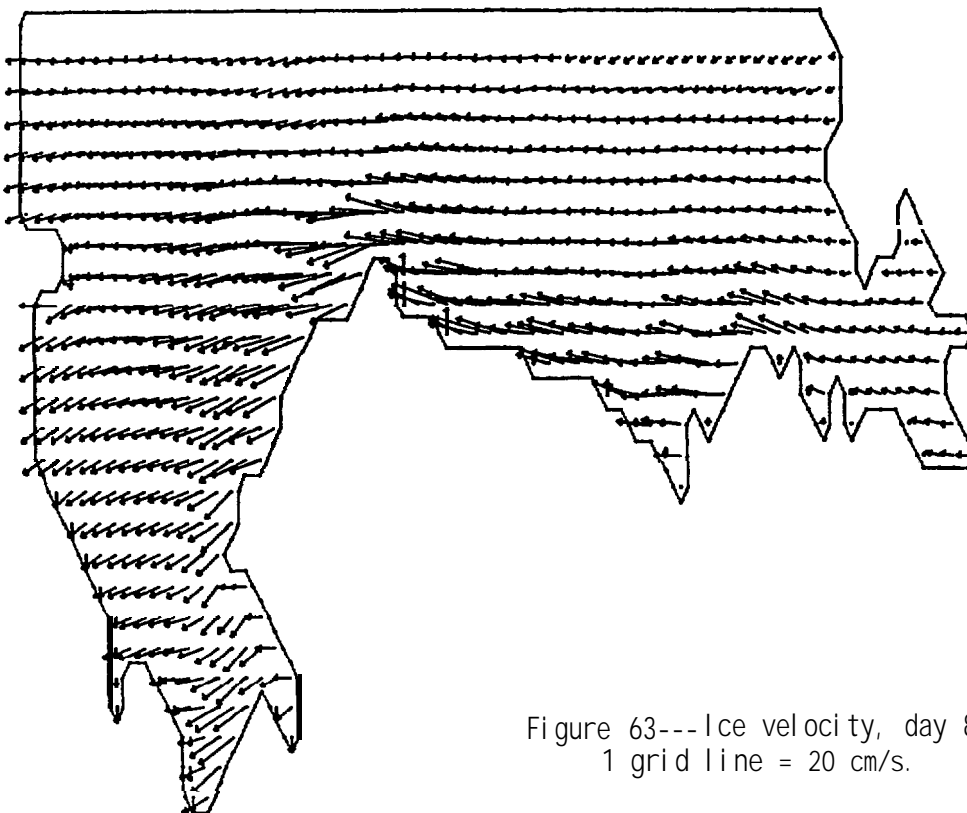


Figure 63---Ice velocity, day 8;
1 grid line = 20 cm/s.

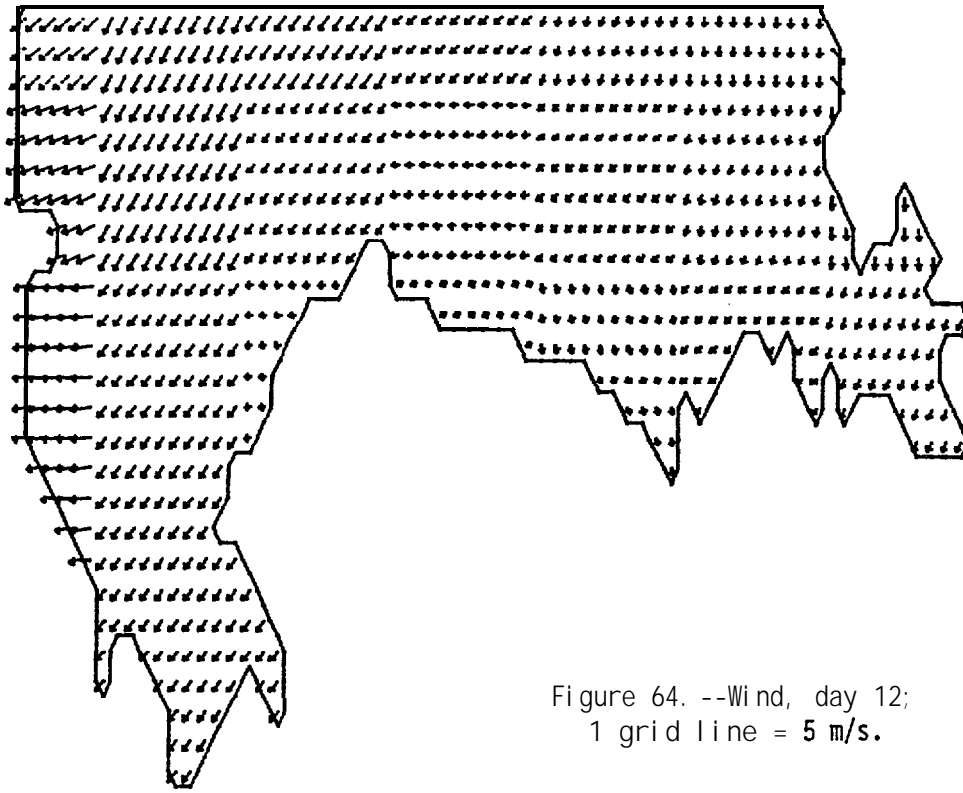


Figure 64. --Wind, day 12;
1 grid line = 5 m/s.

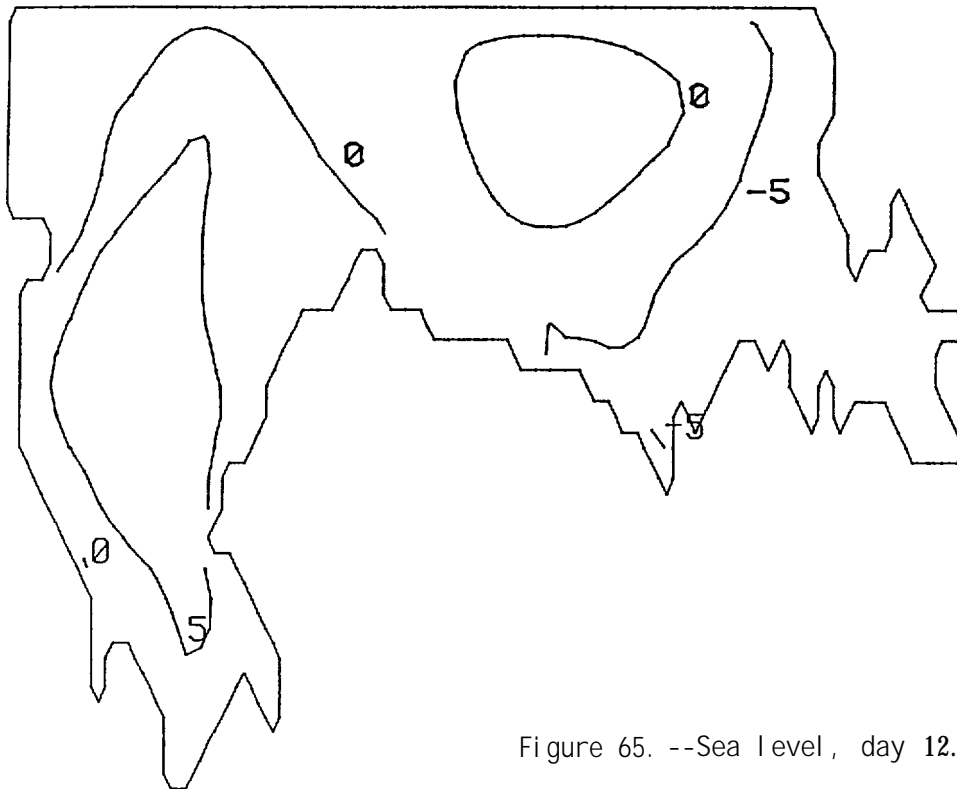


Figure 65. --Sea level, day 12.

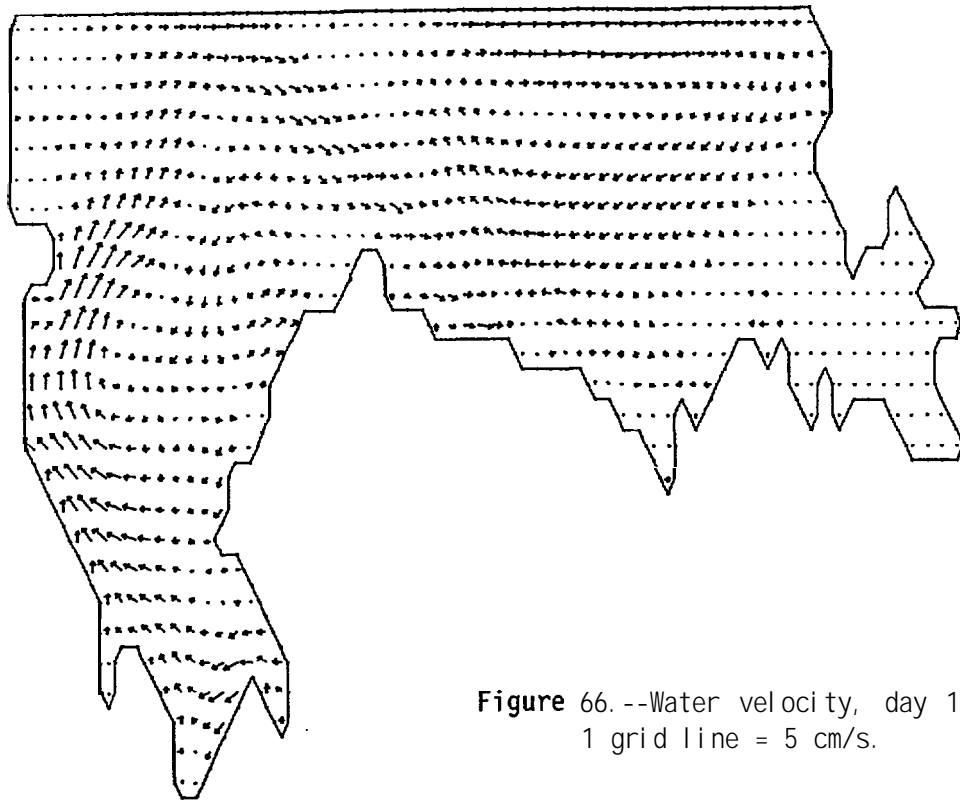


Figure 66.--Water velocity, day 12;
1 grid line = 5 cm/s.

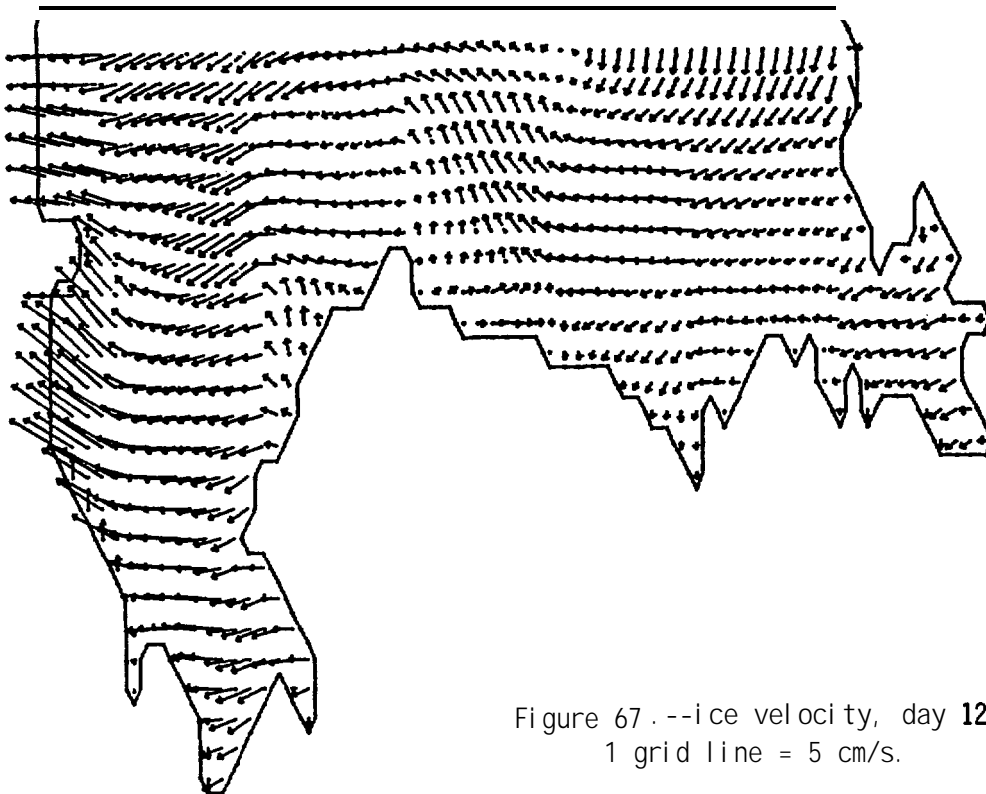


Figure 67.--ice velocity, day 12;
1 grid line = 5 cm/s.

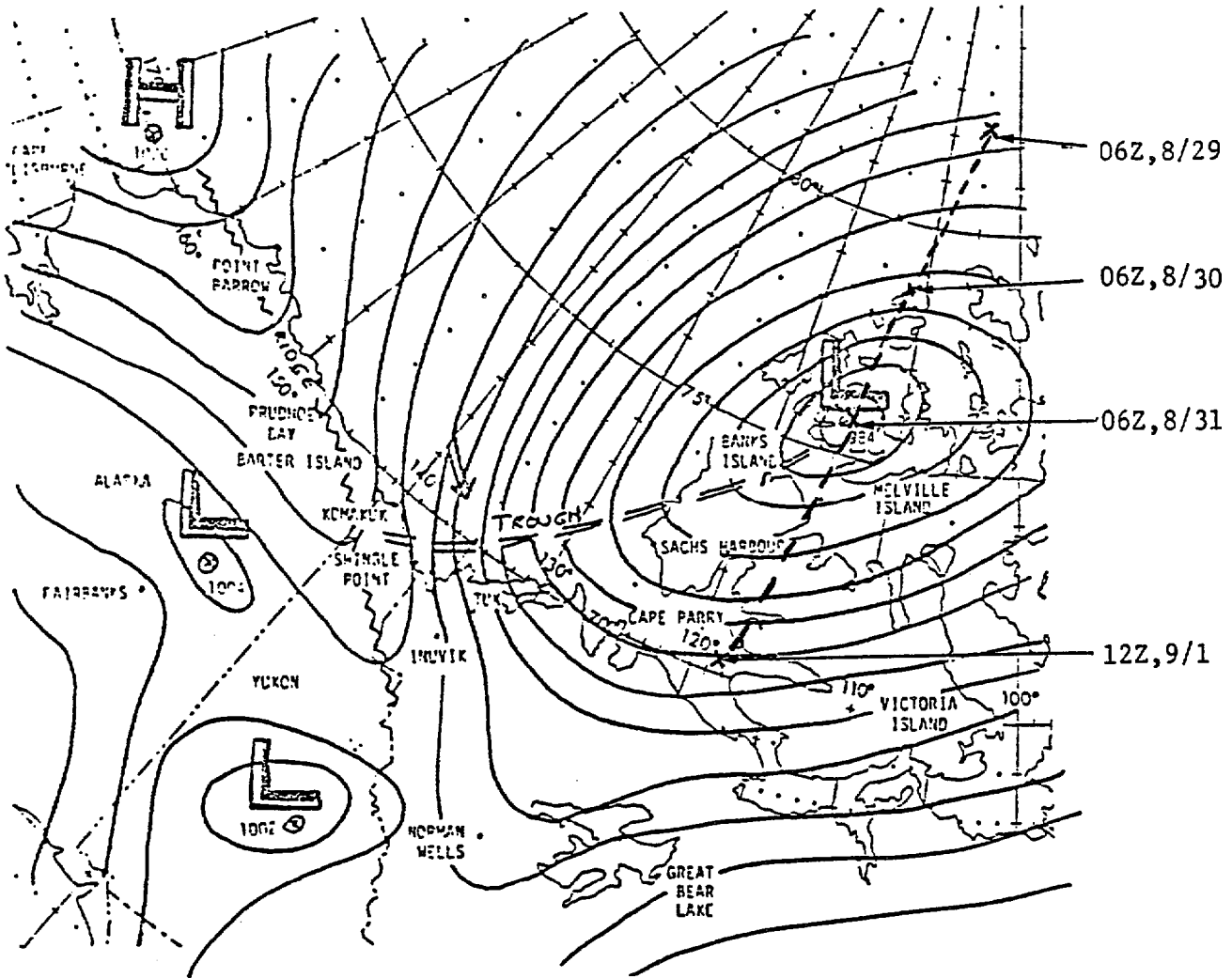


Figure 68. --Surface weather chart for 31 August 1981, 06Z. Pressure in millibars. Dashed line represents the track of the low. From Beaufort Weather and Ice Office 1981 Report.

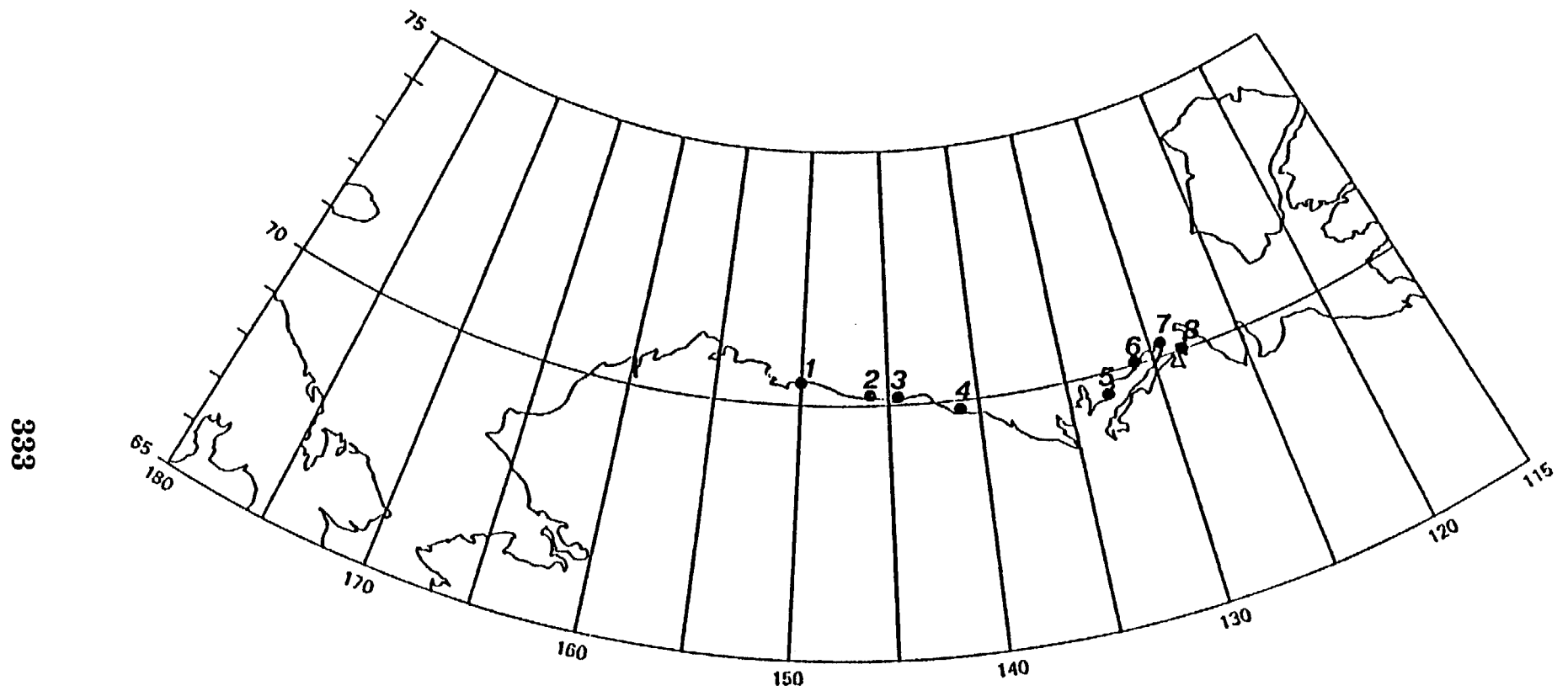


Figure 69.--Positions of the tide gauges deployed along the coast of the Beaufort Sea in August and October 1981: 1, Oliktok; 2, Flaxman Island; 3, Simpson Cove; 4, Demarcation Bay; 5, Tuktoyaktuk; 6, Atkinson Point; 7, Cape Dalhousie; and 8, Baillie Island.

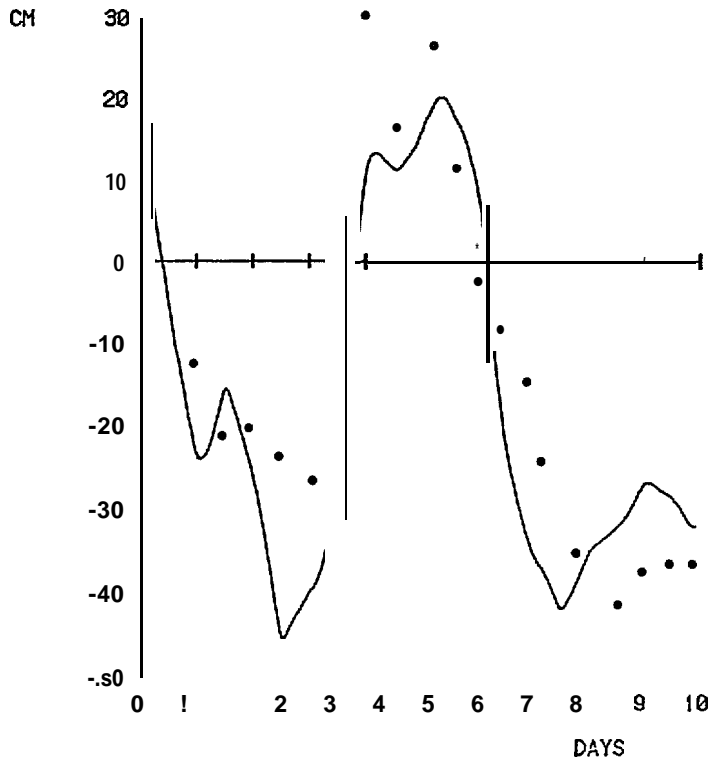


Figure 70. --Sea level variation, OIiktok.

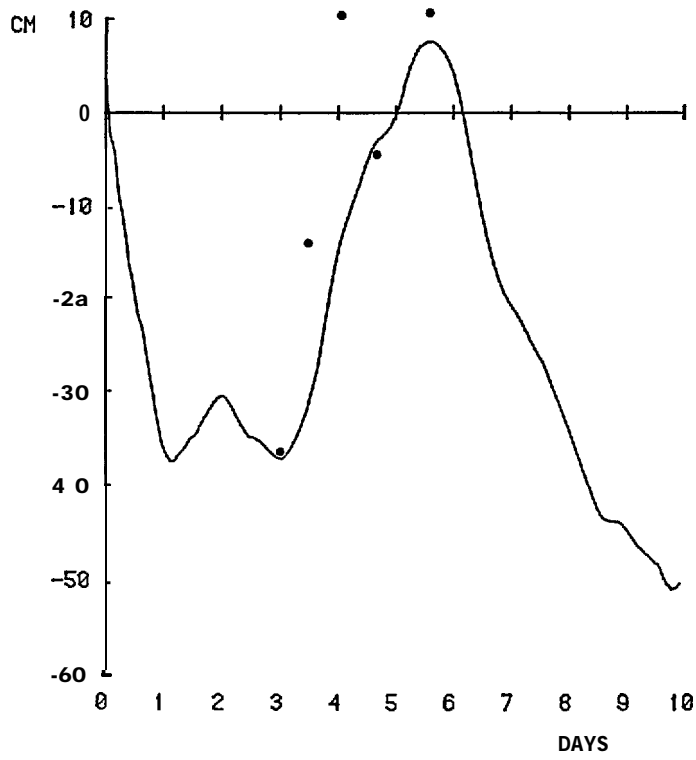


Figure 71. --Sea level variation, Flaxman Island.

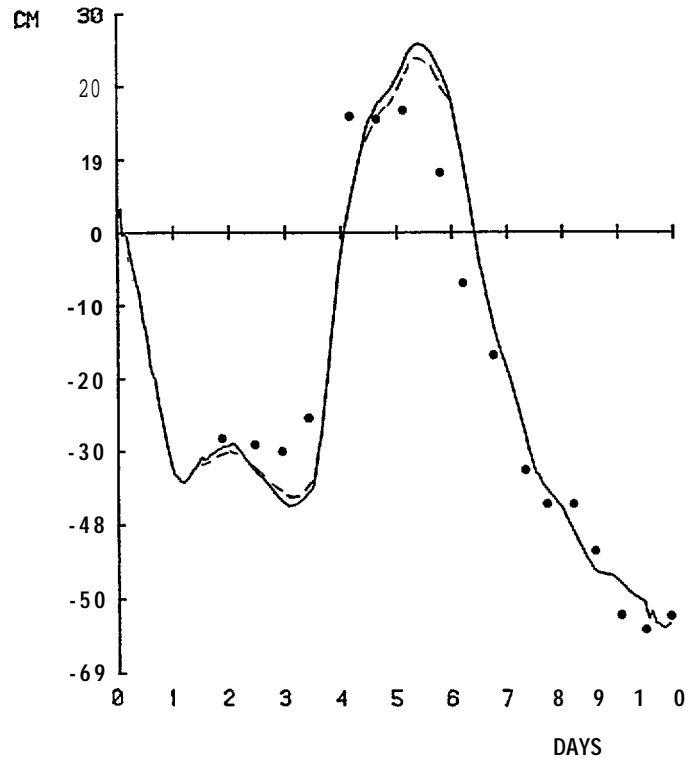


Figure 72. --Sea level variation, Simpson Cove.

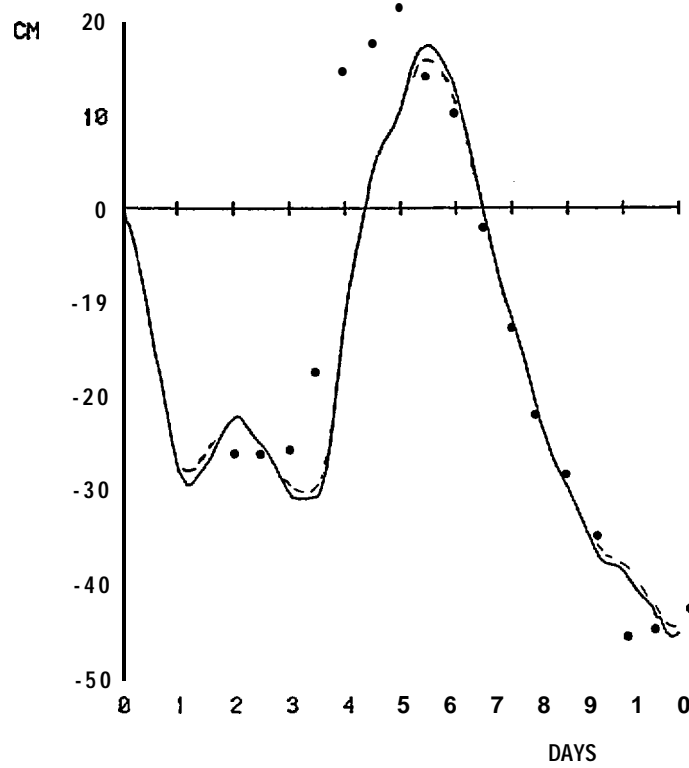


Figure 73. --Sea level variation, Demarcation Bay.

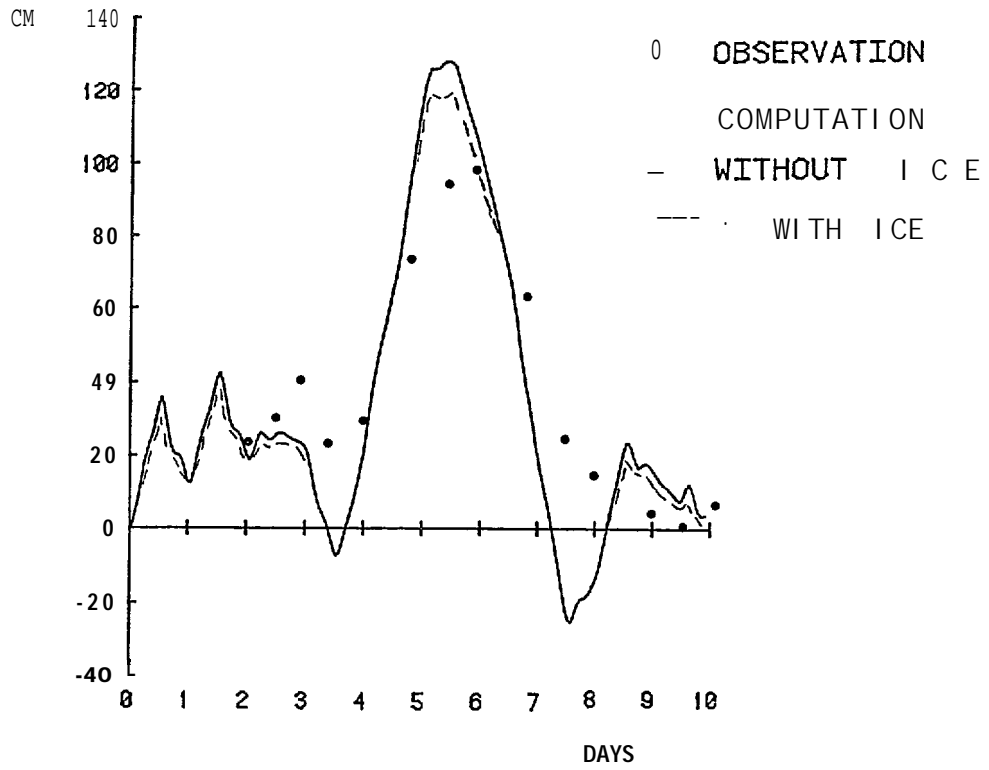


Figure 74. --Sea level variation, Tuktoyaktuk.

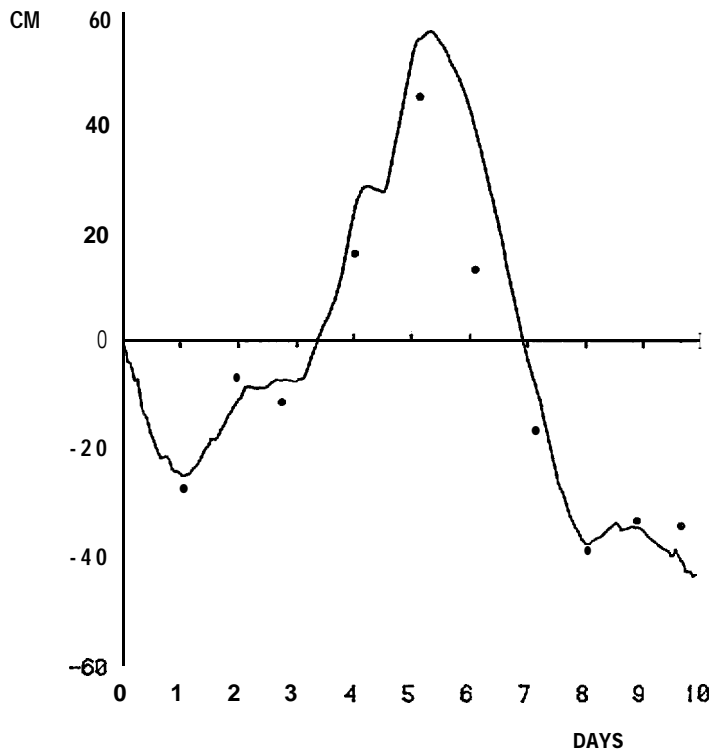


Figure 75. --Sea level variation, Atkinson Point.

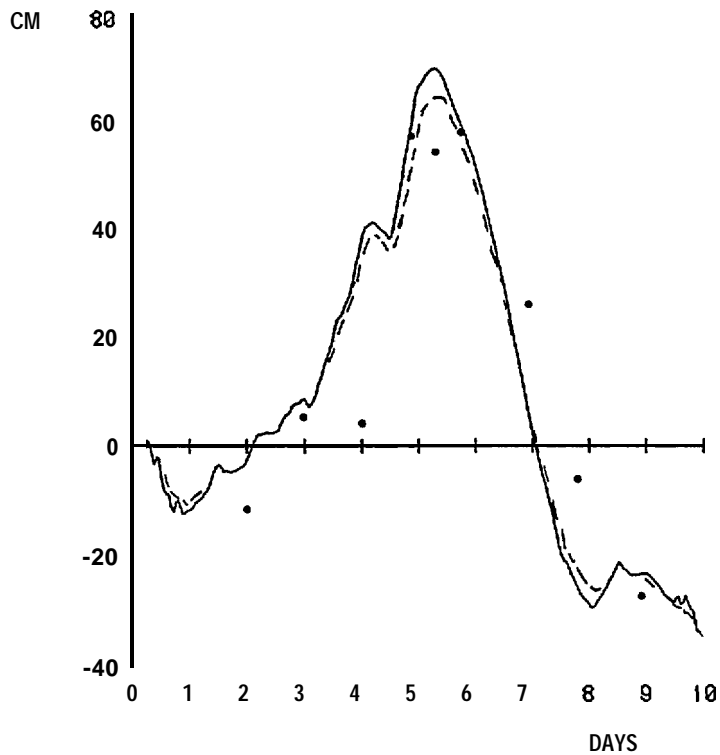


Figure 76. --Sea Level variation, Cape Dalhousie.

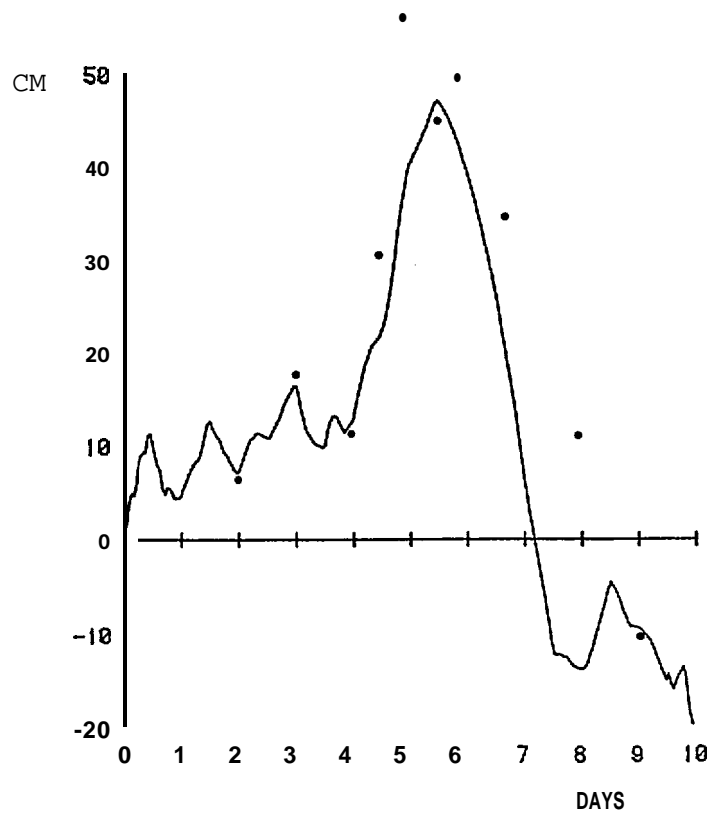


Figure 77. --Sea Level variation, Baillie Island.

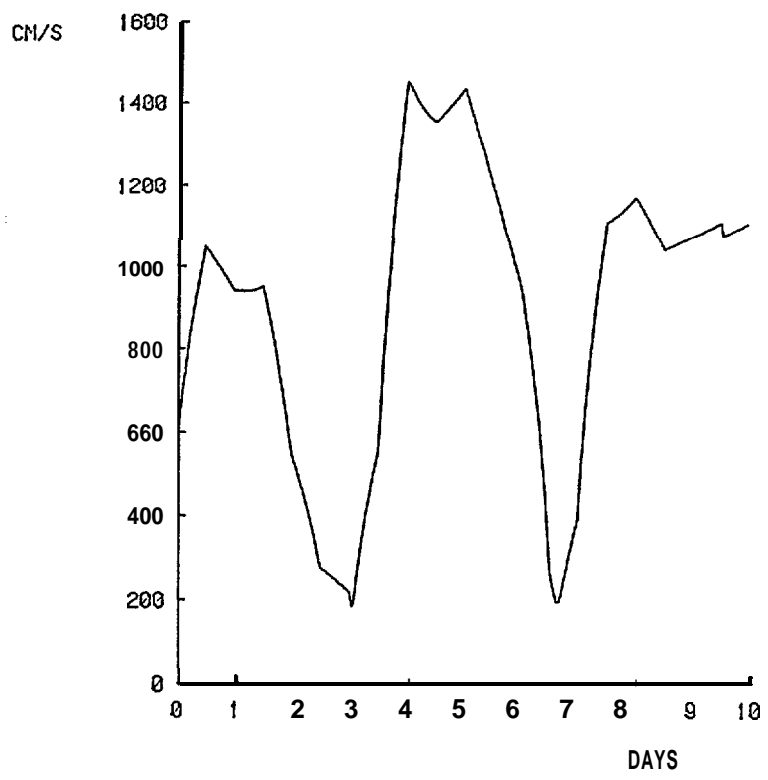


Figure 78---Wind speed at 70°30'N, 135°30'W.

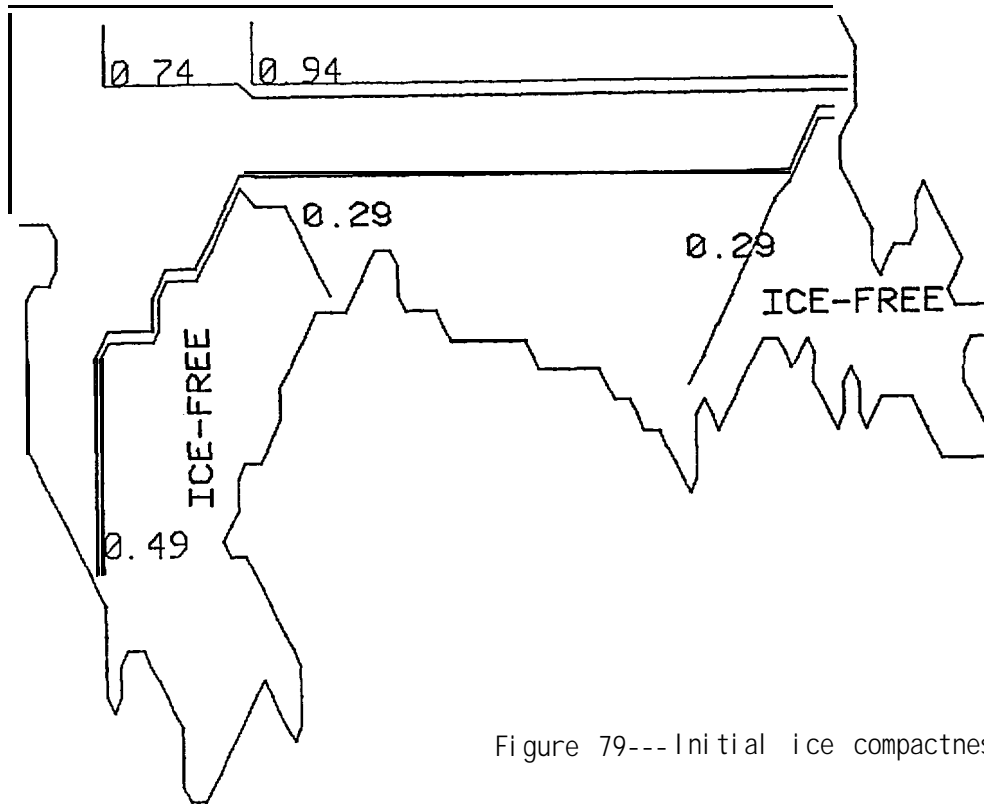


Figure 79---Initial ice compactness.

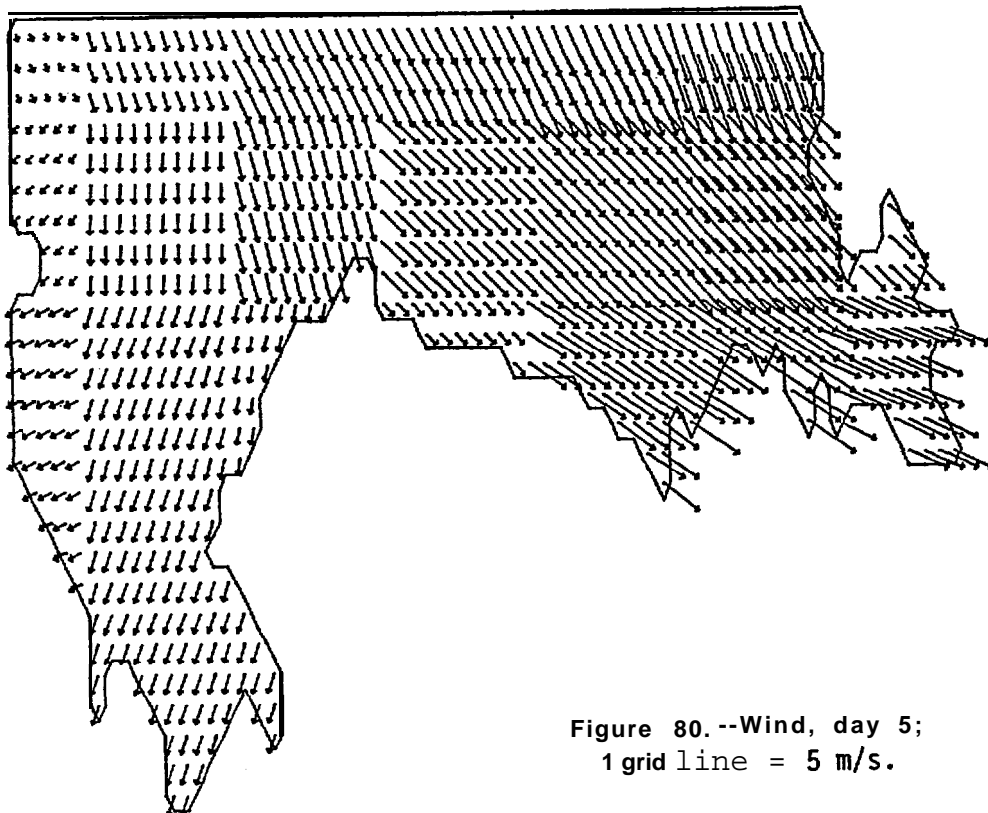


Figure 80.--Wind, day 5;
1 grid line = 5 m/s.

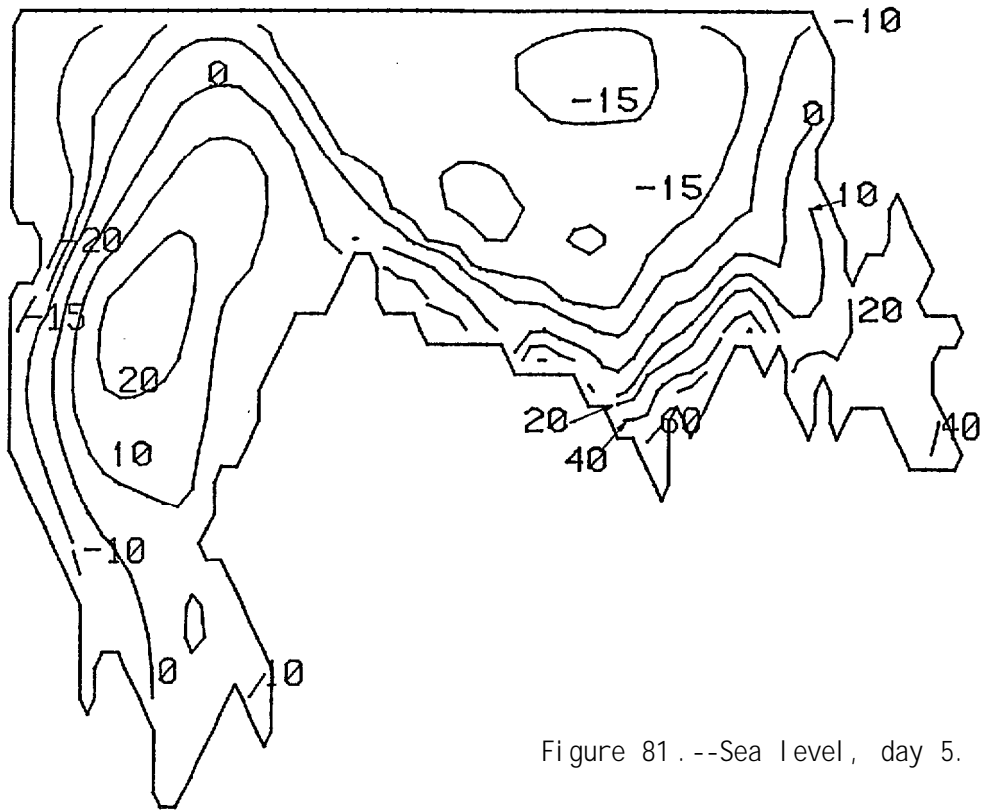


Figure 81 .--Sea Level , day 5.

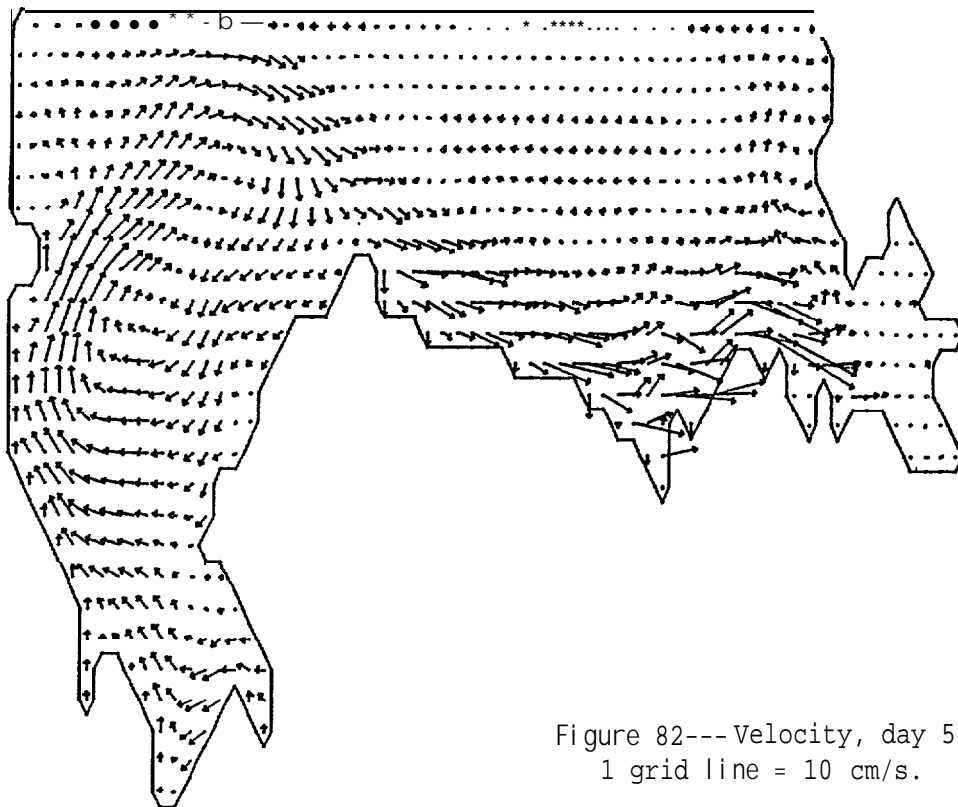


Figure 82--- Velocity, day 5;
1 grid line = 10 cm/s.